國立臺灣大學生命科學院生化科學研究所

博士論文

Graduate Institute of Biochemical Sciences

College of Life Science

National Taiwan University

Doctoral Dissertation

TIFA 磷酸蘇氨酸與其 FHA 結構域分子間交互作用與活化 NF-κB 的機制

Intermolecular binding between TIFA-FHA & TIFA-pT9 mediates TNFα stimulation & NF-κB activation

黃家琦

Chia-Chi Flora Huang

指導教授：蔡明道 博士

Advisor: Ming-Daw Tsai, Ph.D.

中華民國 101 年 7 月

July, 2012

國立臺灣大學博士學位論文
口試委員會審定書

TIFA 磷酸蘇氨酸與其 FHA 結構域分子間

交互作用與活化 NF-κB 的機制

Intermolecular binding between TIFA-FHA and TIFA-pT9 mediates TNFα stimulation and NF-κB activation

本論文係 黃家琦 君（學號 D94B46017）在國立臺灣大學生化科學研究所完成之博士學位論文，於民國 101 年 7 月 18 日承下列考試委員審查通過及口試及格，特此證明。

口試委員：

（簽名）

（召集人）

(指導教授)

Acknowledgement

I would first and foremost like to express my deepest gratitude to my dedicated advisor and mentor, Prof. Ming-Daw Tsai. His wide knowledge, insightful criticisms, and brilliant suggestions are indispensable to the accomplishment of this dissertation. My many discussions with him have provided me invaluable advice and guidance not just in scientific research but also in life. I am very much obliged to his tremendous patience and unconditional trust throughout the course of my postgraduate study. I am sure a lucky graduate student who has been given the opportunity to develop own individuality and self-sufficiency by being allowed to work with such independence.

I sincerely thank all my candidacy qualification and thesis defense committee members for their helpful ideas and comments. Furthermore, I wish to extend my thanks to Ms. Yueh-Mei Chou and members of Cell Biosciences Inc. for their contributions to the NanoPro™ Immunoassay. I would also like to acknowledge the technical assistances provided by Dr. Yo-Ya Kao and Dr. Shun-Chang Wang for preliminary ITC analysis; Dr. Gabriel Wu for stable cell line selection; Dr. Mei-I Su for HSQC and 1-D NMR experiments; Dr. Pang-Hung Hsu and Mr. Eric Chen for MS analysis; Dr. Yu-Hou Chen for AUC analysis; Dr. Chin-Chun Hung for confocal microscopy; Dr. Kai-Fa Huang for

X-ray crystallography; and the IBC core facilities together with Dr. Shui-Tsung Chen and Ms. Yu-Ling Huang for robotic screenings of crystallization conditions, generation of mouse anti-TIFA monoclonal antibody and synthesis of peptides used in this work. I greatly appreciate the gift of pNF-κB-Luc plasmid from Prof. Ling-Pai Ting (National Yang-Ming University, Taipei, Taiwan). I am also deeply indebted to Jim, Jody, Wade, Eric Chen, Dr. Gabriel Wu, Dr. Dongyan Qin, Prof. Ruey-Hwa Chen, and Prof. John Shyy (Univ. of California, Riverside, US) for useful brainstorming and discussions. I would never go this far without their expertises and assistances. Special thanks also go to Karen, Fanny, Emily, Nai-Fang, Chick, and Heather, who have accompanied me through so many ups and downs along the years. Their thoughtfulness and warm encouragements really meant a lot to me. Finally, I would like to thank all the former and current lab members in Rm 310 of the Genomic Research Center and Rm 316 of the Institute of Biological Chemistry for all the helps.

Last but not the least, I'm extremely grateful to my family, especially my parents, for their faith in me. It is through their unwavering love and unending support that I have gained the drives and confidence to tackle the many challenges ahead.

中文摘要

FHA (forkhead-associated) 是一種新發現的結構域，它可以專一性地結合磷酸化蘇氨酸，並藉此調控細胞內許多重要的機制。TIFA 是所有已知人類蛋白質包含 FHA 結構域中最小的一個。先前的文獻已經發現在細胞中大量表現外源性 TIFA 會激活轉錄因子 NF-κB，不過 TIFA 如何參與並調控這訊息傳導仍需要更深入的探討。在此研究中，我們在 TIFA 上發現了一個蘇氨酸(第九個氨基酸)有被磷酸化修飾，並證實這個磷酸化蘇氨酸會與 TIFA 的 FHA 結構域結合。此交互作用會促進 TIFA 蛋白質間的聚合並激活下游的 NF-κB。生化分析的結果顯示在緩衝溶液中，未磷酸化的 TIFA 是以二聚體的形式存在著，意味著 TIFA FHA 結構域和第九磷酸化蘇氨酸(pT9)間的結合是 TIFA 二聚體與二聚體間的交互作用。此外，我們也發現抑制內源性 TIFA 會削弱細胞激素 TNFα引發的訊息傳遞及其功能。根據這些結果，我們認為 TIFA FHA-pT9 的交互作用是 TNFα刺激後活化 NF-κB 傳導途徑中未知的新環節，而此 TIFA 二聚體分子間藉由 FHA-pT9 結合形成聚合體的機制，將是 FHA 結構域研究中另一個全新的範例。

關鍵字/詞: FHA 結構域/轉錄因子 NF-κB/磷酸化蘇氨酸/TIFA/細胞激素 TNFα傳遞訊號機制

Abstract

The forkhead-associated (FHA) domain recognizes phosphothreonine (pT) with high specificity and functional diversity. TIFA (TRAF-interacting protein with a FHA domain) is the smallest FHA-containing human protein. Its over-expression was previously suggested to provoke NF-κB activation, yet its exact roles in this signaling pathway and the underlying molecular mechanism remain unclear. Here we identify a novel phosphorylated threonine site, threonine 9 (pT9), on TIFA and show that this phosphorylation site binds with the FHA domain of TIFA, leading to TIFA oligomerization and TIFA-mediated NF-κB activation. Detailed analysis indicated that unphosphorylated TIFA exists as an intrinsic dimer, and that the FHA-pT9 binding occurs between different dimers of TIFA. In addition, silencing of endogenous TIFA resulted in attenuation of TNFα-mediated downstream signaling. We therefore propose that the TIFA FHA-pT9 binding provides a previously unidentified link between TNFα stimulation and NF-κB activation. The intermolecular FHA-pT9 binding between dimers also represents a new mechanism for the FHA domain.

Running title: TIFA oligomerizes via FHA-pT to activate NF-κB

Keywords: FHA domain/NF-κB/phosphothreonine/TIFA/TNFα-mediated signaling

Table of Contents

Figure List

Table List

Chapter 1. INTRODUCTION

1.1 FHA domain

1.1.1 Conserved folding

The forkhead-associated (FHA) domain, discovered in 1995 (24) and first suggested to bind phosphoproteins in 1998 (59), is known to recognize phosphothreonine (pT) specifically to exert its function (15, 52). Although the sequence homology among different FHA-containing proteins is relatively low, the structural architecture of FHA domains is highly conserved. It consists of a six-stranded and a five-stranded β–sheets, forming a β-sandwich. The β strands are connected by loops which, though varying greatly in length, are responsible for recognition of the specific pT-ligand (**Sup. Figure 1**).

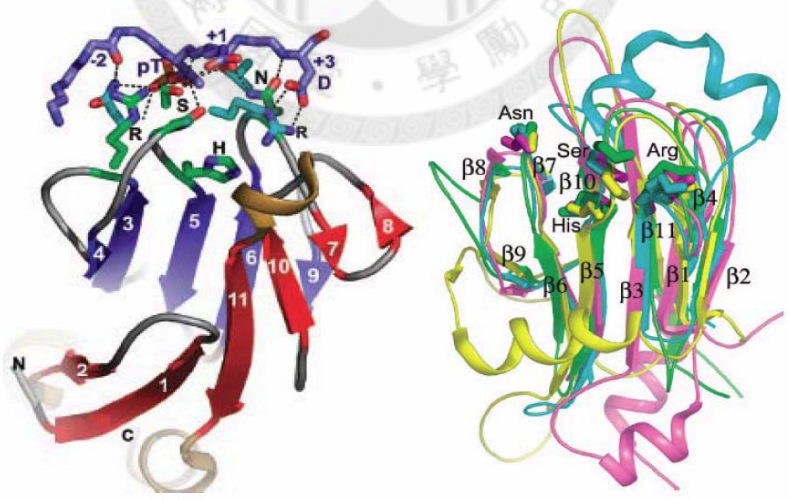

Supplementary Figure 1. Left: Despite sharing low sequence homology, all known FHA domains adopt a strikingly similar tertiary fold: a twisted β sandwich consisted of one β sheet with six anti-parallel strands and the other sheet with five mixed β strands. The hydrophobic side chains are buried in between these two large β sheets (35, 41). **Right:**

The superimposition of yeast RAD53 FHA1 (magenta) and FHA2 (yellow), human CHK2 FHA (cyan), and plant KAPP FHA (green). Side chains of five mostly conserved residues near the phospho-recognition surface are drawn (35).

This functional domain serves not just a solely protein-protein interaction platform but an important activation/inhibition module that participates in establishing or maintaining several essential cellular mechanisms such as DNA damage repair, cell cycle checkpoints, signal transduction, and transcriptional regulations in both eukaryotes and prokaryotes (41). Furthermore, the mechanism of FHA-phosphoprotein binding varies greatly among different FHA-containing proteins. The structure, specificity, mechanism, and biological functions of FHA domains have been summarized in recent reviews (35, 41).

1.1.2 Ligand specificity

The ligand specificity for FHA domain is referring to the amino acid residues surrounding the pT site that are directly recognized by the FHA domain. The most common ligand specificity follows the "pT+3 rule", where the primary determinants of binding are the pT residue and the residue at the +3 position, which could be a hydrophilic type (eg., Aspartic acid) or a hydrophobic type (e.g., Leucine/Isoleucine/Valine) (15, 16, 32, 36). However, as more examples become available, more variations have been found. In addition, even the same FHA domain may have more than one type of ligand specificity. For example, the FHA1 domain of *S. cerevisiae* Rad53 has been shown to bind to ligands with Aspartic acid

(D) (8, 16), Isoleucine (I) (42), and Threonine (T) (29) at the pT+3 positions. In another report, the FHA/BRCT-repeat architecture of Nbs1 (Nijmegen breakage syndrome) was shown to bind the diphosphorylated pSDpTD motif of MDC1 (mediator of DNA damage checkpoint protein 1) (38).

1.1.3 Mechanisms of FHA function

The "mechanism" of FHA function here is defined as how, at the protein level, the FHA domain binds to its biological ligand and confers its biological function. Based on recent reports, the FHA domain appears to be highly diversified in this aspect also. The simplest situation of the mechanism is that *a monomer of the FHA domain binds with a different monomer of its biological ligand intermolecularly* (mechanism a) (**Sup. Figure 2**). An example in this category is the Ki67 FHA – phosphoNIFK (nucleolar protein interacting with the FHA domain of pKI-67) binding. The structure of the Ki67 FHA complexed with fragment 226-269 of NIFK (tri-phosphorylated) shows highly extended interactions beyond the pT site (7), such that it is clear that this is a monomer-monomer complex between two different proteins. The second mechanism is that *a monomer of FHA domain binds with another monomer of the same FHA domain intermolecularly to enhance homo-dimerization* (mechanism b) (**Sup. Figure 2**). A well characterized example in this category is mammalian CHK2, where the FHA-pT68 binding-dependent dimerization has

been well established (2, 31, 72). In the absence of phosphorylated Thr68, weak FHA-FHA interactions (31) and dimer crystallization (9) was also possible. Thus the reciprocal binding of CHK2-FHA domains was suggested to co-operate with the intermolecular interaction mediated by pT68–FHA for the increase of overall avidity for CHK2 dimerization (9). The third mechanism involves *intramolecular binding between an FHA domain and a pT site within the same protein molecule* (mechanism c) (**Sup. Figure 2**). This mechanism was first discovered for the FHA domain of *Mycobacterium tuberculosis* Rv1827, where the intramolecular FHA-pT22 binding switches the FHA domain to a closed conformation and blocks its phospho-independent interaction with three proteins (49). A similar mechanism was also observed for the OdhI (oxoglutarate dehydrogenase inhibitor) protein of *Corynebacterium glutamicum* (3).

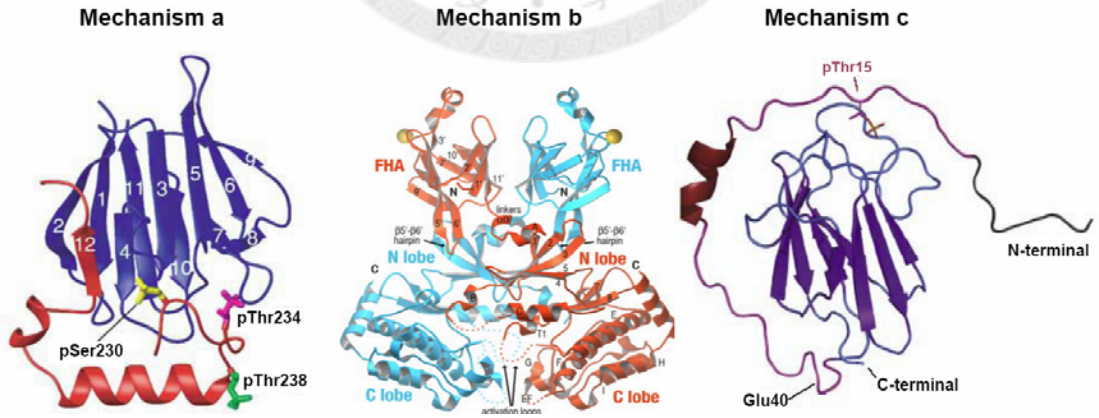

Supplementary Figure 2. Mechanism (a): The ribbon diagram of a representative structure of Ki67-FHA (residues 4 – 99) (blue) and hNIFK226 – 269 (red) with three phosphorylated residues (side chain atom of pSer230 in yellow, pThr234 in magenta, and pThr238 in green) (7). **Mechanism (b):** Schematic representation of the CHK2^{K249R} dimer

with the two protomers colored in red and blue. The yellow spheres indicate the approximate positions of the pThr phosphate group (32). Phosphorylation on Thr68 stabilizes weak FHA-FHA interactions that occur in the unphosphorylated species to form a high affinity CHK2 dimer (9). **Mechanism (c):** A cartoon representation of the phosphorylated OdhI structure, where residues Met1 to Glu9 are represented in gray, Pro10 to Ala39 are in purple; and the side chain atoms of the phosphothreonine anchoring in the FHA domain are in brown. The binding of the phosphorylated N-terminal part of OdhI to its own FHA domain corresponds to a new autoinhibition mechanism (3).

While in mechanisms b-c the pThr site is always located at a site N-terminal to the FHA domain, a new report shows that the FHA domain of MDC1 binds to phosphorylated Thr98, a residue located at the integral part of the FHA domain (40). If further confirmed by biophysical analyses, this could represent yet another new mechanism.

1.2 TRAF-interacting protein with a FHA domain (TIFA)

TRAF-interacting protein with a FHA domain (TIFA) was first identified as a TNF receptor associated factor 2 (TRAF2) binding protein in 2002 and named as TRAF2 binding protein (T2BP) (28). Later T2BP was reported to bind to TRAF6 as well, and renamed as TIFA (61). Consisting of 184 amino acids, TIFA is the smallest FHA domain-containing protein in human. The binding of TRAF2 to TIFA requires the TRAF domain of TRAF2 and almost the entire protein of TIFA (residues 1-162 with FHA domain included) (28). The binding region of TIFA to TRAF6 was mapped to the C-terminus of TIFA, with a consensus binding sequence *XX*P*X*E*XX*-(aromatic/acidic) and binding site at glutamic acid 178 (E178) (61) (**Sup. Figure 3**), indicating different binding mechanisms in

TIFA-TRAF2 and TIFA-TARF6 interactions. The site for TRAF2 binding, however, has not yet been mapped. TIFA has been found to bind to IRAK-1(interleukin-1 receptor-associated kinase-1) and TIFA itself in oligomerization as well (61).

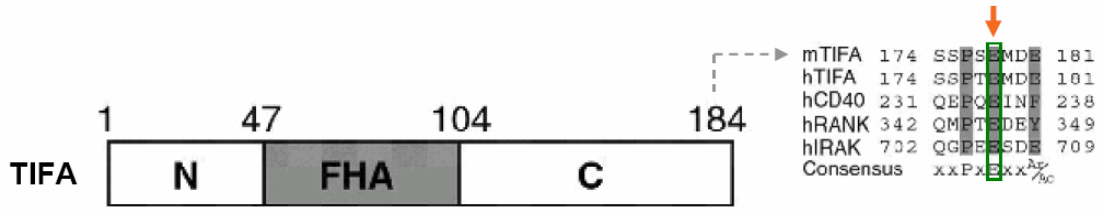

Supplementary Figure 3. The interaction site for TRAF6 has been mapped to be glutamic acid 178 (E178) at the C-terminus of TIFA (61).

In the absence of tumor necrosis factor α (TNFα) stimulation, TIFA over-expression in HEK 293T cells has been shown to activate the master transcriptional factors AP-1 (activator protein 1) and NF-κB (nuclear factor kappa-light-chain-enhancer of activated B cells) (28), and in the latter case, both TRAF2 and TRAF6 are required as demonstrated by RNAi experiments (17). In addition, TIFA over-expression has been shown to activate both NF-κB and JNK (c-Jun amino-terminal kinase) in the absence of cytokine IL-1β (interleukin-1β), possibly through its enhancement of TRAF6 binding to IRAK-1. In a follow-up report, TIFA was shown to promote oligomerization and ubiquitination of TRAF6, leading to activation of IκB kinase (IKK) based on *in vitro* studies (17) (**Sup. Figure 4**). Mutation of TRAF6 E178 residue, on the other hand, abolished the binding of TIFA to TRAF6 and the ensuing activation of NF-κB (61).

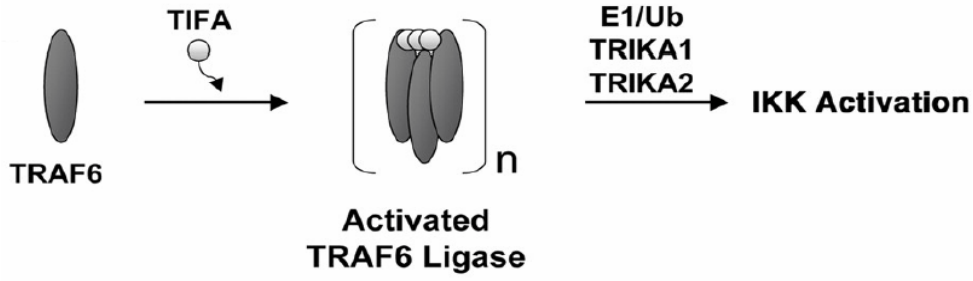

Supplementary Figure 4. TIFA forms oligomers upon stimulation of cells with NF-κB agonists. The oligomerized TIFA then binds TRAF6 to promote TRAF6 oligomerization and ubiquitination which subsequently activate the TRAF6 Ub ligase and downstream IKK (17).

Since NF-κB activation turns on the transcriptions of many genes relevant to inflammation regulations, all these data have suggested a direct involvement of TIFA in TNF-mediated immune responses. It is thus important to further study the physiological functions of TIFA, particularly the roles of TIFA on regulating NF-κB. Furthermore, although FHA domain of TIFA is not required in TIFA-TRAF6 interaction (28, 61), it has been shown that perturbations in FHA domain interfere with TIFA induced IKK and NF-κB activations (17, 61). Altogether, this suggests that an intact FHA domain is important to the biological functions of TIFA, and identification of interaction partner(s) of TIFA-FHA will certainly assist us to understand more about the roles of FHA domain in TNF signaling.

1.3 TNF receptor associated factors (TRAFs)

TNF-mediated cell survival against tumor is a vital response from the immune system, and TRAF proteins are key molecules involved in TNF signaling (11, 55). Mammalian TRAF

is a protein family with 7 members (TRAF1-6 (11), and TRAF7 (71)) that participates the signal transduction of TNFR (tumor necrosis factor receptor) and IL-1R/TLR (interleukin-1 receptor/toll-like receptor) super families. All TRAFs except TRAF7 have a conserved TRAF domain at the C-terminus (also named as meprin and TRAF homology or MATH domain) (55), which is important for TRAF self-association and binding to receptors (62). There are one RING (really interesting new gene) domain and several zinc finger (ZF) motifs located at the N-terminal portion and one coiled coil (CC) region in the middle of TRAF2-7. The structures of TRAF domains, RING and partial zinc finger domains of TRAF2 (51, 81) and TRAF6 (74, 75) have been solved (**Sup. Figure 5**).

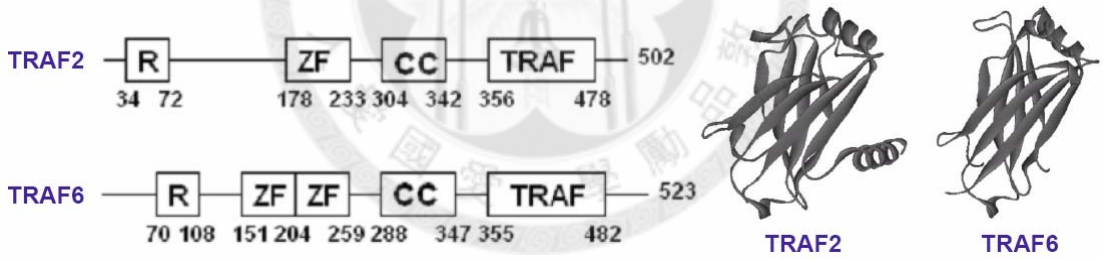

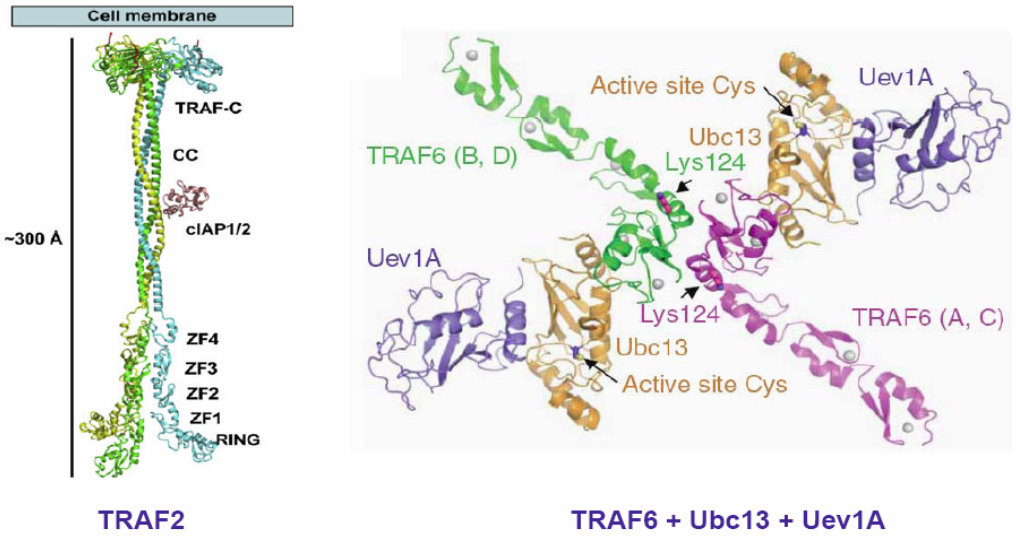

Supplementary Figure 5. Top left: Functional domains of TRAF2 and TRAF6 (13). **Top right:** Structures of TRAF-C domains of TRAF2 and TRAF6. Both global structures mainly contain β-sheets (51). **Bottom left:** Atomic model of full-length TRAF2 built from the current solved partial structures of TRAF2 (**PDB: 1CA4, 1CA9, 3M06, 3M0A, 3M0D, 3KNV**) (81). **Bottom right:** A dimeric TRAF6/Ubc13/Uev1A complex built based on the dimeric TRAF6 N-terminal domains structures (**PDB: 3HCS, 3HCT, 3HCU**) (75).

In addition, several post-translational modifications of TRAF2 and TRAF6 have been reported to be involved in TNFα signaling. Upon TNFα stimulation, TRAF2 undergoes K48- and K63-linked ubiquitination (21, 58, 69). The phosphorylation status of TRAF2 has also been identified in some works (5, 33, 63, 77, 78, 79). Among the several phosphorylation sites characterized, threonine 117 (T117) at the RING domain of TRAF2 has been reported to be TNFα-dependent. NF-κB activation has been attenuated when T117 was rendered to unphosphorylatable alanine (33). Subsequent report has identified the kinase responsible for this phosphorylation to be PKCε (protein kinase C) (34). On the other hand, TRAF6 has been suggested to be polyubiquitinated at its RING domain to activate the ubiquitin (Ub) E3 ligase activity (17). It has also been reported that TRAF6 transduces signals when oligomerized. It activates the transforming growth factor β–activated kinase (TAK1) when TRAF6 was artificially oligomerized without IL-1 stimulation (4, 65). In addition, TRAF2 and TRAF6 over-expression has been observed in pancreatic cancer (PANC-1 cell line) and leukemia (ALL cell line), respectively (64, 68). TRAF6-deficient mice are defective in IL-1 signaling (39, 48). TRAF3 has been reported capable of inhibiting TARF2-mediated non-canonical NF-κB activation and promoting the

activities of TRAF6 (22). Moreover, cells from TRAF2 and TRAF5 double knockout mice demonstrate severely impaired TNFα-induced NF-κB activation, implying that TRAF5 may compensate for TRAF2 deficiency (60).

1.4 TNFα-mediated NF-κB activation

The activation of the transcriptional factor NF-κB mediated by cytokine TNFα has been one of the three well-established inflammatory signaling pathways (30). Phosphorylation and ubiquitination are two major post-translational modifications in the NF-κB pathway. Phosphorylation has been shown to regulate IκB and NF-κB (23) while proteasome-independent K63-linked polyubiquitination has been documented for various components in the NF-κB signaling pathway (1). Recent evidence shows the existence of two branches of NF-κB pathways (canonical and non-canonical), leading to either cell death protection or lymphatic tissue development (6, 53). The classic scheme of canonical signaling transduction for TNFα-induced NF-κB activation is summarized as follows (**Sup. Figure 6, Left**). When inflammatory stimulation occurs, TNFα trimers will bind to the extracellular domains of TNFR on the cell membrane and cause the intracellular domains of receptors to trimerize. Although TRAF2 has been reported to be a double-edged sword in this pathway, and exactly how the signals are propagated at this stage of signal cascade is not well-understood yet, it is known that TRAF2 oligomerizes and interacts with the

trimeric TNFR or the CD40 cytoplasmic domain with high affinity (30). Subsequently, TRAF6 will oligomerize as well to activate its ubiquitin E3 ligase activity and to catalyze K63-linked polyubiquitination in conjunction with the Ubc13-Uev1A E2 complex (ubiquitin-conjugating enzyme E2 13-ubiquitin-conjugating enzyme E2 variant 1A, the complex is also known as TRIKA1) at its RING domain (17). Ubiquitinated TRAF6 is then recruited to the TRIKA2 complex, which contains TAK1 and the Ub receptor TAB2 (TAK1-binding protein 2) (65). Once the protein kinase TAK1 is activated, it will phosphorylate one of the two catalytic IKK subunits, IKKβ, at key serine residues within the activation loop, thereby activate the whole IKK complex including IKKα and one other essential subunit NEMO (NF-κB essential modulator) (1). Activated IKK will in turn phosphorylate IκB, the inhibitor of NF-κB, and thus facilitate the degradation of IκB by proteosome. Once IκB is removed, NF-κB heterodimers will be free to enter the nucleus to turn on several downstream inflammatory responsive genes that will ultimately lead to cell survival.

1.5 Inflammatory signaling

The important defense mechanisms in the human body against infection, injury, and immunological challenges comprise the innate and adaptive immunities. Other than the TNFα/TNFR pathway mentioned in section 1.4, there are two other important signaling

pathways that mediate inflammatory responses through the recognition of IL-1β and lipopolysaccharide (LPS) by IL-1R and TLR4, respectively (**Sup. Figure 6, Right**). The biological functions of TNFR, IL-1R, and TLR are very similar, which is quite remarkable given the fact that they belong to different structural classes. IL-1β, also known as catabolin, is a human pro-inflammatory cytokine protein that is produced by monocytes and activated macrophages as a precursor protein. It has to be proteolytically processed by caspase 1 (interleukin-1β convertase) to turn into its active mature form. As an important mediator of the inflammatory response, how IL-1R-mediated signals link to the downstream protein kinase cascades has been studied extensively (25). Members of the MAP3K (mitogen-activated protein kinase kinase kinase) family, including TAK1 (25), MEKK1 (MAPK/ERK kinase kinase 1) (4), MEKK2 (80), MEKK3 (73), NIK (NF-κB-inducing kinase) (43), and Tpl2 (tumor progression locus 2) (14), are critical in this process. Upon receptor engagement, IL-1R forms a heterodimer with IL-1 receptor accessory protein (IL-1RAcP), which functions as a co-receptor. IRAK 1 and 2 then transmit downstream signals by serving as adapter proteins as well as protein kinases to recruit TRAF6 to the IL-1 receptor complex via an interaction with IL-1RAcP. Oligomerization of TRAF6 and subsequent formation of TAK1/MEKK3 signaling complexes then relay the signal via NIK to IKK, leading to NF-κB activation (25). In a similar fashion, TLR4 signaling occurs on dimerization of the TLR4 upon LPS binding.

Once TLR4 goes through conformational change, adaptor protein myeloid differentiation 88 (MyD88), a member of the TIR (toll/interleukin-1 receptor) family, is recruited (12). This will then lead to subsequent recruitment of IRAK4, IRAK1, and IRAK2 that will phosphorylate and activate TRAF6, which in turn polyubiquitinate TAK1 to facilitate the binding of TAK1 to IKKβ (61). As mentioned previously, despite total absence of chemical and structural similarities, occupancy of IL-1R and TLR leads to activation of NF-κB signaling that ultimately elicits acute and chronic inflammatory responses.

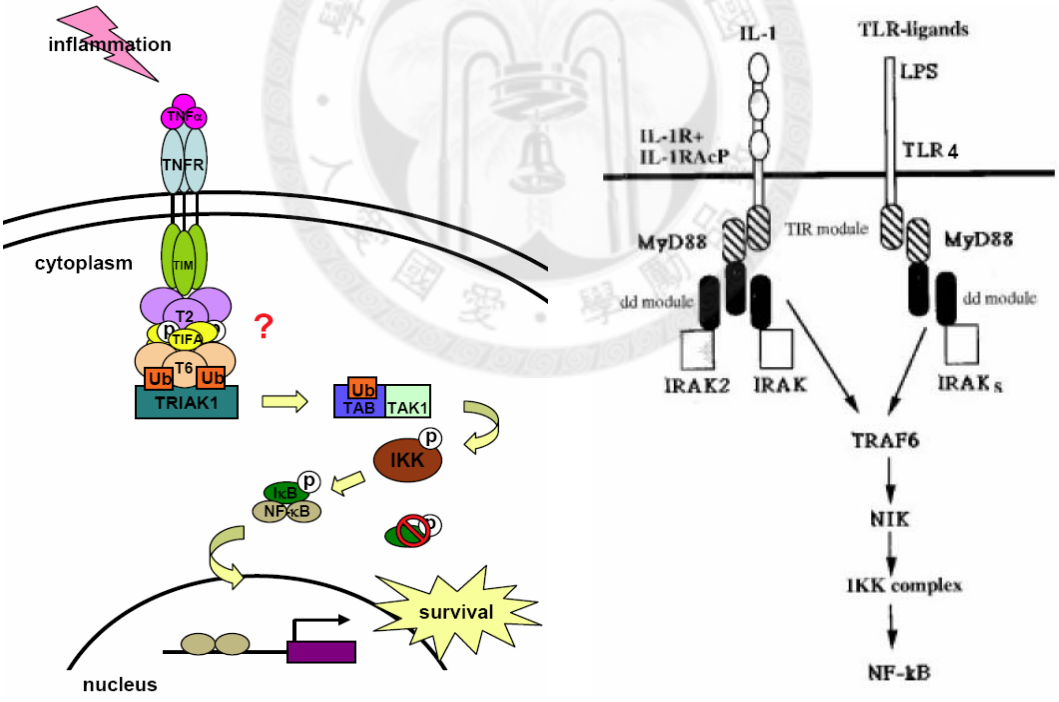

Supplementary Figure 6. Left: The classical pathway of TNFα/TNFR-mediated activation of NF-κB (13). **Right:** The signaling is triggered through the recognitions of IL-1β and LPS by IL-1R and TLR4, respectively, and is then propagated by members of IRAK and MAP3K families (47). Although belonging to different structural classes, signaling mediated by these three receptors all lead to the activation of IKK and NF-κB.

1.6 Other proteins relevant to TIFA

The signaling involving TIFA gets more complicated when TIFAB, a TIFA-binding and inhibiting protein, was recently discovered by the same group who identified TIFA (45) (**Sup. Figure 7**). TIFAB seems to bind to TIFA and causes conformational changes on TIFA. The conformational changes likely disrupt TIFA-promoted TRAF6 oligomerization, which in turn blocks the TIFA-mediated NF-κB activation (44). The impact of TIFAB on TIFA- mediated AP-1 activation, however, is still unknown.

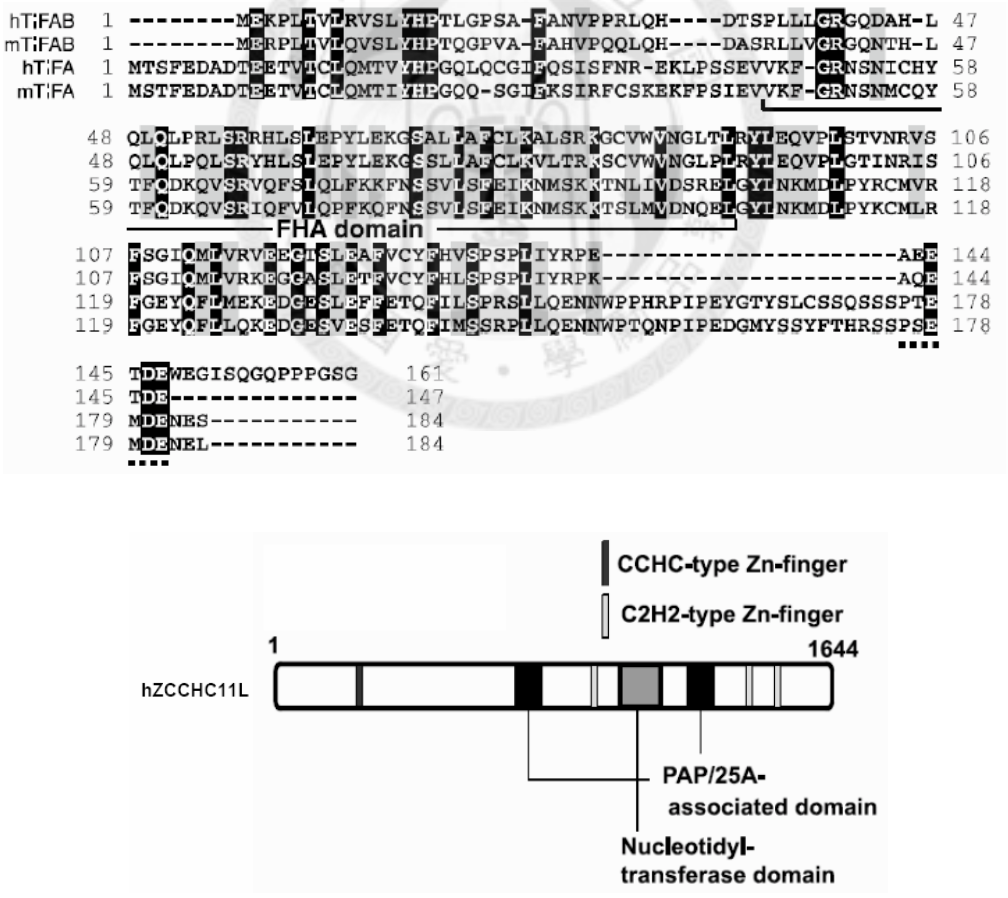

Supplementary Figure 7. TOP: Sequence alignment of human and mouse TIFAB with human and mouse TIFA (45). **Bottom:** Schematic diagram of ZCCHC11L protein (46).

Other than TIFAB, ZCCHC11L, a novel zinc finger protein, has also been identified to interact with TIFA and modulate TLR signaling (46). Locating in the nucleus most of the time, ZCCHC11L is translocated into the cytoplasm in response to LPS and bound to TIFA. Over-expression and RNAi experiments have indicated that ZCCHC11 functions as a negative regulator of TLR-mediated NF-κB activation after LPS treatment. The N-terminal region (ZCCHC11S) including CCHC-type Zn-finger motif has been mapped to be sufficient for suppression of NF-κB (46).

1.7 Significances

The main focuses of this work is to study the biological functions of TIFA and to determine the involvement of TIFA in inflammatory signaling pathways. Although the studies of Takatsuna *et al.* (61) and Ea *et al.* (17) have previously established the key function of TIFA in its interaction with TRAF6, several issues still remain inconclusive. For example, TIFA has been suggested to be phosphorylated as unpublished result (61), but no data has been reported subsequently. Also, the integrity of the FHA domain of TIFA has been suggested to be required for downstream activation of NF-κB (17, 61), but little information about the molecular basis of TIFA phosphorylation and oligomerization were unveiled. Therefore, in this thesis, we aimed to characterize the phosphorylation status of TIFA and depict its functional consequences. In addition to

study the molecular mechanism of TIFA, we also tried to confirm the TIFA-TRAF2 binding *in vivo* as well as to map the sites important for this interaction. One other emphasis of this work is to study the biochemical properties of TIFA *in vitro* and hopefully to solve its full-length structure using X-ray crystallography.

As a result, we identified threonine 9 (T9) as a novel phosphorylation site of TIFA and showed that the phosphorylation level of T9 increased upon TNFα treatment. Based on *in vivo* and *in vitro* evidences, we concluded that TIFA-FHA binds to this phosphorylated T9 (pT9) site, and that TIFA-FHA/pT9 binding directs TIFA self-association and promotes NF-κB activation through the oligomerization process. Further biophysical analyses indicate that TIFA-FHA/pT9 binding occurs between dimers of TIFA, leading to oligomerization. We also observed *in vivo* the speckle formation of oligomerized TIFA which co-localizes with TRAF6, and the increase of the TIFA protein level upon stimulation by TNFα. Moreover, our studies suggest that the TNFα-mediated signaling is attenuated when endogenous TIFA is knocked-down. Accordingly, we proposed that FHA/pT9 binding of TIFA is a critical link between TNFα stimulation and NF-κB activation. Our findings provide not only a new molecular insight into the TNFα-mediated signaling pathway but also a new functional mechanism of FHA-containing proteins. Considering NF-κB is constitutively activated in most cancers, the information gathered on

TIFA could thus lead to some potential therapeutic windows. Together with the corresponding structural studies, this work may further shed light on the FHA domain researches since most of the solved human FHA structures to date are only domains and none of them is from a full-length protein. Should the full-length structure of TIFA to be solved in the near future, it will be a good demonstration about how FHA domain fits into a full-length protein. Furthermore, structural information regarding full-length TIFA and its interaction partner(s) could serve as another good model to elucidate some significant issues lingering in FHA research field, such as the mechanism of substrate recognition and binding specificity.

Chapter 2. RESULTS

2.1 Identification of phosphorylation at Thr9 on TIFA

To elucidate the function of TIFA, it is important to first identify the biological ligand of the FHA domain of TIFA. On the basis of the known mechanisms of FHA-pT binding, and considering that there are five Thr residues at the N-terminus of TIFA (T2, T9, T12, T14, and T19) **(Figure 1A)**, we hypothesized that one of these Thr residues could be phosphorylated and then recognized by the FHA domain of TIFA. In order to validate our hypothesis, we first analyzed the phosphorylation status of exogenously expressed Flag-TIFA derived from HEK-293T cells using *in vivo* pull-down assay in combination with mass spectrometry (MS) analysis. The MS data, with 80% sequence coverage, revealed that Flag-TIFA was clearly phosphorylated at Thr9 (T9) (**Figure 1B**).

2.2 Phosphorylation status of pT9

Because both TNFα stimulation and TIFA over-expression can activate NF-κB (28, 61), it is likely that T9 phosphorylation is correlated with TNFα-elicited signaling. We thus used the recently developed NanoPro^{TM} immunoassay (18, 50) to examine the effect of TNFα treatment on T9 phosphorylation. The method involves separation of cell lysates in the capillary isoelectric focusing step, followed by analysis of specific protein isoforms (i.e., different phosphorylation forms of TIFA) using conventional immune-detection (50).

As shown in trace 1, **Figure 1C**, the exogenously expressed Myc-TIFA, revealed by the anti-Myc antibody, exhibited a major peak at pI 4.75. This was close to the theoretical pI value of 4.92 deduced by the Scansite data base (http://scansite.mit.edu/calc_mw_pi.html). Among the several smaller peaks detected, the one with pI 4.63 was consistent with singularly phosphorylated TIFA, since addition of one phosphate group is expected to decrease pI by 0.12. Treatment of TNFα also led to increase of the peak with pI 4.63 (traces 2), suggesting phosphorylation at one single amino acid residue. However, TNFα did not have such effect on the T9A mutant (traces 3 and 4). When traces 1-4 were repeated in the presence of alkaline phosphatase (traces 5-8, respectively), only one single peak at pI 4.75 was observed. These results support that the exogenously expressed TIFA was phosphorylated (at T9 based on the MS result), and that the phosphorylation increased upon TNFα treatment.

The subsequent question would be whether we can also observe the same TNFα–stimulatable pT9 phosphorylation on the endogenous TIFA proteins. In order to answer this question, we raised a mouse monoclonal antibody (mAb) against bacterial-expressed full-length TIFA protein and used it to examine endogenous TIFA through the same NanoPro immunoassay. In **Figure 1D**, the endogenous TIFA from 293T cells showed the same results as that seen in **Figure 1C** (comparing traces 1-4 in **Figure 1D**

with traces 1, 2, 5, 6, in **Figure 1C**). Of note, since the endogenous TIFA was not tagged, the pI values differed slightly from those in **Figure 1C**.

In vitro kinase assay was then used to further confirm that TIFA T9 phosphorylation is TNFα-dependent. We incubated recombinant TIFA with TNFα-stimulated cell extracts in the presence of [γ-^{32}P]ATP. All the TIFA proteins were then immobilized by anti-His beads, separated by SDS-PAGE and visualized by auto-radiography. As shown in **Figure 1E**, the band intensity of ^{32}P-labeled His-TIFA increased when TNFα stimulated cell extract was used, relative to that from control cells (lanes 3, 4 in **Figure 1E**). On the other hand, there was no TNFα-dependent increase in the band intensity for the T9A mutant (lanes 6, 7 in **Figure 1E**), indicating that TNFα-increased TIFA phosphorylation most likely occurs at T9. In the control lanes 1, 5, 8, and 9, no ^{32}P-labeled TIFA band was observed when the sample was treated with phosphatase, or when TIFA protein or cell lysates was omitted. Taken together, the results in this section strongly support that the TIFA phosphorylation at Thr9 residue occurs in a TNFα-dependent manner.

2.3 Search for potential kinase

To explore the kinase that mediates the TNFα-dependent T9 phosphorylation, cells were treated with caffeine, a general inhibitor for the PI3K pathway, or kinase inhibitor cocktails

for AKT, IRAK, TAK, and PKC before TNFα treatment. Autoradiography (**Figure 1F**) showed that caffeine, AKT and PKC inhibitors (Go 6976 and Go 6983), but not IRAK or TAK inhibitors, decreased the level of TNFα-induced phosphorylation of His-TIFA wild-type (WT), while none of these inhibitors affected the basal phosphorylation level of T9A. These results suggest the involvement of Ser/Thr kinases in the PI3K-AKT signaling pathway in T9 phosphorylation.

2.4 Interaction of TIFA-FHA and TIFA-pT9

As mentioned in section 2.1, we hypothesize that one of the TIFA N-terminus Thr residues could be phosphorylated and recognized by TIFA-FHA, and it was suggested that TIFA can associate with each other to form homo-oligomers (61). Therefore, we then examined whether the phosphorylated T9 binding to TIFA-FHA is the basis of TIFA-TIFA self-association. Flag-tagged WT TIFA and Myc-tagged TIFA (WT or mutants) were over-expressed in HEK 293T cells. The Myc–tagged WT TIFA was detected in the anti-Flag pull-down (**Figure 2A**, lane 1). To provide further support that TIFA-TIFA association occurs in a phosphorylation-dependent manner, we incubated anti-Flag antibody pulled-down samples with phosphatase and found a reduced interaction between Myc- and Flag-tagged WT TIFA (lane 2). This reduction of interaction, however, can be rescued by EDTA which blocks the phosphatase activity (lane 3). In contrast, the T9A mutant was

marginally detected under the same conditions, with or without phosphatase (lanes 4-6), supporting that T9 phosphorylation is critical for the TIFA self-association.

We next tested whether FHA mutants impair the TIFA-TIFA association. On the basis of sequence alignment of different FHA domains shown in **Figure 2B**, we replaced two of the highly conserved Arg51 and Asn89, and a non-conserved but potentially important Lys88 (due to its charge neighboring to the conserved Asn89), with Ala. As shown in **Figure 2C**, Gal-tagged mutant TIFA could no longer be detected in the anti-Flag immunoprecipitants, indicating that each of the three residues is essential for the TIFA-TIFA interaction. Similar result was observed in previous study using a G50ES66A double mutant (61), although the role of pT9 was not then known.

To further support the results of immuno-precipitation experiment, a direct evidence to demonstrate the binding between the FHA domain and the pT9 residue of TIFA would be valuable. Hence we proceeded to evaluate the binding *in vitro* using isothermal titration calorimetry (ITC). The expressed His-tagged WT TIFA and two FHA mutants were purified by a nickel-column and then analyzed for association with a synthetic pT9-containing peptide spanning residues 1-14 of TIFA. As shown in **Figure 2D** (panel II), ITC showed that the pT9-peptide binds to the unphosphorylated recombinant WT TIFA

with a K_d of 50 ± 1.3 μM (stoichiometry N = 1.04). In contrast, ITC could not detect binding for the corresponding unphosphorylated peptide with WT TIFA (panel I), or binding for the pT9-peptide with mutants R51A and R51AK88A (panels III-IV). These results reinforce the notion that the *TIFA self-association is mediated through binding of pT9 to the FHA domain of TIFA.*

2.5 Expression and purification of recombinant TIFA

For subsequent structural studies and assays, full-length human TIFA cDNA has been cloned into several different expression vectors containing HIS or GST tag(s). Several expression and purification trials (**Table 1** and **2**) have been carried out trying to find the optimal working conditions for recombinant TIFA protein using the *E.coli* system and the Ni-NTA columns. As a result, full-length human TIFA protein turned out to be quite sensitive to salt concentrations (**Figure 3A**), buffer pH, temperatures of purification environment, and centrifugation speed. As shown in **Table 1**, the best expression vector screened is pET43.1 with a C-terminal HIS tag and the expression host cells are BL21 Codon Plus (RIPL). The optimal IPTG induction amount used is 600 μL per liter of cell culture that reached an O.D. of 0.7. After induction, the incubation temperature for the culture would be lowered from 37°C to 16°C to allow more time for the newly translated proteins to fold correctly.

In terms of optimal purification conditions for the full-length TIFA protein (**Table 2**), we found that TIFA would not precipitate in Tris buffer with a pH range of 7.5 to 8.5, and it could only tolerate salts with a concentration range from 200mM to 250mM. TIFA has to be purified and kept at low temperature (4^{o}C) all the time. It would remain stable in both low (0.5mg/mL) to high (16mg/mL) protein concentrations as long as the centrifugation speed during the concentration step did not exceed 3000rpm. The proteins have to be re-suspended frequently to avoid high local concentration at the bottom of the amicon tubes. TIFA protein can easily precipitate when any of the purification conditions mentioned above were not met. Based on the secondary structure prediction (**Figure 3B**), Circular dichroism (CD) analysis (**Figure 3C**), and HSQC TROSY analysis (**Figure 3D**), TIFA contains many loop regions (approximately 66% of the whole protein) at both its core and its two termini. These unstructured regions are probably the causes for protein instability. Although 1-D NMR spectrum (**Figure 3E**) suggested that full-length TIFA WT protein had appropriate folding in phosphate buffer (pH 6.5) as well, tiny signals representing partial degradation were observed in the HSQC TROSY spectrum (**Figure 3D**) of the protein sample with high concentration. Moreover, the peak signals on TIFA HSQC spectrum were not well distributed and scattered. Instead, a lot of peaks were clustered in the middle of the spectrum suggesting that, in agreement with the CD spectrum and secondary structure prediction, the full-length TIFA contained a lot of random coils. We therefore tried to

remove these flexible regions at both termini (**Table 3**) hoping to render the protein stable. However, purification of these truncated TIFA showed no improvement in protein stability (**Figure 3F**). At the end, we decided to proceed with the structural and all other necessary studies using the full-length TIFA (in pET43.1 construct) purified with the optimized conditions mentioned previously.

2.6 Recombinant TIFA exists as intrinsic dimer in solution

As a hallmark of the TRAF family, oligomeric formation appears to be critical for TNFα signaling (4, 26, 54). Since TIFA is able to promote oligomerization of TRAF6 (17), the self-associated TIFA may serve as building blocks for oligomerization. This in turn raises a question whether the quaternary state of TIFA may exist in high-ordered protein architecture. The recombinant TIFA has been reported to exist in trimers (61), even though the vast majority of FHA domains are known to exist as monomers (41). Unexpectedly, results from our experiments using FPLC (**Figure 4A**) or AUC (**Figure 4B**) indicated that unphosphorylated TIFA WT existed as a 46 kD intrinsic dimer which was stable between pH 7.5 and 8.5 (**Table 2**) in a range of protein concentrations (**Figure 4C**). This finding suggests that the TIFA self-association observed in Fig. 2 represents an oligomer formation (dimer associates with dimer) through FHA-pT9 interaction rather than a dimer formation (monomer associates with monomer). To further investigate the dimerization mechanism of

TIFA, we performed FPLC and AUC again to analyze three mutants T9A, R51A, and R51AK88A (RK mutant) (**Table 9**). Since these mutants showed reduced self-association (**Figure 2A & 2C**), they should not remain as stable dimers if the self-association reflected the formation of dimers. As the mutants still exist as dimers in **Figure 4A-B**, the results provide further support that TIFA exists as intrinsic dimers in solution. In addition, the fact that the peptide-protein complex in **Figure 4D** (panel III) remained as dimer suggests that the dimeric interface does not involve the pT-FHA binding sites so that the dimer is not disrupted by the pT9-peptide. Finally, we found that TIFA WT still dissociates into monomers in non-reduced condition (**Figure 4E**), excluding involvement of disulfide bond in the intrinsic dimer. Taken together, our results suggest that unphosphorylated TIFA forms intrinsic dimers in solution, and that the binding between FHA and pT9 of TIFA in vivo likely occurs "intermolecularly" between dimers. This represents a new mechanism for the FHA domain function.

2.7 Crystallization of recombinant TIFA

After obtaining pure and stable TIFA proteins, the next phase of this work would be to determine the structural basis of free TIFA and functionally significant TIFA-pT9 peptide complex and attributing such information to TIFA's biological functions. Since full-length

TIFA appears to be a dimer in solution, its total molecular size impeded us from solving its structure by using NMR. X-ray crystallography was therefore employed.

As mentioned in section 2.5, tremendous efforts were spent on reproducing and optimizing the tricky purification conditions of full-length TIFA protein. Confirmed by MS analysis (**Figure 5A**), batches of native TIFA proteins with concentrations ~15mg/mL and purities greater than 95% were then sent for robotic screenings to find initial crystallization conditions. Also, numerous refinements and additive screenings were carried out manually for the four listed crystallization conditions that grew microcrystals (**Table 4**). As a result, TIFA protein can crystallize using sitting vapor diffusion method at 4^{o}C in buffers containing 0.1M Tris-Base (pH ranging from 8.0 to 9.0), 10% PEG1500, 10% EtOH, and 0.1M ATP disodium salt as an additive. The crystal packing seemed to favor only one dimension, thus the crystals appeared to be thin but long (**Figure 5B**). These "rod" shape crystals were quite small and they diffracted weakly. In order to enlarge the sizes and refine the qualities of the crystals, several crystallization techniques such as macroseeding and microseeding have been applied. Unfortunately, TIFA crystals can only be grown in low temperature. These crystals had to be manipulated in cold room, snap-froze and kept in liquid nitrogen prior to in-house X-ray and synchrotron radiation shootings. To prevent ice formation on the crystals that would normally generate ice rings and affect the data

resolution, skillful looping of crystals and tolerance of low temperature were required. Apart from the temperature disadvantage, our crystallization buffer conditions consisted of ethanol, which is least favoured by crystallographers as EtOH evaporated easily once it was in contact with the air. The crystallization condition could thus be highly variable and hard to be reproduced. Altogether, the complexities of the purification and crystallization conditions make every single crystal acquired costly and precious. Moreover, the precipitant of our crystallization buffer could not protect TIFA crystals from radiation damage during data collection. Therefore, an ideal cryo-protectant had to be applied to the crystals. After trials of different methodologies like oil microbatches and serial dilutions were performed, the best cryo-protectant found for TIFA crystals is 28-32% of PEG1500 (**Table 5**). Up to this point, we managed to grow native crystals that can diffract to 2.3 Å (**Figure 5B** and **Table 8**). Although it is possible to determine the partial structure using the molecular replacement (MR) method, this resolution is not sufficient for us to see the flexible loop regions. On the other hand, less than 50% of our unsolved structure could find models for molecular replacement. Available models are scarce and they all share low sequence homology (**Figure 5C**). Taken together, these drawbacks make the phase problem almost unfeasible to solve by the molecular replacement method. In order to solve the phase problem encountered, multi-wavelength anomalous dispersion (MAD) strategy was applied.

Heavy atom soaking is one approach carried out. Native crystals were soaked with different heavy-atom reagents (**Table 6 and Figure 5D**) hoping to generate anomalous signals. In addition to the heavy atom soaking method, selenomethionine (Se-Met) labeled TIFA protein was expressed, purified (**Figure 5E**), and crystallized (**Table 7**). However, Se-Met labeled crystal appeared to be even smaller and harder to grow than the native protein crystals (**Figure 5B**). In order to collect high quality X-ray diffraction data for these small crystals, only the synchrotron radiation equipped with fluorescence scans in multiple wavelengths as well as an intense X-ray source could satisfy the need. Synchrotron beamlines with distinguishing features such as high photon flux and narrow beam size were also helpful to needle/rod-shaped TIFA crystals. Since the advance collecting mode allowed the beam to move gradually along the long axis of the targeted crystal during data collection (**Figure 5F**), the X-ray exposed regions could be changed and the radiation damage of the whole crystal could be minimized.

To date, several data sets with acceptable qualities have been collected at SPring-8 beamline 44XU in Japan or NSRRC beamline 13B1 in Hsin-Chu. The best resolution obtained for the Se-Met labeled crystal so far is 3.0 Å (**Table 8**). However, the phase problem has not yet been solved and only ambiguous models for the core regions of TIFA could be calculated. In short, correct phase plus data sets with higher resolutions and, more

importantly, better qualities are what we're trying to achieve before the structural details of TIFA can be unraveled and a clear and defined model can be computed.

2.8 Oligomerization status of native TIFA

To provide further support that pT9-FHA binding does promote TIFA oligomerization, we next evaluated the molecular weight of native TIFA proteins using non-denaturing gels. We examined over-expressed Myc-tagged or Flag-tagged TIFA and mutants from mammalian HEK 293T cells and found that native T9A and RKN mutants of TIFA protein migrated faster than the WT protein during electrophoresis, suggesting that the mutations repressed the formation of oligomeric TIFA (**Figure 6A**). We also performed *in vitro* kinase assay and analyzed the native samples. As a result, the recombinant His-TIFA WT protein that had been phosphorylated by TNFα-treated cell lysates up-shifted to a larger molecular weight whereas the PBS-treated control WT and both T9A samples remained in lower molecular weight (**Figure 6B**), suggesting that TNFα-induced TIFA Thr9 phosphorylation is important to TIFA oligomer formation.

Next, we employed immunostaining to study the role of FHA-pT9 binding in TIFA oligomerization in cells. U2OS cells were transfected with Gal-tagged WT TIFA or its various mutants. Out of our expectation, there was a particularly significant result from the

IFA study. As shown in the top panel of **Figure 6C** (column I, row 1), a number of discrete punctate spots recognized by anti-Gal (indicated by white arrows) were found in the peri-nuclear region of the cytoplasm of U2OS cells (representing possible protein aggregates or oligomers) transfected with WT Gal-TIFA. In parallel experiments in which cells were transfected with T9A or FHA domain mutants (columns II-V, row 1), no aggregates of Gal-TIFA were observed.

This unreported aggregation/oligomerization formation of exogenously expressed TIFA WT proteins behave similarly to what have been observed for members involved in the same inflammatory signaling pathway, including TRAF6, IRAK, sequestosome 1/p62, etc. (20, 56, 57, 66, 67, 76). Studies have demonstrated that these punctuate spots were the sites where ubiquitinated TRAF6 co-localized with IRAK, sequestosome, and proteasome (20, 56, 57, 66, 67, 76). Accordingly, we extrapolated that the speckles observed in cells exogenously expressing TIFA could be part of the whole protein complex. Indeed, the confocal section (**Figure 6D**) showed that, when TIFA WT and Flag-tagged TRAF6 were co-expressed, most of the punctuate spots of TIFA (column I) co-localized with that of TRAF6 (column II) in the cytoplasm of the cells (indicated by white arrows) (column IV). These findings suggest that intermolecular FHA-pT9 interactions between TIFA dimers are crucial for TIFA/ TRAF6 oligomerization.

2.9 TIFA-mediated activation of NF-κB

Previous reports showed that over-expression of exogenous TIFA can activate NF-κB without the stimulation of TNFα (17). It was also demonstrated that the oligomeric forms of TIFA can activate IKK (17), and that interaction of TIFA with TRAF6 is indispensable for NF-κB activation (61). In order to validate previous findings, we first measured and compared the activation levels of NF-κB for endogenous and exogenous TIFA with and without TNFα treatment using a luciferase-based reporter assay (**Figure 7A**). The result indicated that NF-kB can be highly activated in the absence and presence of TNFα in HEK 293T cells over-expressing exogenous TIFA. However, for the endogenous case, NF-κB can only be activated upon TNFα stimulation.

Given that TIFA-TIFA interaction occurs *via* pT9-FHA binding between TIFA dimers leading to oligomerization, we subsequently tested whether the pT9-FHA interaction is necessary for NF-κB activation. HEK 293T cells were transfected with the NF-κB luciferase reporter together with expressing plasmids encoding the wild-type TIFA or its various mutants. As shown in **Figure 7B**, the NF-κB-driven luciferase activity was much lower in cells co-transfected with the unphosphorylatable T9A or the FHA domain mutant R51AK88AN89A (RKN) when compared with that of WT TIFA. In line with previous observation (61), the NF-κB activity mediated by E178A mutant was also drastically

decreased, which supports that TRAF6 binds to TIFA via E178. Considering that a remarkable feature of NF-κB activation is its translocation into the nucleus, we then monitored the subcellular localization of endogenous NF-κB affected by exogenously expressed TIFA. In agreement with the reporter assay, Gal-tagged WT TIFA in U2OS cells did promote the nuclear translocation of NF-κB (**Figure 6C**, column I, row 2). Such a nuclear translocation of NF-κB was not observed when T9A, R51A, K88A, or R51AK88A was transfected (**Figure 6C**, columns II-V, row 2). Altogether, our results suggest that FHA-pT9 binding is required for TIFA-mediated activation of NF-κB.

2.10 Extracellular stimulation augments TIFA protein amount

The above results provide mechanistic insight for the effect of exogenously expressed TIFA in leading to NF-κB activation. These results, along with previous reports, suggest that the functional role of TIFA is broad based. Our work has mainly focused on the role of pT9-FHA binding in NF-κB activation, and it is beyond the scope of this work to further examine the effect of pT9-FHA interaction on every network that mediates NF-κB activation. However, based on what we had observed, we speculated that a concentration-dependent phenomenon may be involved in NF-κB signaling since the presence of large amount of exogenous TIFA, TRAF2, or TRAF6 is sufficient to activate NF-κB without the stimulation of cytokines. To test this hypothesis, we used the

monoclonal anti-TIFA antibody to monitor the endogenous TIFA protein amount after various stimulations. As shown in **Figure 7C**, the amount of endogenous TIFA protein increased in the first 15 minutes upon treatment with TNFα, interleukin-1β (IL-1β), and lipopolysaccharide (LPS). The protein amounts kept increasing until 12 hours, while no change in the TIFA amount was observed in the control set with PBS treatment. In parallel, the levels of phospho-IκB (pS32/pS36) and NF-κB also increased (second and third rows of **Figure. 7C**). The results therefore indicated that external inflammatory stimulations affect the cellular levels of TIFA proteins.

Since NF-κB plays important roles in transactivation of a panel of genes (23), it is necessary to find out if the promoted TIFA amount a consequence of transcriptional activity up-regulated by NF-κB. The transcriptional level of TIFA under the same stimulatory condition was accessed through semi-quantitative RT-PCR. Briefly, total RNA of the cells treated by TNFα in the same time scales was extracted, and cDNA was synthesized in the presence of oligo (dT) and reverse transcriptase. PCR reactions were then carried out using the synthesized cDNA as templates. As presented in **Figure 7D**, the mRNA levels of endogenous TIFA did not change between the PBS control group and the TNFα-treated sample group, no matter in low or high amplification cycle numbers. This result indicated

that the change in endogenous TIFA protein amount upon TNFα treatment was mainly due to post-translational modification, instead of up-regulation of transcription of *tifa* gene.

2.11 Silencing of endogenous TIFA

In order to establish the significance of TIFA protein in NF-κB signaling *in vivo*, small interfering RNA (siRNA) was used to silence the endogenous TIFA in HEK 293T cells, which was down to approximately 20% of the original level (**Figure 7E**). Reporter assay and Western blot analysis were performed again to examine NF-κB activation while endogenous TIFA was silenced in HEK 293T cells. When compared with those in positive controls using non-transfected cells or cells transfected with scramble RNA, the TNFα-induced activation of NF-κB (**Figure 7F** upper bar graph) or elevation level of phosphorylated IκB and total NF-κB proteins (**Figure 7F** lower bar graphs) were reduced to a level similar to the PBS control for the TIFA-silenced group. Similar attenuation of TNFα-mediated signaling was also observed when endogenous TIFA was silenced in the human acute monocytic leukemia cell line, THP-1 (**Figure 7G**). These findings altogether demonstrate that TIFA is necessary, and the FHA-pT9-induced TIFA oligomerization is important, for TNFα-mediated NF-κB activation.

2.12 Interaction of TIFA and TRAF2

From previous studies carried out by Kanamori *et al.*, TIFA was shown to bind to TRAF2 in mammalian-two-hybrid (MTH) assay and co-immunoprecipitation (Co-IP) experiments. They have also tried to narrow down the interaction regions by constructing truncated TIFA and TRAF2 in different lengths. As a result, they concluded that TIFA-TRAF2 interaction requires the TRAF domain of TRAF2 and almost the entire TIFA (FHA domain plus C terminus). However, the exact binding sites for TIFA-TRAF2 interaction have not been mapped and the biological significance of such interaction has yet been established. Thus, as a side project, we also tried to study the involvement of TIFA in TRAF2 signaling regulation. First of all, we confirmed TIFA-TRAF2 interaction *in vivo* by performing Co-IP experiment (**Figure 8A**) as well as immunofluorescence assay (IFA) (**Figure 8B**). For Co-IP experiment, Flag-tagged TIFA and TRAF2 were over-expressed in HEK 293T cells. TRAF2 protein was detected in the anti-Flag pull-down (**Figure 8A**). The overlapping of red and green fluorescence intensity signals shown in the confocal section (**Figure 8B**) also suggested co-localization of Flag-TIFA and TRAF2 proteins in the cytoplasm of HEK 293T cells. Once again, in line with **Figure 6C** and **6D**, red punctate spots representing possible aggregation/oligomerization of exogenous TIFA were observed in the cytoplasm.

To map site(s) on TRAF2 that are important for TIFA-TRAF2 association, sequence of TRAF2 TRAF domain was aligned with human NIFK protein (**Figure 8C**). Four residues

on TRAF2 were rendered to Ala, Asp, Glu, Cys individually or in combinations using site-directed mutagenesis (**Table 10**). Among the four residues chosen, Thr349 and Ser 378 aligned with two phosphorylated threonine (Thr234 and Thr238) residues on hNIFK that are important for Ki67-NIFK interaction. MTH assays were subsequently carried out by over-expressing GAL4-TIFA (bait) and VP16-TRAF2 (prey) fusion constructs with a luciferase reporter plasmid in HEK 293T cells. Luciferase signals would be detected when GAL4 DNA binding domain of the bait protein interacted with the VP16 activation domain of the prey protein. According to the results of the MTH assay (**Figure 8D**), interaction between GAL4-TIFA WT and VP16-TRAF2 T349AS378A mutant were severely impaired, indicating that these two residues are crucial to TIFA-TRAF2 interaction.

Next, we tried to identify the phosphorylation status of exogenous Flag-TRAF2 protein immunoprecipitated from mammalian cells that were treated with TNFα. The mass analysis revealed thirteen phosphorylation sites including T7, S11, S102, S123, S160, S162, T188, T226, S274, S318, S327, T401 and S408 on TRAF2 (**Figure 8E**). Phosphorylation on S11 of TRAF2 was later on suggested to be essential for TNFα-induced secondary and prolonged IKK activation by another research group (5). No phospho-modifications, however, were observed on T349 and S378 so far.

Since partial structure of TRAF2 was solved by X-ray crystallography already, we have also looked at the locations of T349 and S378 on the structure. Prior to that, we have examined the size of exogenous full-length TRAF2 protein immunoprecipitated from HEK 293T cells using AUC. It turned out to be a dimer in solution (**Figure 8F**). Interestingly, the solved TRAF domain of TRAF2 appeared to be a trimer in crystal. The overall structure of the trimeric TRAF2 TRAF domain looks like a flower bouquet with TNF receptor binding sites on the edge of the flower pedals (top) and T349 and S378 on the top of the stem (in between α-helix and the core of TRAF domain) (**Figure 8G**).

In summary, T349 and S378 are two sites on TRAF2 that seemed to be important for TIFA-TRAF2 interaction. Nevertheless, further studies are required to validate whether these two sites interact with TIFA in a TNFα- and phosphorylation-dependent manner. Mechanisms regarding the regulation of such interaction will be investigated as well in the near future.

Chapter 3. DISCUSSION AND CONCLUDING REMARKS

In this study, we first identified phosphorylation of TIFA at Thr9 and demonstrated its up-regulation upon TNFα treatment. We next showed that TIFA-FHA binds directly to this pT9 site and this binding drives TIFA self-association and promotes NF-κB activation. Importantly, we found that recombinant TIFA protein exists as a dimer and the pT9-FHA binding likely occurs between individual TIFA dimers, by which the oligomerization of TIFA is promoted. We subsequently showed that speckles formed by oligomerized TIFA co-localizes with TRAF6 *in vivo*. Finally we demonstrated that the protein level, but not the mRNA of *TIFA* gene is up-regulated by TNFα stimulation. In parallel, we also validated TIFA-TRAF2 interaction *in vivo* and mapped T349 and S378 residues on TRAF2 to be important for such interaction. The regulation mechanism and functional consequences of such interaction, however, will be investigated in future studies.

On the basis of the results presented here, we proposed a working model for the function of TIFA as shown in **Figure 9**. In this model, external stimulation by TNFα (possibly also IL-1β and LPS) activates a kinase (yet to be identified but may be a serine/threonine kinase involved in the PI3K-AKT pathway) that phosphorylates Thr9 of TIFA. Phosphorylation of TIFA T9 residue then triggers binding by TIFA FHA domain, which occurs between dimers (AA, BB, CC…) in the fashion of AA-BB-CC-…, leading to oligomerization of

TIFA. Since TRAF6 is constitutively bound with E178 residue at the c-terminus of TIFA, the oligomerization of TIFA consequently induces TRAF6 oligomerization which in turn enhances the E3 ligase activity of the RING domain of TRAF6 and activates the downstream signaling (17). Thus, this newly defined mechanism has important translational implications, particularly inflammatory responses in mammalian cells.

Using MS, NanoPro immunoassay, and *in vitro* kinase assay, we confirmed the T9 phosphorylation and semi-quantified its changes responding to TNFα stimulation. These assays also showed that, in addition to T9, there are other basal phosphorylations for both exogenous and endogenous TIFA (trace 1 in **Figure 1C-D**). However, it is not clear whether these basal phosphorylations are specific. It remains to be established the exact kinases responsible for the TNFα-induced phosphorylation of T9 and the basal phosphorylation of TIFA. Furthermore, because the pT9-FHA binding plays a pivotal role not only in mediating TIFA self-association/oligomerization but also in provoking TRAF6 oligomerization/NF-κB activation, antagonizing such a putative kinase may intervene with the TNFα-related inflammation.

Considering the activation of an unknown kinase which phosphorylates TIFA T9 residue upon stimulation as an “on” switch of the signal cascade, it is rational to hypothesize the

existence of another unknown regulatory mechanism that terminates the transduction. Among the several phosphatases involved in the inflammatory signaling pathways, protein phosphatase 4 (PP4) has been suggested to directly interact with the TRAF domain of TRAF6 in a LPS-dependent manner. PP4 has also been shown to exert a negative role on LPS-induced and TRAF6-mediated NF-κB activation by suppressing the ubiquitination of TRAF6 (10). Altogether, these results have made PP4 one potential candidate as the "off" switch of the signal transductions initiated by cytokines/LPS (**Sup. Figure 8**). To test this hypothesis, the first future experiment to carry out will be to confirm if PP4 interacts with TIFA upon stimulations and to examine the time kinetics of such interaction.

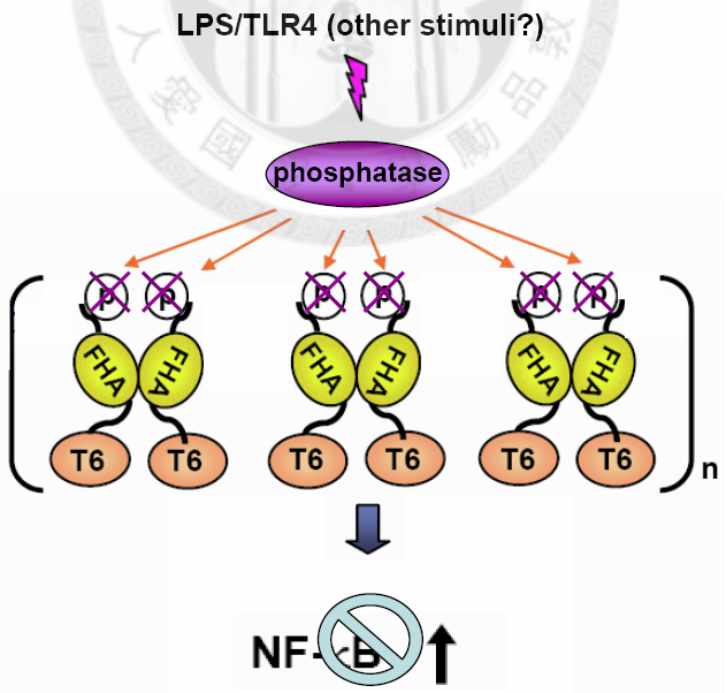

Supplementary Figure 8. An unknown phosphatase may serve as the "off" switch of the signal cascade by removing the phosphorylation on T9 to impair the oligomerization of TIFA, hence the oligomerization of TRAF6 and the subsequent activation of NF-κB.

As mentioned in the introduction section, the mechanisms of FHA domain function appear to be highly diversified (41). Up to date, three major mechanisms have been characterized and they are summarized here once again: a) *a monomer of the FHA domain binds the pT residue(s) of a different monomer of its biological ligand intermolecularly* (7), b) *a monomer of FHA domain binds with the pT residue of another monomer of the same FHA protein intermolecularly to enhance homo-dimerization* (9, 31, 72), and c) *intramolecular binding between a FHA domain and a pT site within the same protein molecule* (3). Since the model for the aggregation of TIFA does not represent any of the above mechanisms, we therefore propose that a new mechanism for FHA domain functions is uncovered - the unphosphorylated FHA domain-containing protein exists as *an intrinsic dimer that oligomerizes via the intermolecular FHA-pT bindings between dimers*. Interestingly, the FHA domain of both human and mouse Mediator of DNA Damage Checkpoint 1 (MDC1) protein was recently shown to exist as an intrinsic dimer in solution and in crystals (27, 37, 70).

The study of Takatsuna *et al.* (61) has established the key function of TIFA-TRAF6 interaction (61), which has been fully supported by our results in **Figure 6D** and **Figure**

7B. However, one relatively minor point in their report is inconsistent with one finding in our work. In their study, GST-tagged N-truncated TIFA protein was able to pull-down Flag-tagged wild-type TIFA and promote NF-κB activation, whereas our T9A mutant was not capable of either. Such discrepancy for the requirement of N-terminus portion of TIFA (a.a. 1-46) in TIFA functions may be due to the functional delineation by domain deletion or by site-specific residue substitution. Despite the minor discrepancy mentioned, one interesting and consistent observation was perceived throughout our study. Unlike TIFA T14A and T19A with which the single mutations have disturbed the expression yield or stability of the protein, TIFA amount seemed to be boosted when Thr12 was mutated to alanine. Coincide with the enhanced interaction between TIFA WT and TIFA T12A mutant, the level of NF-κB activation was relatively unaffected when over-expressing T12A in cells (**Sup. Figure 9**). These preliminary data have suggested that Thr12 may play a negative role in regulating TIFA oligomerization. Since TIFAB has been demonstrated as a TIFA interacting protein (45) as well as a negative regulator of TIFA-mediated NF-κB activation (44), we would like to find out if TIFAB has anything to do with Thr12. Interestingly, the phosphorylated interacting partner of the FHA domain of TIFAB hasn't been identified. In addition, TIFAB is short of the first 8 amino acids at its N-terminus when compared to TIFA and it contains neither the corresponding Thr9 nor Thr12 (**Sup. Figure 7**). Thus, we will first try to see if TIFA Thr12 is phosphorylated under

non-stimulated condition. If so, we will next determine if TIFA-TIFAB interaction is phosphorylation- and FHA domain-dependent. If not, then it is still worth the effort to map the TIFA-TIFAB interaction region on both proteins and to investigate the regulatory mechanism of TIFAB on TIFA-mediated oligomerization using structural studies.

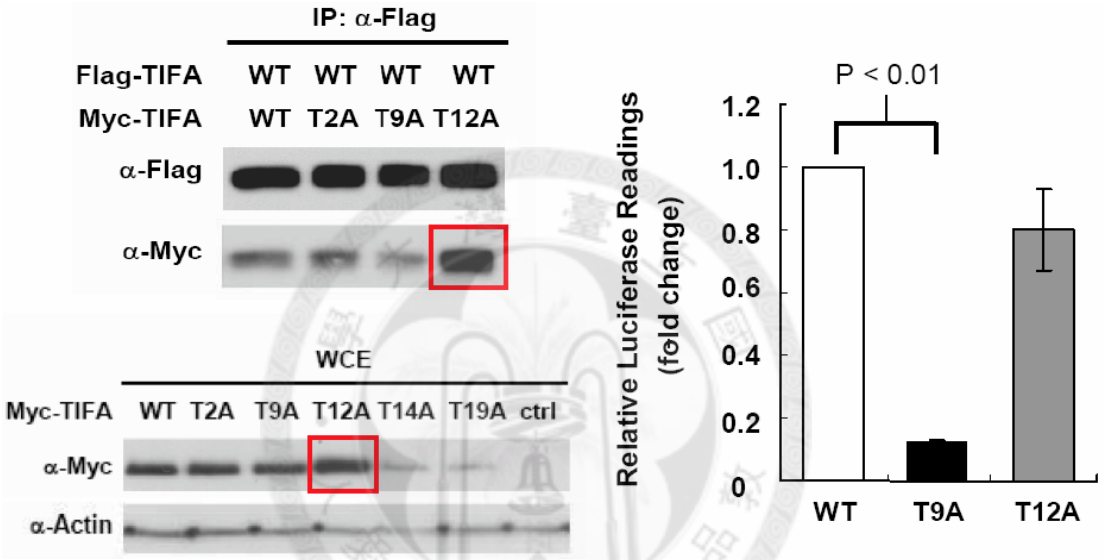

Supplementary Figure 9. Left: TIFA T12A expression and its association with other TIFA seemed to be enhanced. **Right:** Mutating Thr12 into alanine did not impair the TIFA-mediated NF-κB activation.

On the other hand, how TNFα stimulation directs TIFA protein amount is also a worthy topic for further study. Since the transcriptional level of TIFA was not elevated after TNFα stimulation, one possible process triggering the augmentation of TIFA amount could be prevention of degradation, which could possibly be correlated with the phosphorylation-induced oligomerization of TIFA. Understanding the detailed mechanism of these processes can be a key to decipher the dominant positive nature involved in most

of the TRAF members (26, 67). Given the existence of basal-level phosphorylation, it will also be interesting to see whether such stimulation-independent phosphorylation of TIFA correlates with the homeostasis of the total TIFA pool in cells.

Furthermore, in view of the fact that TIFA seems to play a critical role in the master signaling pathway of NF-κB activation, whether the *tifa* gene is essential for inflammatory response elicitation and/or other diseases is a crucial issue. So far, the involvement of TIFA in diseases can be linked to several types of cancers, such as leukemia (68), pancreatic cancer (64), and breast cancer (data not shown), in which TRAF6, TRAF2, and TIFA are screened to be highly expressed, respectively. On the other hand, three cases of an autosomal recessive TIFA mutation in human patients have been reported. Preliminary data has shown that this deficiency in TIFA may compromise the immune system so the patients developed chronic sinusitis, and are prone to invasive bacterial infection and pneumonia (data not shown). Future effort therefore will be spent on examining the molecular mechanism behind this TIFA deficiency using the EBV-B cells obtained from the patient. A mouse model with *tifa* being knocked-out will also be generated to study the relevant clinical consequences in more depth.

Finally, detailed atomic structures of free full-length TIFA dimer or full-length TIFA complexed with a pT9-peptide, when available, will be very valuable to interpret molecular mechanisms of the signaling pathway. Once the structure of free full-length TIFA is solved, we are aiming to mutate the residues responsible for dimerization formation. So far, one possible scenario to explain why TIFA forms unique intrinsic dimers in solution is that this dimer formation not only speeds up the oligomerization process, but also serves as a platform for interactions with much larger binding partners such as TRAF2 and TRAF6. It will thus be interesting to see what functional consequences will result from the disruption of TIFA dimer. Moreover, before we identify the responsible kinase of pT9, we're also working on generating a full-length pT9-containing recombinant TIFA *in vitro* using the native peptide ligation method (31). In order to do so, a relatively stable N-truncated TIFA will need to be constructed prior to the ligation. We also need to make sure that Cys15 residue does not form intramolecular disulfide bond with other cysteine residues in TIFA before we can conjugate the pT9-containing peptide onto it. If we ever manage to succeed in obtaining phosphorylated recombinant TIFA, our next move will be to reconstitute TIFA oligomerization *in vitro* and hopefully to solve the structure of full-length TIFA in complex with phosphorylated full-length TIFA. This will be a much more challenging task than complexes of small phosphopeptide, but the information generated will definitely be of great help in terms of understanding the molecular basis of the function of TIFA. Most

importantly, it will provide us chances to design regulatory compounds against NF-κB activation and properly manage inflammatory response, autoimmune diseases, viral infection, and cancer development.

Overall, our work herein, along with previous reports, has provided a mechanistic insight for TIFA oligomerization and the critical role of TIFA in NF-κB activation. The TIFA pT9-directed oligomerization of molecules involved in TNFα-mediated inflammatory responses may have a broad impact in understanding the mammalian immunity. Further studies will be required to address the specific roles of TIFA in the entire network, or family of networks, between external stimulation and NF-κB activation. Nevertheless, our results have provided a basis for future studies into these significant issues.

Chapter 4. MATERIAL AND METHODS

Cell culture. The human embryonic kidney (HEK) 293T cell line and human osteosarcoma cell line U2OS were cultured in Dulbecco's modified Eagle medium (DMEM) (Gibco). The human acute monocytic leukemia cell line THP-1 was cultured in Roswell Park Memorial Institute medium (RPMI-1640) (Gibco). All media were supplemented with 10% heat-inactivated fetal bovine serum (FBS) (Gibco), 200 mM L-glutamine (Gibco), 100U/mL penicillin (Gibco), 100 μg/mL streptomycin (Gibco), and 1% sodium pyruvate (Gibco). Cells were kept in 37 ^{o}C incubator with 5% CO_2. Cells were starved by replacing the complete media with serum-free DMEM 8 to 10 h prior to the addition of 50 ng/mL of TNFα at indicated time points.

TIFA and TRAF2 plasmids. All the plasmids involved in this study, including: Flag-tagged pCMV-Tag2a (Stratagene), pcDNA3.1-Myc (EQKLISEEDL) (Invitrogen), pNF-κB-Luc (Clontech), His-tagged pET43.1a (Novagen), His-tagged pET28a (Novagen), His-tagged pET-Duet (Novagen), GST-tagged pGEX-4 (Promega), Gal-tagged pBIND (Promega), VP16-pACT (Promega), pBIND-Id (Promega), pACT-MyoD (Promega) and pG5luc (Promega) were obtained from commercial sources.

Antibodies. The anti-TIFA monoclonal antibody (mAb) was produced by the core facility at IBC, Academia Sinica. Other mAbs used in the current study are: anti-Flag (Sigma), anti-Myc (Millipore), anti-Gal (Abcam), anti-β-actin (GeneTex), anti-His (Signal Chem), anti-pIKKα (pT23) (Abcam), anti-pIκB (pS32/pS36) (Santa Cruz) and anti-NF-κB p65 (Millipore). The polyclonal antibodies used in this work are: anti-NF-κB p65 (Santa Cruz), HRP-conjugated anti-mouse IgG (Millipore), FITC-conjugated anti-mouse IgG (Millipore), and rhodamine-conjugated anti-rabbit IgG (Millipore).

Site-directed Mutagenesis. Point mutations in TIFA and TRAF2 cDNA sequences were introduced by PCR-based, site-directed mutagenesis (QuickChange™ mutagenesis kit, Stratagene) according to standard procedures. The original amino acids were switched to desired ones using PfuTurbo™ DNA polymerase (Invitrogen) and the mutant oligonucleotide primers. A *Dpn I* endonuclease (NEB) specific for methylated and hemimethylated DNA was applied to select for mutation-containing synthesized DNA as it can only digest the parental DNA template. All mutants were verified by DNA sequencing.

NanoPro™ immunoassay. The method involves separation of cell lysates in the capillary isoelectric focusing step, followed by analysis of specific protein isoforms (i.e., different phosphorylation forms of TIFA) using conventional immune-detection (50). Cells were

collected and centrifuged at 1.0 krpm for 5 min. The cell pellet was then re-suspended in 250 μL Bicine/CHAPS lysis buffer plus 1X DMSO inhibitor mix™ and 1X aqueous inhibitor mix™. The cell lysates were cleared by centrifugation at 13.2 krpm for 1 h at 4 °C. When indicated, 5 mg total cell lysate was incubated with alkaline phosphatase (Fermentas) together with 10X reaction buffer and incubated at 37 °C for 1 h. Final supernatants were transferred to a fresh tube and snap-frozen with liquid nitrogen. Nanofluidic proteomic immunoassay was performed with NanoPro-1000 system. Cell lysate was diluted to 2X of final protein concentration in Bicine/CHAPS buffer in the presence of DMSO inhibitor mix™ and 20 mM DTT. Diluted Cell lysate was combined with an equal volume of IEF™ buffer solution (50% v/v pH 3-10 Pre-mix solution, 50% v/v Servalyte pH 3-6), 1 μM pI standard 4.4, and 1 μM pI standard 5.5. The charge-based separation was performed in a capillary at 45,000 μW for 40 min and immobilized by 80 sec irradiation with UV light. After separation and immobilization, the sample was incubated with primary antibody for 120 min. Each over-expressed sample was then incubated with HRP-conjugated goat-anti-mouse IgG for 1 h. Endogenous sample was detected by biotin-labeled goat-anti-rabbit IgG for 1 h followed by 10 min incubation with SA-HRP-conjugated antibody. Chemiluminescence signal for the target proteins was detected by adding Luminol and Peroxide XDR detection reagents and analyzed by the Compass software.

***In vitro* kinase assay.** After washing with PBS, TNFα-stimulated or non-stimulated 293T cells were lysed with CHAPS lysis buffer. The cell lysates were pre-cleaned with sheep anti-mouse IgG M-280 dynabeads^{TM} (Invitrogen) at 25 °C for 30 min then incubated with the recombinant His-tagged TIFA WT or T9 mutant in a buffer containing 40 mM HEPES, pH 7.5 and 20 mM $MgCl_2$), 100 μM ATP and γ-^{32}P ATP (1 mCi/mL) (Perkin Elmer) at 37 °C for 30 min. His-TIFA was pulled-down with M-280 dynabeads^{TM} coated with anti-His mAb. The reaction was terminated by addition of SDS sample buffer and heating at 95 °C for 10 min prior to SDS-PAGE.

Co-immunoprecipitation analysis. The protein coding sequences of TIFA cDNA were sub-cloned into the expression vector pCMV-Flag or pcDNA3.1-Myc. HEK 293T cells (~2 x 10^7) were co-transfected with 3 μg of the expression vectors containing Flag-TIFA and Myc-TIFA using JetPEI^{TM} (Polyplus transfection). After 36 h, cells were lysed with TNE buffer containing 10 mM of Tris-HCl (pH 7.8), 1% NP-40, 0.15 M NaCl, 1 mM EDTA, 1 mM PMSF and 1X protease inhibitor cocktail. An amount of 6.5 μg of anti-Flag mAb was pre-coated with M-280 dynabeads^{TM} overnight at 4 ^{o}C. The cell lysates were incubated with anti-Flag-dynabeads^{TM} at 4 ^{o}C overnight. The protein-beads complex was then washed with TNE buffer and 1X TBST buffer. The immunoprecipitants were then eluted using 50 μg of the 3X Flag peptide (Sigma) and subjected to Western blot analysis.

Western blotting. For Western blotting, cell lysates were separated by 15% SDS-PAGE and transferred onto PVDF membrane (Perkin Elmer). The membranes were then blotted with primary antibody at 4 ^{o}C overnight followed by HRP-conjugated anti-mouse IgG. The blotted protein bands were revealed by the ECL system (Millipore).

Mammalian-two-hybrid (MTH) assay. TIFA and TRAF2 cDNA were cloned into GAL4 DNA binding domain-containing vector (pBIND) and VP16 activation domain-containing vector (pACT). 3 μg of these two plasmids were then transfected together with 3 μg of reporter plasmid pG5luc (Promega) into 70% confluent HEK 293T cells seeded in 6-well plates. After 48 hours of incubation, the luciferase reporter activity was measured with the Dual-Luciferase Reporter Assay System (Promega).

Native PAGE experiment. For native PAGE experiment, cells were lysed using the NativePAGE^{TM} (Invitrogen) sample buffer in the presence of 10% DDM and 5% Digitonin. After centrifugation at 4 ^{o}C for 1 h, the whole cell lysates were separated by gradient PAGE (4-16%). A buffer containing 0.5 M Tris-Base, pH 9.2, and 0.5 M glycine was used for protein transfer. After transfer, PVDF membrane was incubated in 20 mL of 7.5% acetic acid for 15 min at room temperature to fix the proteins. The membrane was subsequently rinsed with methanol and deionized water to remove the residual Coomassie

G-250 dye. Finally, TIFA proteins were detected by Western blot analysis using mouse-α-Flag Ab or mouse-α-Myc Ab.

NF-κB activation assay. 293T cells in 6-well plates were transiently transfected with 1.5 μg of the TIFA WT or mutant expression plasmids together with 1.5 μg of the pNF-κB-Luc reporter. After 36 h, cells were lysed with 1X Passive Lysis Buffer (Promega) and 20 μL of cell lysates were dispensed into the 96-well plate followed by addition of 100 μL of Lyophilized Luciferase Assay Substrate (LARII) (Promega) and 100 μL of Stop & Glo Reagent (Promega). The luciferase activity was measured as relative luminescence unit (RLU). When indicated, Western blot analysis for the total cell lysate was carried out in parallel in order to justify the expression levels of each sample. The firefly luciferase readings were then normalized to the internal renilla luciferase readings as well as the corresponding band intensities of the samples.

Immunofluorescence assay (IFA). An amount of 7 x 10^5 U2OS cells seeded on coverslips were transfected with 3 μg of TIFA or mutants vectors. Thirty-six hours post transfection, cells were washed with cold PBS and fixed with 4% paraformaldehyde (Electron Microscopy Sciences) for 30 min. Cells were permeabilized with 0.2% Triton X-100 and blocked with PBS containing 10% BSA, then incubated with primary antibodies,

fluorescence-labeled secondary antibodies, and DAPI sequentially. The fluorescence image sections were taken by Zeiss LSM 510 confocal microscopy.

RNA extraction, cDNA synthesis, and RT-PCR. Total cell contents from HEK293T cells were collected and re-suspended in 200 μL PBS after TNFα treatment. Isolation of total RNA was then performed using High Pure RNA Isolation Kit (Roche) according to manufacturer's instructions. First strand cDNA was prepared with SuperScript™ II reverse transcriptase (Invitrogen) and oligo-dT(20) primer as suggested by manufacturer's guidelines. 5 μg of total cDNA was then subjected to specific amplification by PCR with Taq DNA polymerase (New England Biolabs). Endogenous TIFA cDNA was amplified with primers TIFA-RT-f (5'-AAC AGC TGA AGA GAG TTC ACT GAC TCC C-3') and TIFA-RT-r (5'-GTG TCT ATA CAG CAT CTA CAG AGC TCT TCA TCC-3') using the following protocol: 95 °C / 5 min, 32 or 40 cycles of [95 °C / 45 sec – 58 °C / 35 sec – 72 °C / 60 s], and 72 °C / 10 min. GAPDH cDNA was amplified with primers GAPDH-RT-f (5'-GCC AAA AGG GTC ATC ATC TC-3') and GAPDH-RT-r (5'-GGC CAT CCA CAG TCT TCT-3') using the following protocol: 95 °C / 5 min, 25 or 33 cycles of [95 °C / 45 sec – 55 °C / 10 sec – 72 °C / 30 s], and 72 °C / 10 min. Amplified cDNA products were then separated by agarose electrophoresis, revealed by EtBr staining, and subjected to analysis.

RNA interference. 200pmol of double-stranded siRNA oligomers (Invitrogen) corresponding to the sequence of TIFA (UCAGGACAAACAGGUUUCCCGAGUU) or scramble control oligomers (Invitrogen) were transfected into HEK 293T or THP-1 cells. Cells were collected after 72 hours of incubation.

Recombinant TIFA purification. Various human TIFA WT and mutants were expressed as His fusion proteins in *Escherichia coli* BL21 Codon Plus and affinity purified with nickel resin (Millipore). Approximately 30 mg of purified recombinant His-TIFA were applied to a HiLoad 16/60 Superdex 75 pg column or a Superdex 75 10/300 GL column (GE Healthcare). The separated fractions were analyzed on 15% SDS-PAGE and proteins were visualized by Coomassie Brilliant Blue Staining. Protein concentration was measured using Bradford dye (BioRad). Standard molecular weight marker proteins were analyzed under the column conditions described above.

Protein crystallization. The purified native and selenium-labeled TIFA proteins were crystallized at 4^{o}C from a solution containing 0.1M Tris-Base, pH 8.0 to 9.0, 10% PEG1500, 10% EtOH, and additives 0.1M ATP disodium salt or 3.0M NDSB-195 using the sitting vapour diffusion method. The crystals belong to space group p321 with cell dimensions of a=41.21 Å, b=41.21 Å, c=178.91 Å and $\alpha=90^{o}$, $\beta=90^{o}$, $\gamma=120^{o}$.

Circular dichroism (CD) spectroscopy. CD spectra were collected in 50 mM sodium phosphate (pH 8.0), 200 mM NaCl using a Jasco J-815 spectropolarimeter (Jasco, Tokyo, Japan) with 1-mm path length. Experiments were performed at 25 °C and maintained by circulating water baths. The spectra were collected in the range of 190 to 240 nm and corrected for the buffer background. The data was calculated/fitted using CDSSTR method (variable selection method: reference set 7).

1-D NMR and HSQC TROSY experiment. 1-D NMR and HSQC experiments were carried out on Bruker UltraShield Plus (600 MHz/ 54 mm Plus) equipped with 5mm Z gradient TXI ($^{1}H/^{13}C/^{15}N$) CryoProbe at Genomic Research Center, Academia Sinica. ^{15}N-^{1}H heteronuclear single quantum correlation (HSQC) spectra were recorded by using ^{15}N-labeled recombinant TIFA protein samples dissolved in 50 mM sodium phosphate (pH 6.5), 200 mM NaCl and 5% D_2O.

Mass (MS) spectrometry. The phosphorylation sites were analyzed using high resolution and high mass accuracy nanoflow LC-MS/MS on an LTQ-FT (Linear quadrupole ion trap-Fourier transform ion cyclotron resonance) mass spectrometer (Thermo Fisher Scientific) with procedures described previously (19).

Isothermal titration calorimetry (ITC) analysis. ITC experiments were performed using a MicroCal iTC200 instrument (Northampton, US). Two TIFA N-terminal peptides, i.e., MTSFEDADTEETVT or MTSFEDAD(pT)EETVT (2 mM), were used to titrate TIFA protein (100 μM) at 25 °C in the calorimeter cell (0.2044 mL) with automatic injections of 1.6 μL each time. With the use of software provided by the manufacturer, each peak corresponding to the injection was integrated and corrected with baseline. The titration heat had been calculated to eliminate the effect of heat generated from diluting the ligand into buffer. Thermal data was fitted to a two-independent-site binding model to yield the value of the equilibrium dissociation constant (K_d).

Analytical ultra centrifugation (AUC) analysis. Sample and buffer were loaded into 12-mm standard double-sector Epon charcoal-filled centrepiece and mounted in an An-60 or An-50 Ti rotors of a Beckman-Coulter XL-I analytical ultracentrifuge (Fullerton, US). The rotor speed was 40,000 rpm at 20 ^{o}C. The signal was monitored at 280 nm. The partial specific volume of TIFA protein is 0.724. The raw experimental data was analyzed by Sedfit (http://www.analyticalultracentrifugation.com/default.htm) and the plots of *c(s, fr)* and molecular mass versus the s-value were generated by MATLAB (MathWork, Inc.).

Chapter 5. FIGURES

Figure 1. Enhancement of TIFA phosphorylation by TNFα stimulation.

Figure 1A. TIFA domain structure and sequence alignment of different TIFA orthologues.

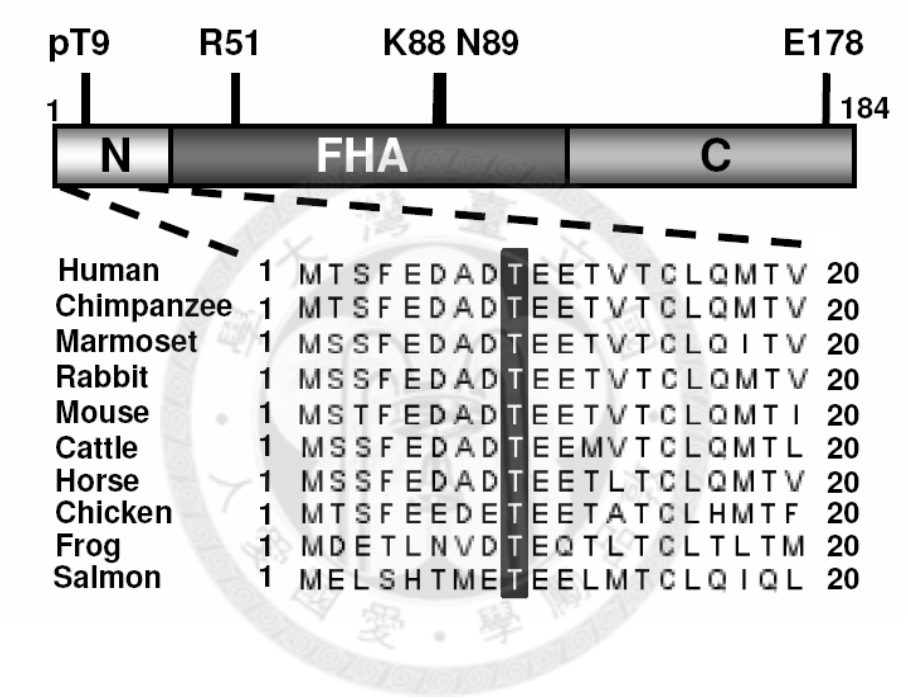

Figure 1. (A) Schematic overview of TIFA domain structure (top) and N-terminal sequence alignment of different TIFA orthologues from the indicated organisms (bottom). Over-expressed human Flag-TIFA protein is phosphorylated at threonine 9 (colored in dark gray).

Figure 1B. MS spectrum of TIFA peptide containing pT9.

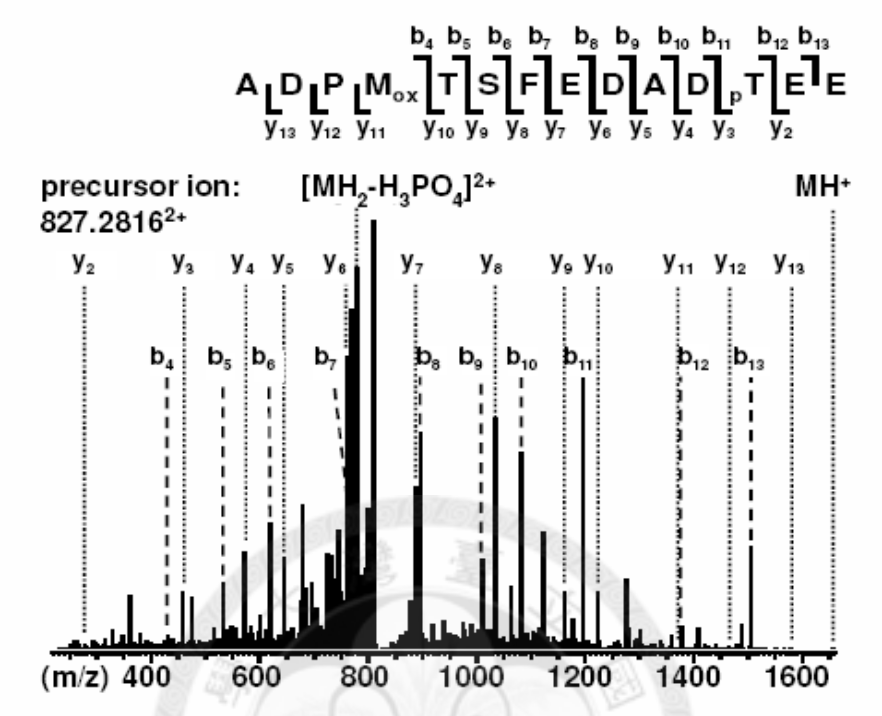

Figure 1. (B) The MS^2 spectrum of peptide containing pT9 in TIFA. The precursor ion 827.2816^{2+} is from ADPMTSFEDAD(pT)EE.

Figure 1C. Phosphorylation status of over-expressed TIFA.

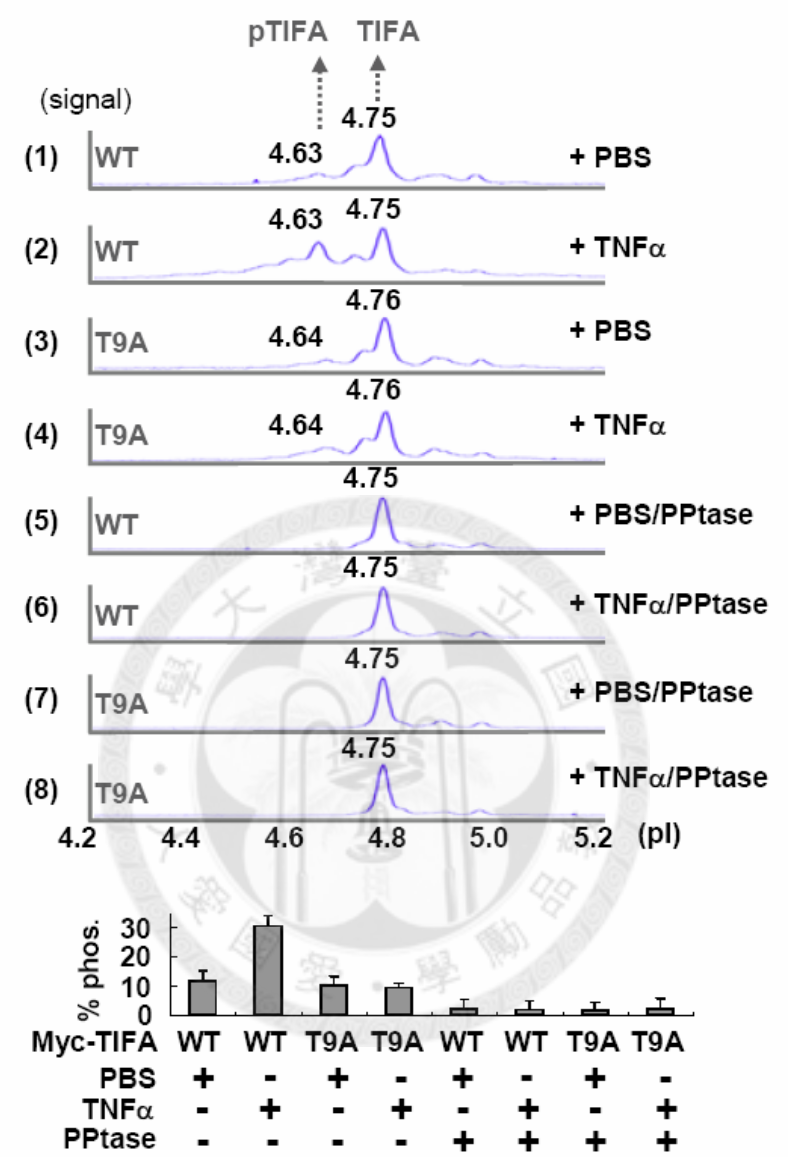

Figure 1. (C) NanoPro™ immunoassay demonstrates the phosphorylation status of over-expressed Myc-tagged TIFA WT and T9A mutant with or without TNFα and phosphatase treatment. The peaks at pI 4.75 and pI 4.63 are assigned to unphosphorylated TIFA and singularly phosphorylated TIFA, respectively. The bar graph in the lower panel represents the ratios of peak areas of singularly phosphorylated TIFA over total TIFA in percentage. The results represent mean ± SD from at least 3 independent experiments.

Figure 1D. Phosphorylation status of endogenous TIFA.

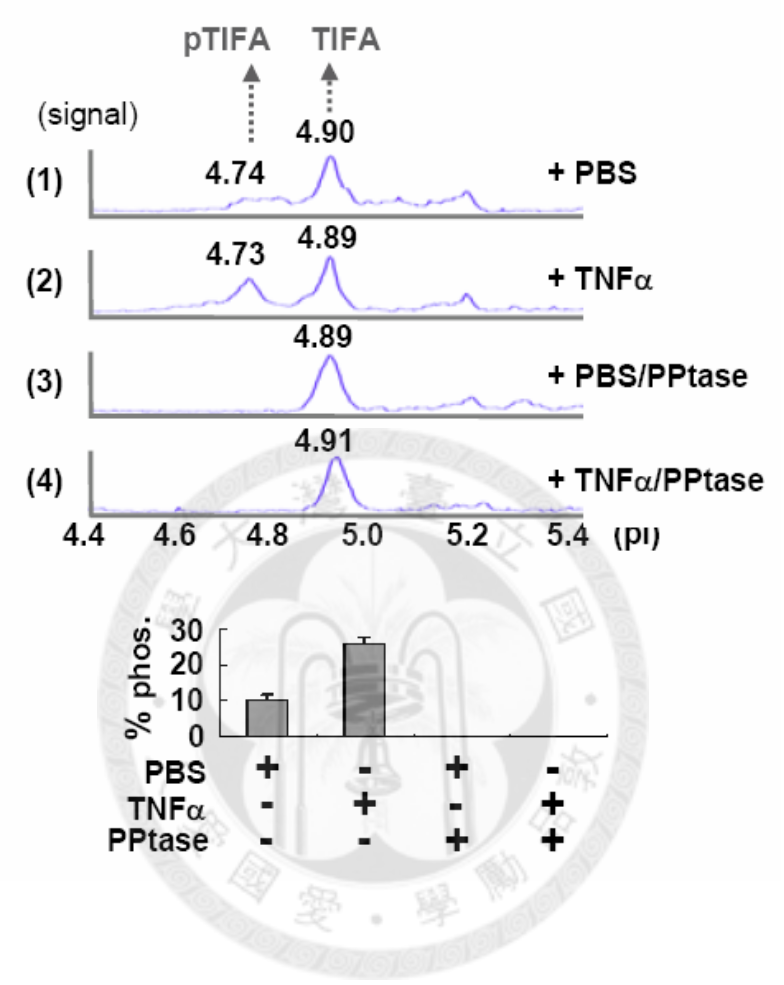

Figure 1. (D) NanoPro™ immunoassay of endogenous TIFA. The conditions were the same as those in (C). The pI values differ from the peaks in (C) due to lack of the Myc tag.

Figure 1E. *In vitro* kinase assay.

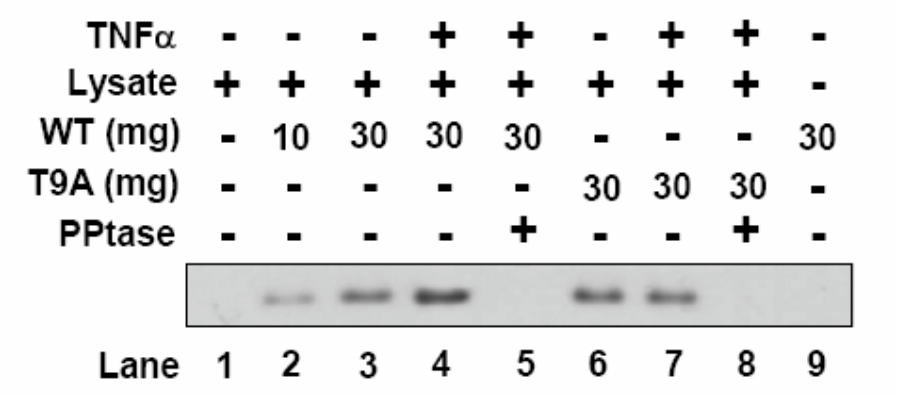

Figure 1. (E) Recombinant TIFA or T9A mutant were incubated with [γ-^{32}P]ATP and lysates from cells treated with or without TNFα for 30 min. During incubation, alkaline phosphatase (PPtase) was added as indicated. The reaction mixtures were separated by SDS-PAGE and the bands were revealed by autoradiography.

Figure 1F. Identification of kinase for TIFA T9 phosphorylation.

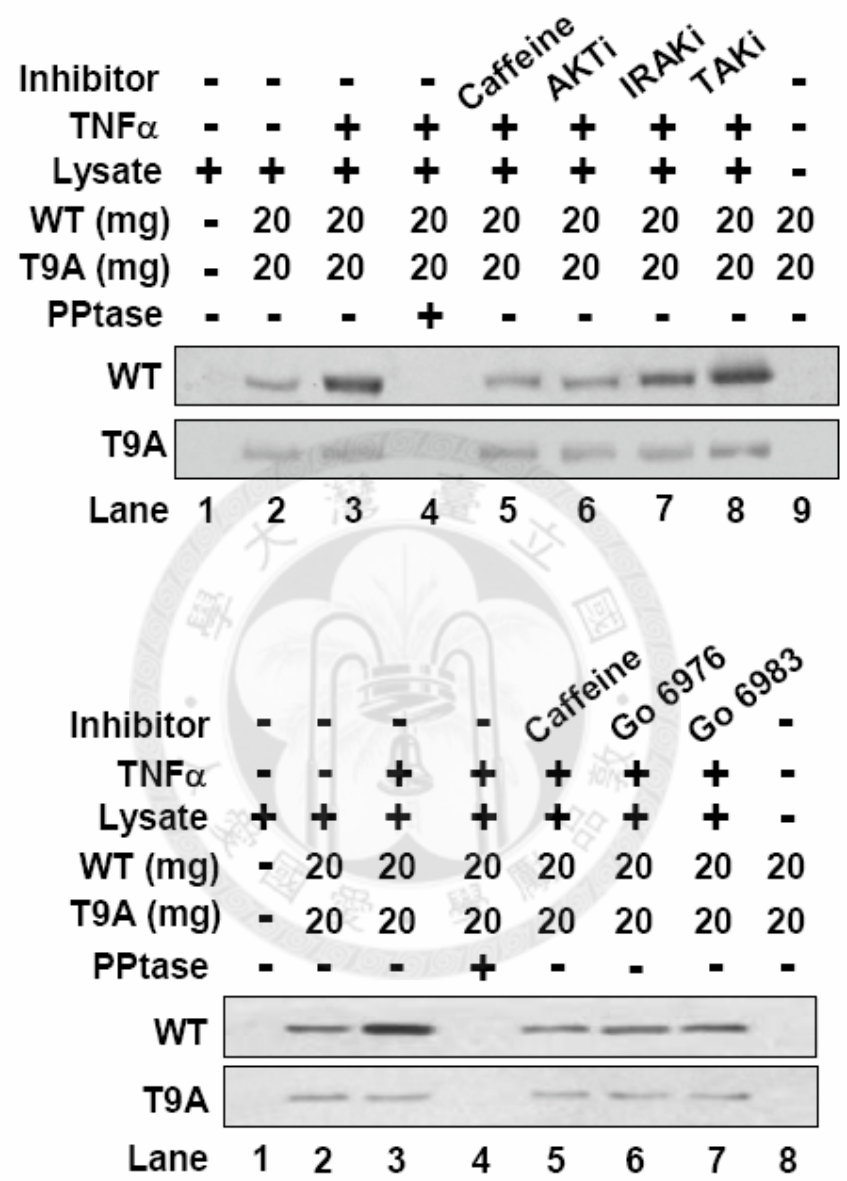

Figure 1. (F) The experimental conditions were the same as those in (E) except the inclusion of caffeine or inhibitor cocktails for AKT, IRAK, TAK, or PKC (Go 6976 and Go 6983).

Figure 2. pT9 and FHA domain are required for TIFA self-association.

Figure 2A. TIFA pT9 is important for TIFA-TIFA association.

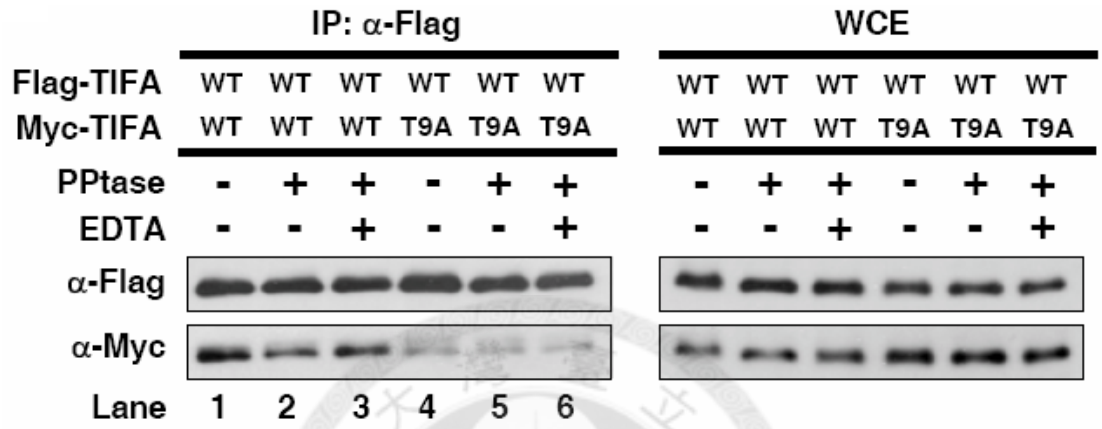

Figure 2. (A) The Flag-tagged WT and Myc-tagged WT and T9A were co-expressed in HEK 293T cells. The anti-Flag coated Dynabeads™ was used in immunoprecipitation (IP). The co-precipitated proteins were detected by anti-Myc antibody in immunoblotting. The whole cell extracts (WCE) used as IP inputs are shown in the right panel. PPtase or EDTA was included as indicated.

Figure 2B. Sequence alignment of different FHA domain proteins.

Figure 2. (B) Sequence alignment of the conserved pT-contacting residues within the FHA domain of different FHA domain-containing proteins. Conserved residues among homologues are colored in light gray. The residues chosen for mutation in this work are labeled in dark gray. RAD53＊: RAD53 FHA1.

Figure 2C. TIFA FHA domain is important for TIFA-TIFA association.

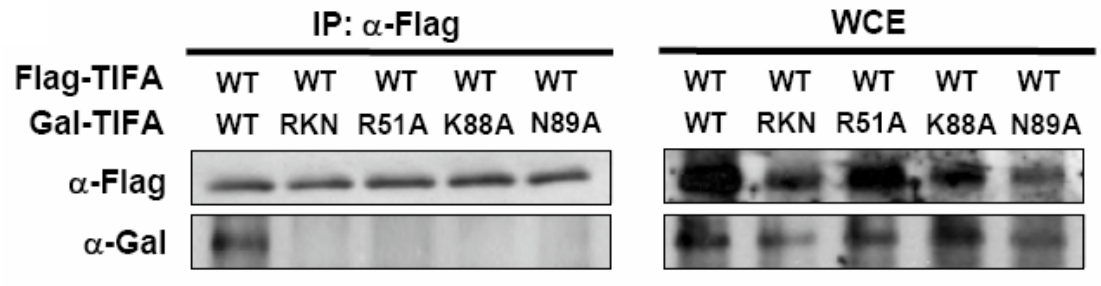

Figure 2. (C) The effect of FHA domain mutations on the self-association of TIFA. The experiments were performed as described in (A), except that the co-precipitated TIFA and its mutants were detected by anti-Gal antibody. RKN: R51AK88AN89A.

Figure 2D. *In vitro* binding of TIFA with pT9 peptides.

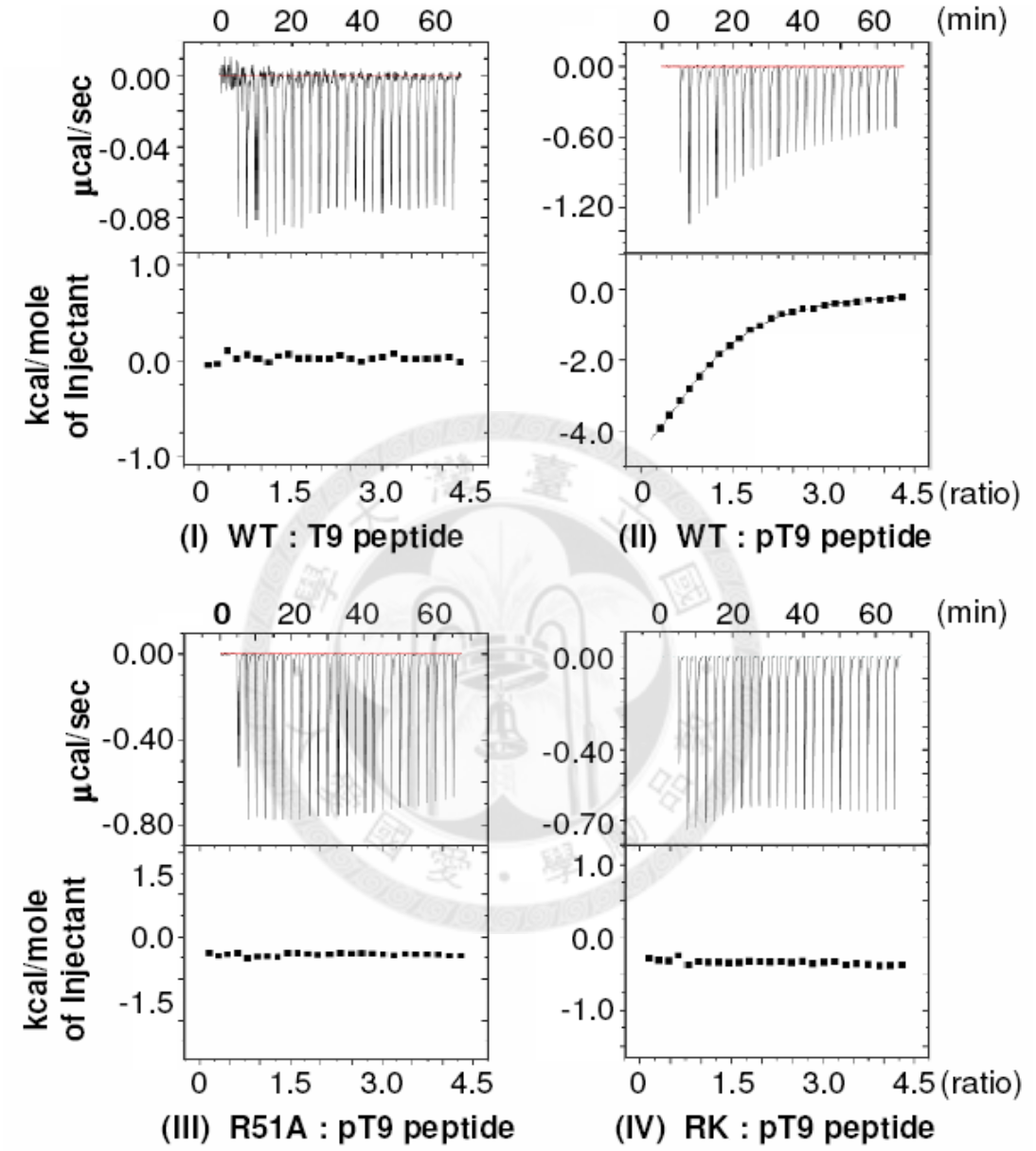

Figure 2. (D) ITC analysis of the *in vitro* binding of TIFA WT and its R51A and R51AK88A (RK) mutants with the T9-peptide [^{1}MTSFEDADTEETVT^{14}] or pT9-peptide [^{1}MTSFEDAD(pT)EETVT^{14}]. Binding was observed only when the WT TIFA was incubated with the pT9-peptide.

Figure 3. Expression and purification of recombinant TIFA.

Figure 3A. Salt concentration screening for recombinant TIFA purification.

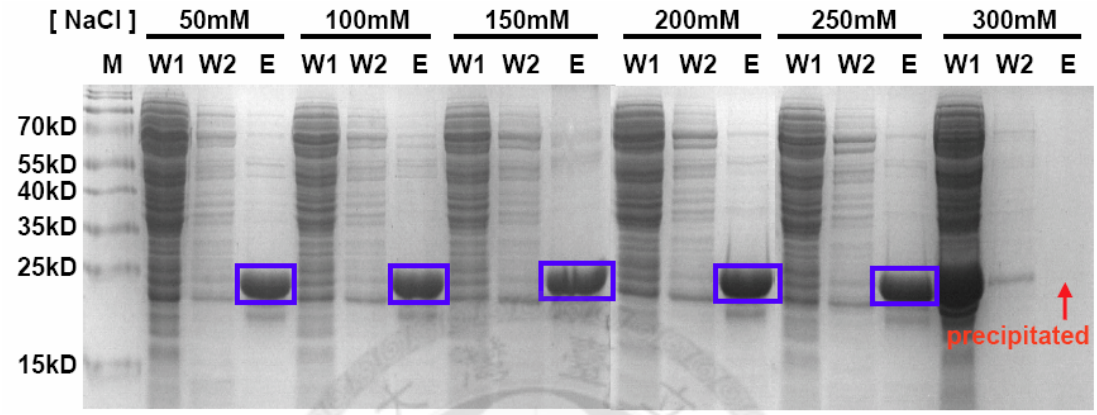

Figure 3. (A) Screenings of optimal purification conditions for full-length recombinant TIFA WT protein. The wash 1 (W1) buffer contained 50mM Tris-HCl (pH 8.0), various concentrations of NaCl (as indicated), and 40mM Immidazole. The contents of wash 2 (W2) buffer and elution (E) buffer were the same as that of W1 buffer except 80mM and 400mM Immidzaole were used, respectively. TIFA protein remains stable in a very narrow range of salt concentrations, from 200mM to 250mM.

Figure 3B. Human TIFA secondary structure prediction.

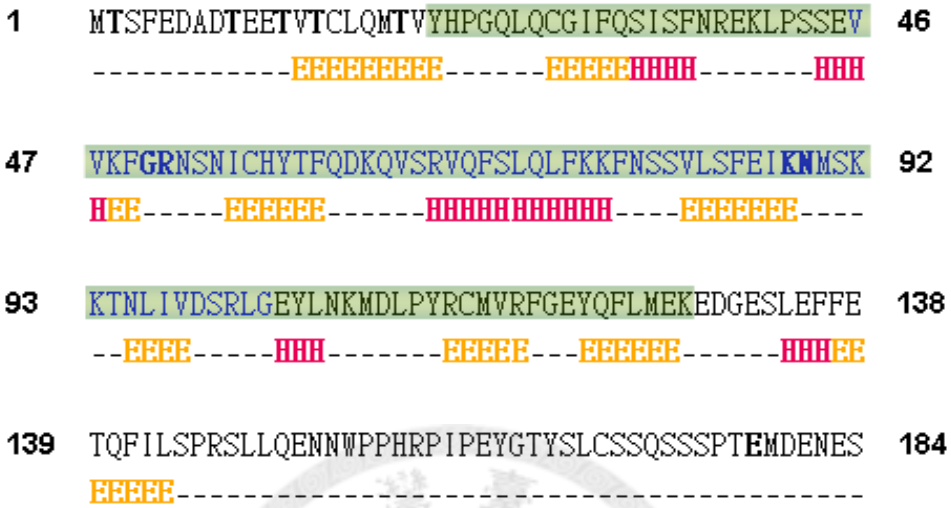

Figure 3. (B) Prediction of the secondary structure of human TIFA protein using Jpred. β-sheets regions are labeled as "E" in orange color and α-helices regions are labeled as "H" in magenta color. Unstructured turns or random coils are indicated by dashes "-". Residues of TIFA FHA domain are highlighted in blue color, but the structural boundary for the conserved FHA domain folding is predicted to be the region shadowing in light green color.

Figure 3C. CD analysis of recombinant TIFA.

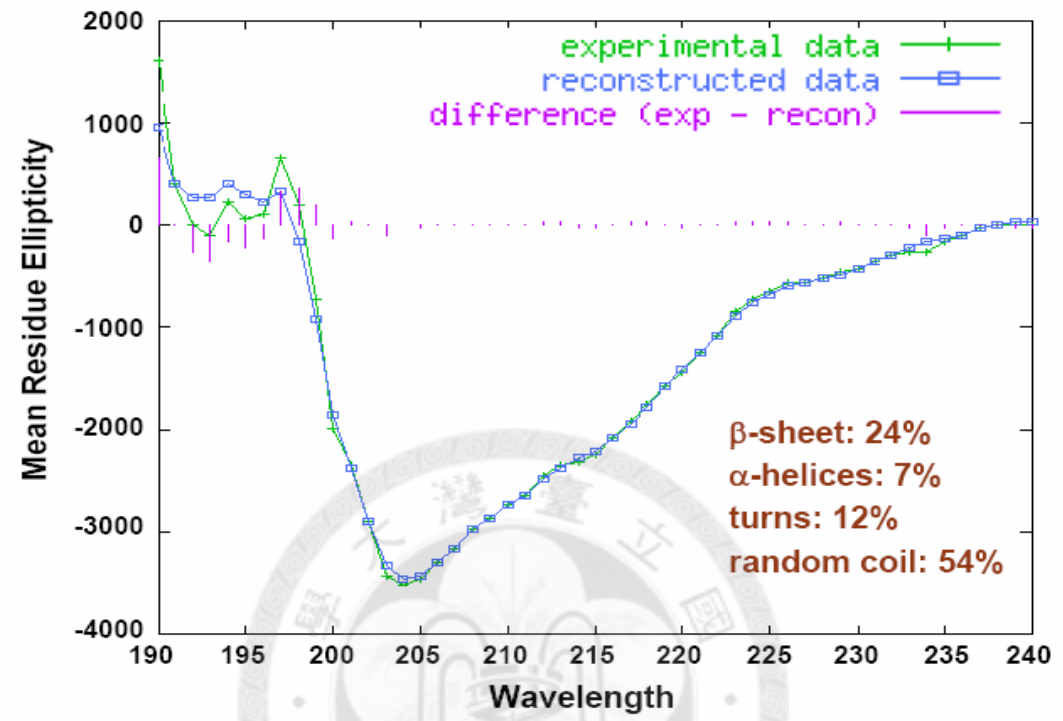

Figure 3. (C) CD analysis of recombinant TIFA. Data was calculated and fitted using CDSSTR method (variable selection method: reference set 7). About 24% of the structure was predicted to be β-sheets, 7% to be α-helices, 12% to be turns and 54% to be random coils.

Figure 3D. HSQC TROSY spectrum of recombinant TIFA.

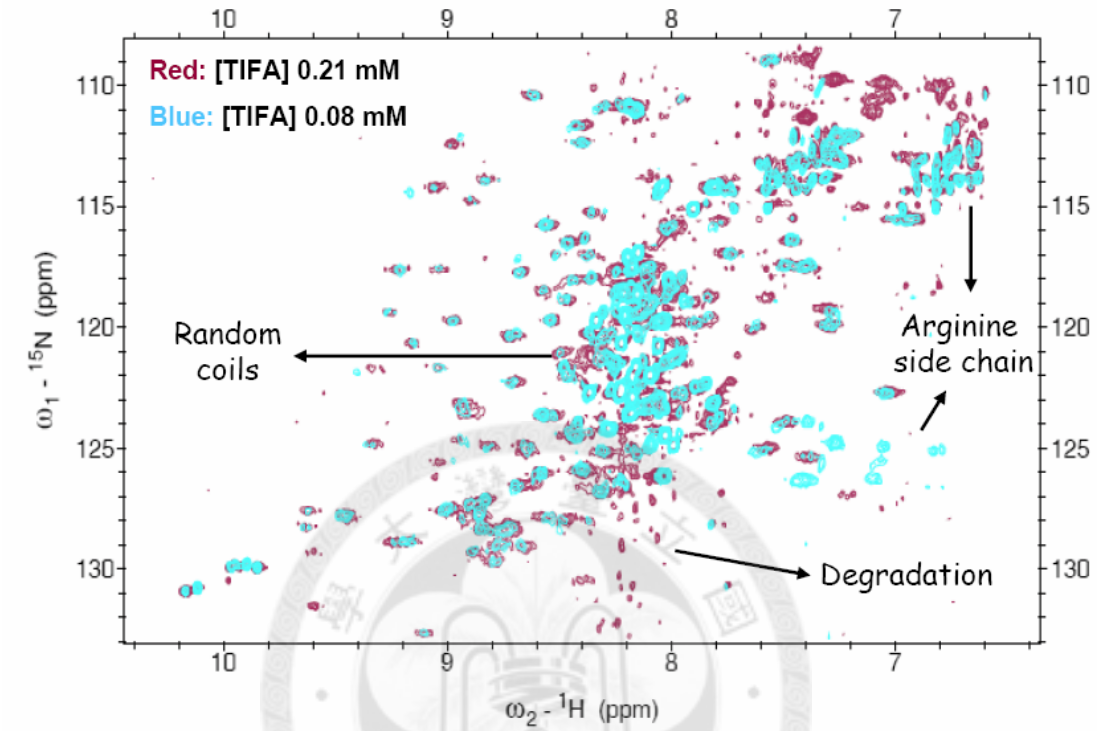

Figure 3. (D) Two HSQC TROSY spectra of recombinant TIFA WT protein in different protein concentrations were overlaid. The concentration of the protein sample (Red batch) was 2.5 fold greater than the other batch (Blue batch), thus the intensity for the new spectrum improved nearly 7 fold. A few tiny signals appeared only in highly concentrated Red batch suggested potential partial degradation of the sample (signal detected because it was intensified due to the increased protein concentration). Most peaks matched well (rough peak count: ~200) and the peak distribution pattern suggested that TIFA protein has conformation (β-sheets: scattered peaks, random coils: in the middle).

Figure 3E. 1-D NMR spectrum of recombinant TIFA.

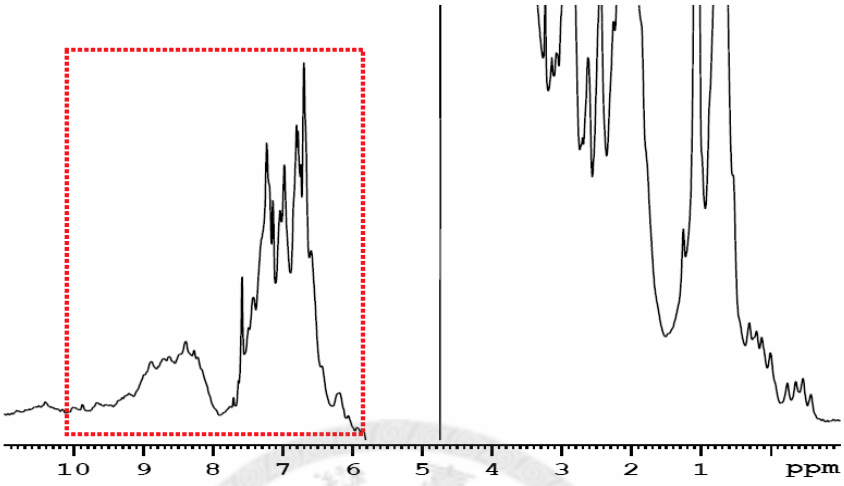

Figure 3. (E) 1-D NMR spectrum of recombinant TIFA WT protein. Tris buffer was exchanged to phosphate (NaH_2PO_4) buffer during sample preparation. However, Tris buffer was accidentally mixed into D_2O while adjusting the salt concentration, thus a large Tris reaction peak was observed at around 4 ppm. The peaks enlarged at the region of 6~10 ppm suggested that several NH groups were protected by the structure thus the folding seemed fine for the TIFA WT protein.

Figure 3F. Purification of truncated TIFA.

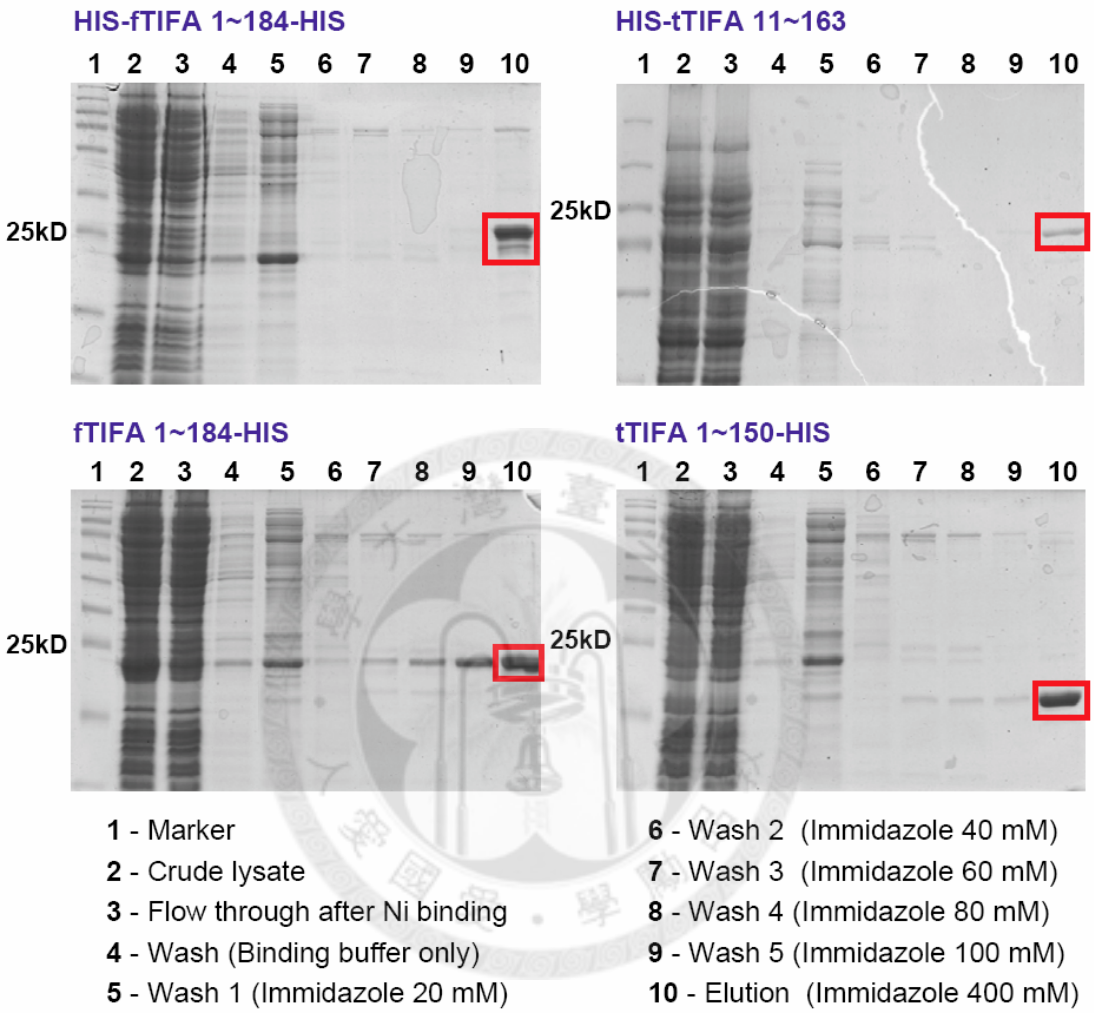

Figure 3. (F) Purification of full-length and truncated TIFA proteins that have His-tag at different positions. Full-length recombinant TIFA with the His-tag at the C-terminus seemed to achieve the best expression yield, purity, quality (least degradation observed) and stability.

Figure 4. TIFA exists as an intrinsic dimer in solution.

Figure 4A & B. Size-exclusion chromatography and AUC analysis of recombinant TIFA WT and mutants.

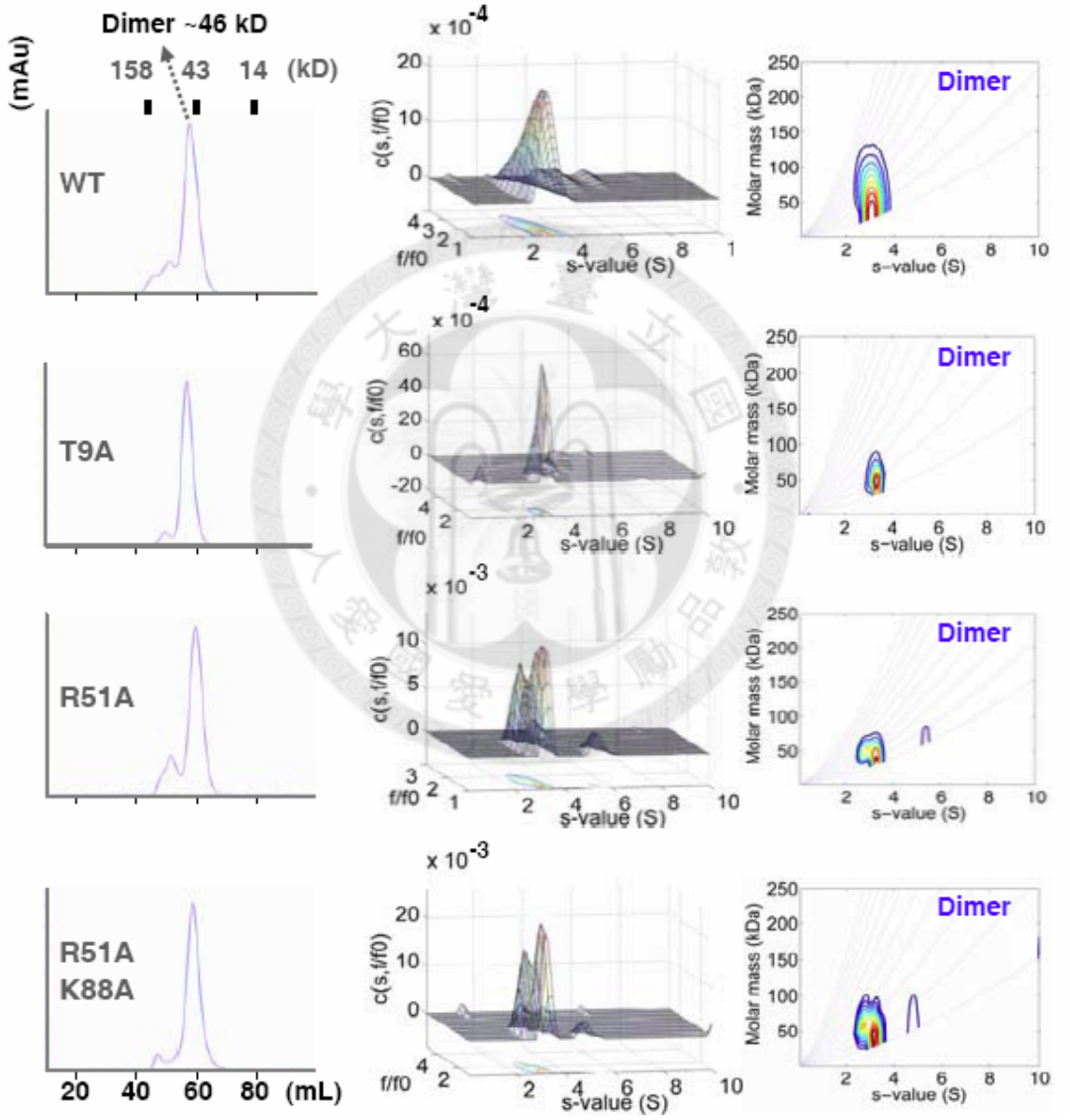

Figure 4. (A) Size-exclusion chromatography (HiLoad 16/60 Superdex 75 pg column) and **(B)** AUC analysis show that recombinant TIFA and mutants exist as dimers in solution.

Figure 4C. Recombinant TIFA in different concentrations.

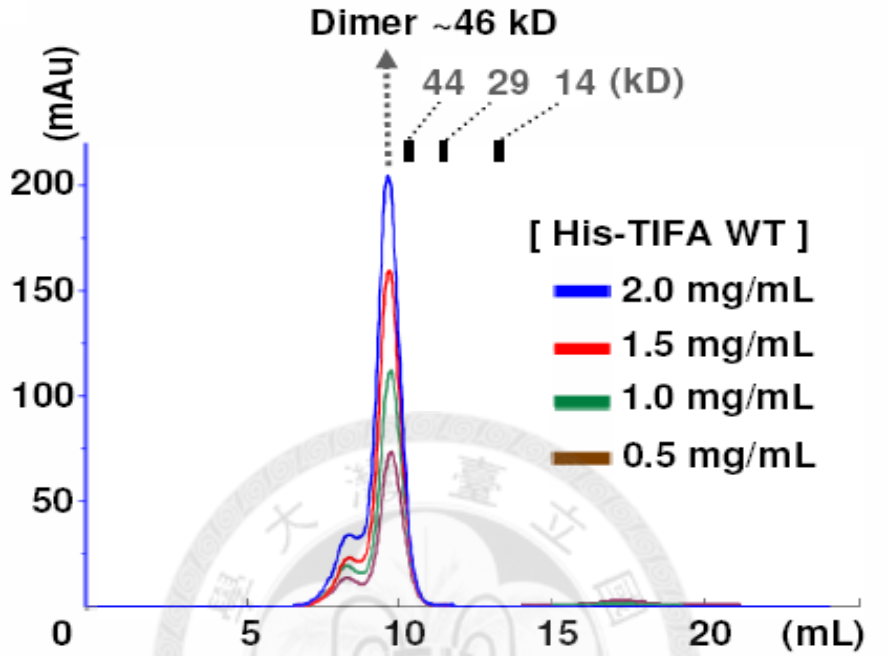

Figure 4. (C) Recombinant TIFA WT appeared as a dimer from low (0.5 mg/mL) to high (2 mg/mL) protein concentrations in size-exclusion chromatography (Superdex 75 10/300 GL column).

Figure 4D. AUC analysis of recombinant TIFA with peptides.

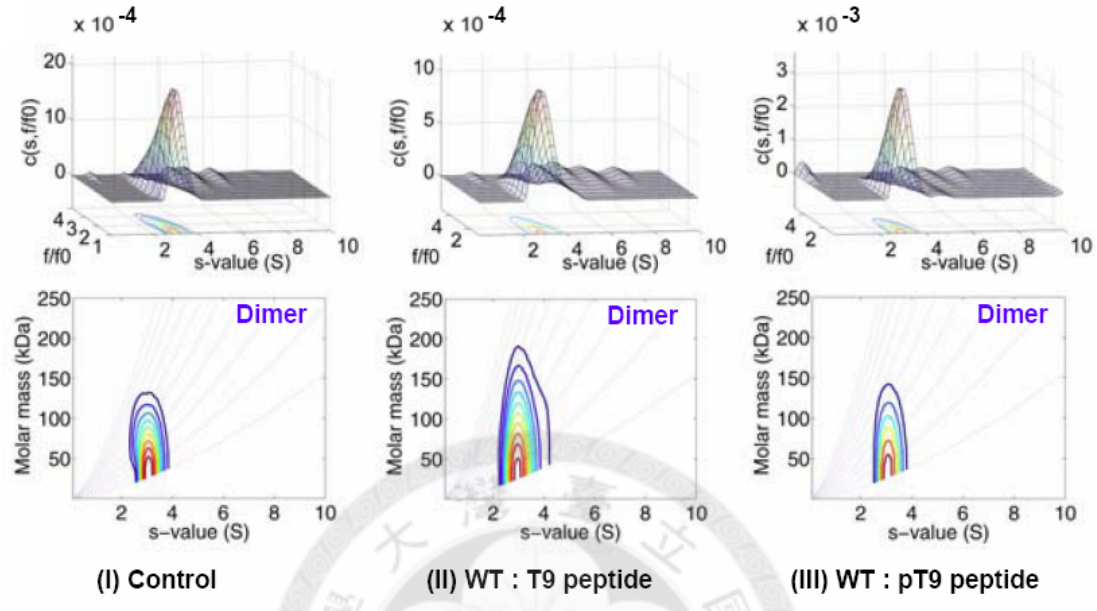

Figure 4. (D) AUC analysis of WT recombinant TIFA alone (I), with the T9-peptide (II) or pT9-peptide (III). The concentration of TIFA WT used was 10 mM and the peptides were presented at a molar ratio of 1:10 (protein: peptide).

Figure 4E. TIFA not dimerize through disulfide bonds.

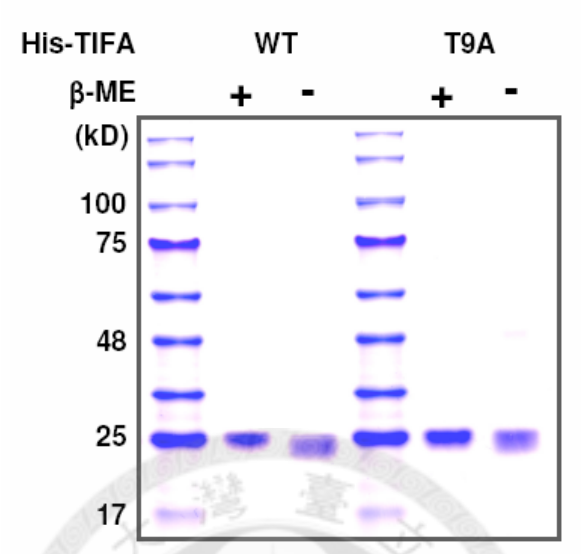

Figure 4. (E) TIFA remained in the monomeric form on SDS-PAGE in a non-reduced condition, demonstrating that TIFA did not dimerize through disulfide bonds.

Figure 5. Crystallization of recombinant TIFA.

Figure 5A. Purification and MS analysis of full-length TIFA.

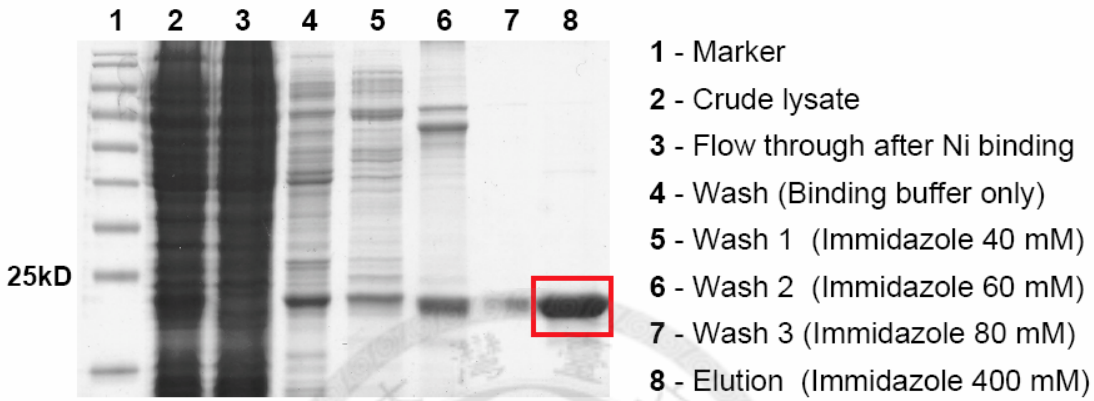

TRAF-interacting protein with a forkhead-associated domain [Homo sapiens]

Sequence Coverage: **72%**

```
  1 MTSFEDADTE ETVTCLQMTV YHPGQLQCGI FQSISFNREK LPSSEVVKFG
 51 RNSNICHYTF QDKQVSRVQF SLQLFKKFNS SVLSFEIKNM SKKTNLIVDS
101 RELGYLNKMD LPYRCMVRFG EYQFLMEKED GESLEFFETQ FILSPRSLLQ
151 ENNWPPHRPI PEYGTYSLCS SQSSSPTEMD ENESLEHHHH HH
```

Figure 5. (A) Purified full-length recombinant TIFA WT protein was digested by enzymes trypsin together with chymotrypsin and analyzed by MS. With a purity greater than 95% and a peptide sequence coverage of 72%, human TIFA WT protein obtained was confirmed to contain no mutation(s) and was then used for crystallization.

Figure 5B. Native and Se-Met TIFA protein crystals.

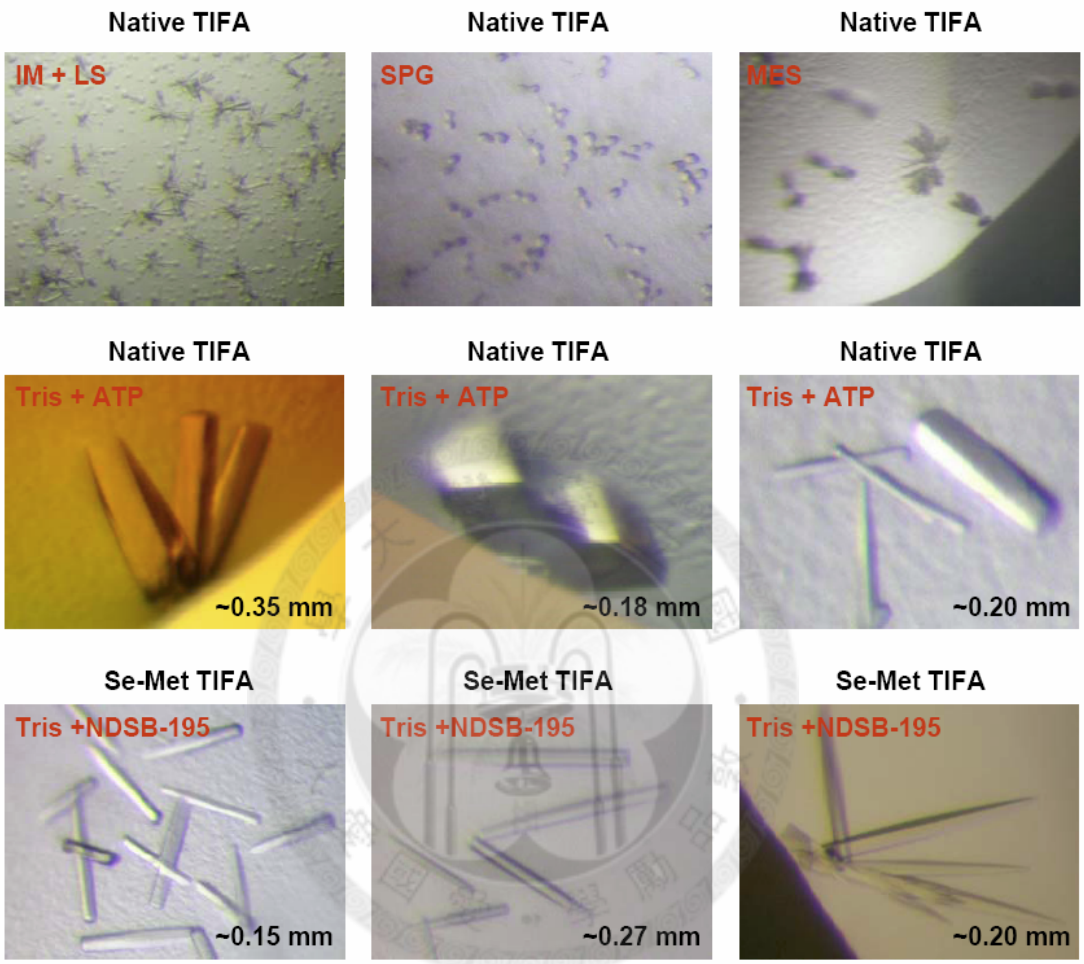

Figure 5. (B) Native and Se-Met labeled TIFA crystals in different crystallization conditions all appeared to be thin but long (needle/rod shape).

Figure 5C. Low sequence homology between FHA proteins.

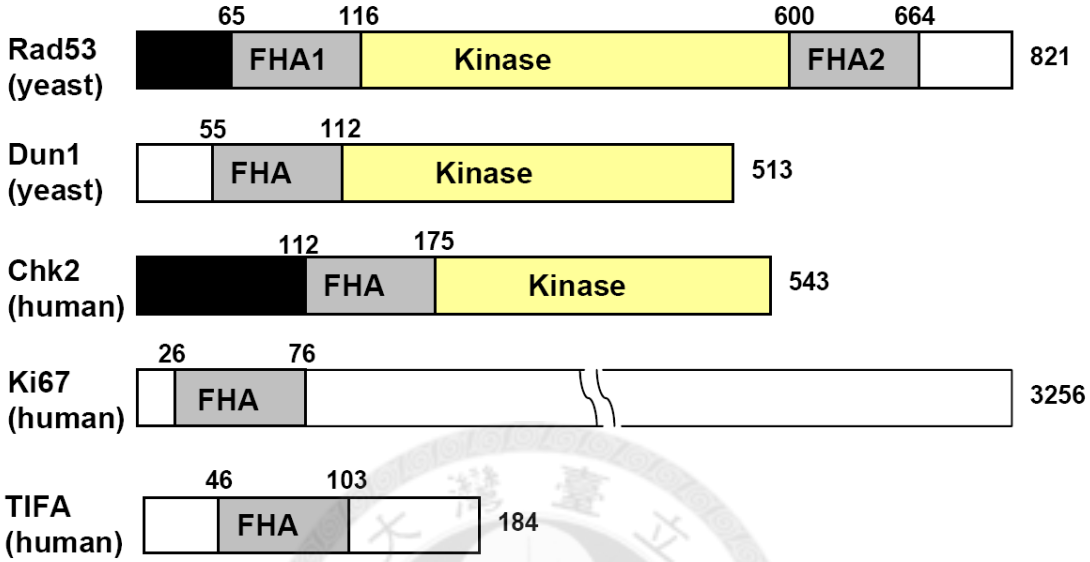

Figure 5. (C) For molecular replacement, only less than 40% of TIFA may find a few models (other solved FHA domain structures, indicated in blue color) that share low sequence homologies.

Figure 5D. Heavy atom soakings for native TIFA crystals.

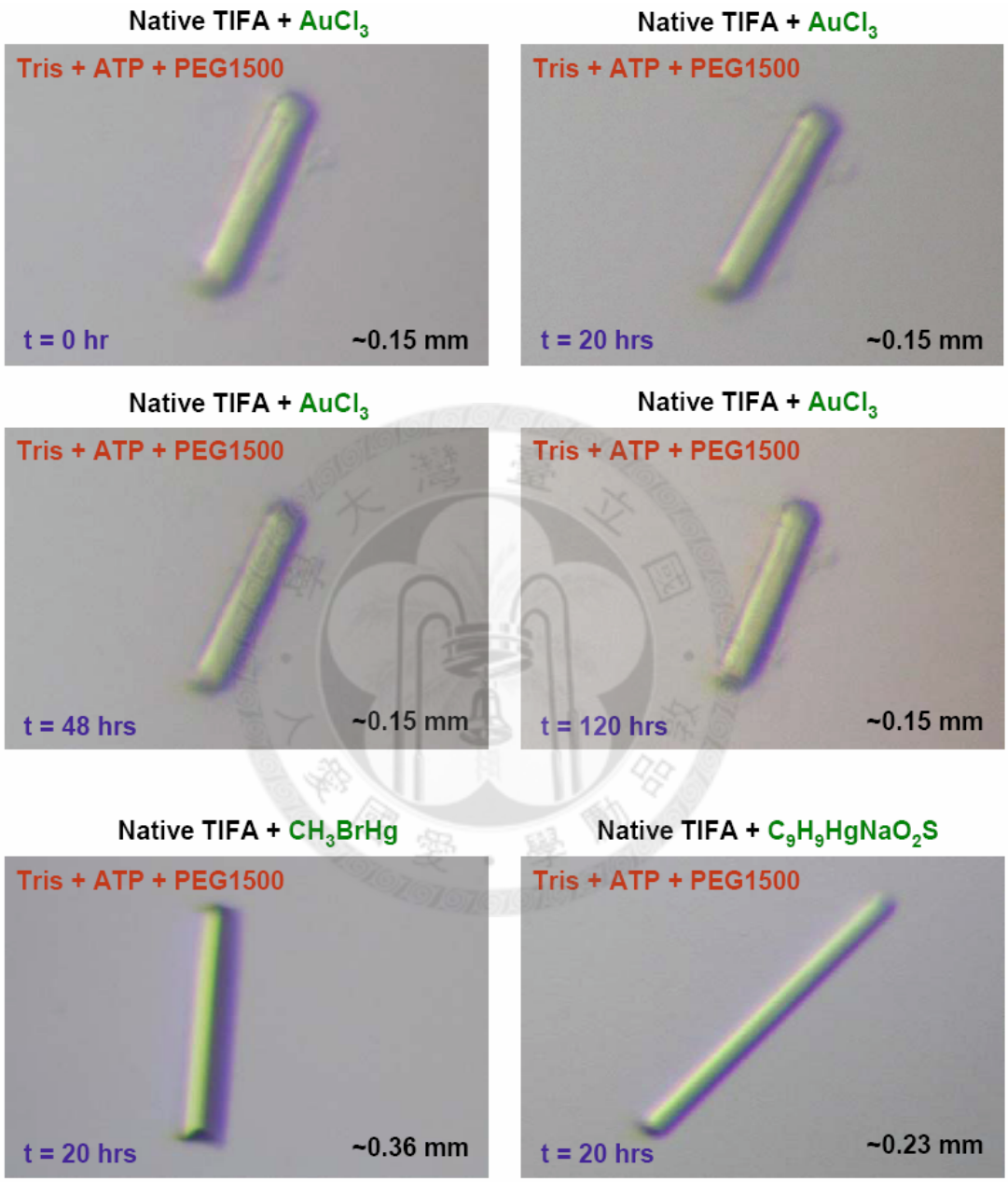

Figure 5. (D) Native TIFA crystal soaked in crystallization buffer with additive (ATP), cryo-protectant (22% PEG1500) and heavy atom (1mM $AuCl_3$, CH_3BrHg or $C_9H_9HgNaO_2S$) for the time indicated.

Figure 5E. Purification and MS analysis of Se-Met TIFA.

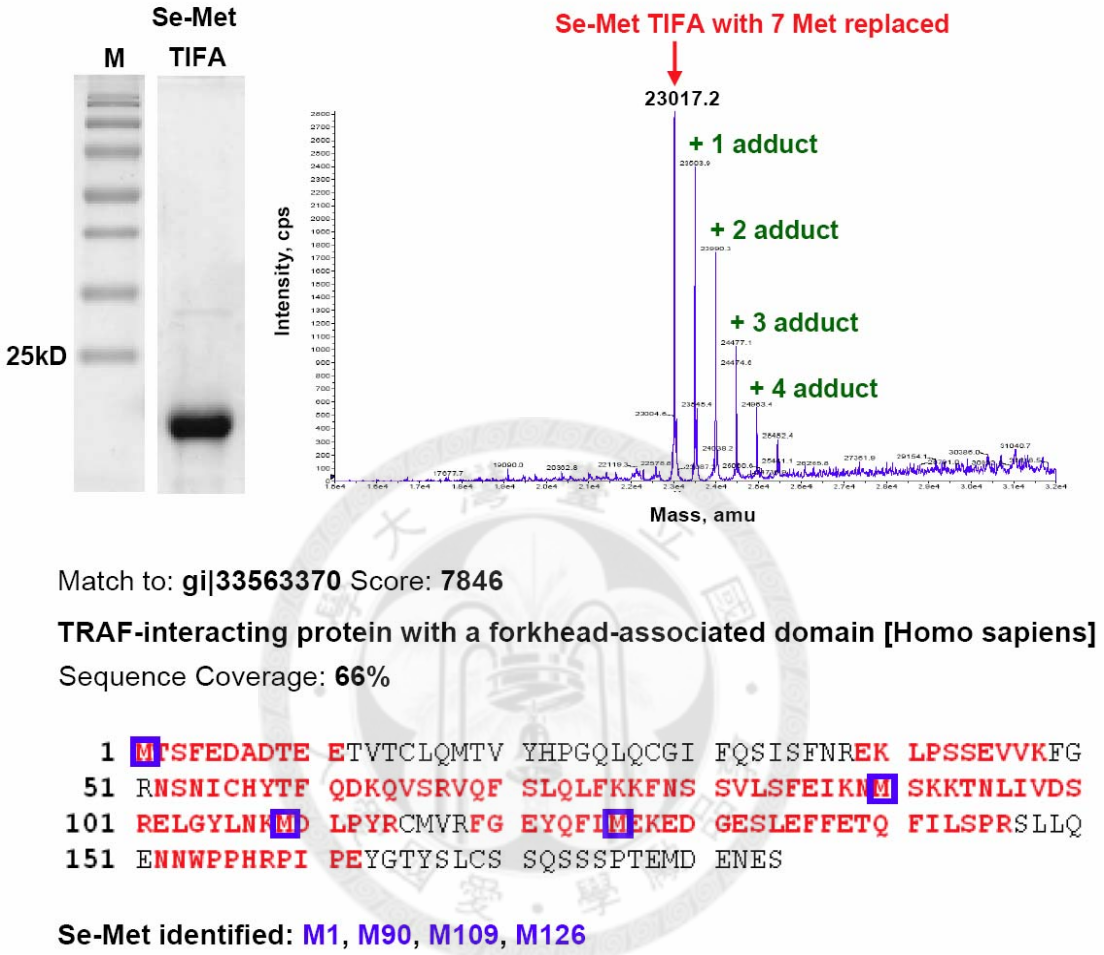

Figure 5. (E) Purified Seleno-methionine (Se-Met)-labeled recombinant TIFA protein was digested by enzymes trypsin together with GluC and analyzed by MS. It was confirmed that four among a total of seven methionine residues in TIFA have been labeled with selenium. The Se-Met TIFA protein was further subjected to crystallization as well.

Figure 5F. Diffraction patterns of different TIFA crystals.

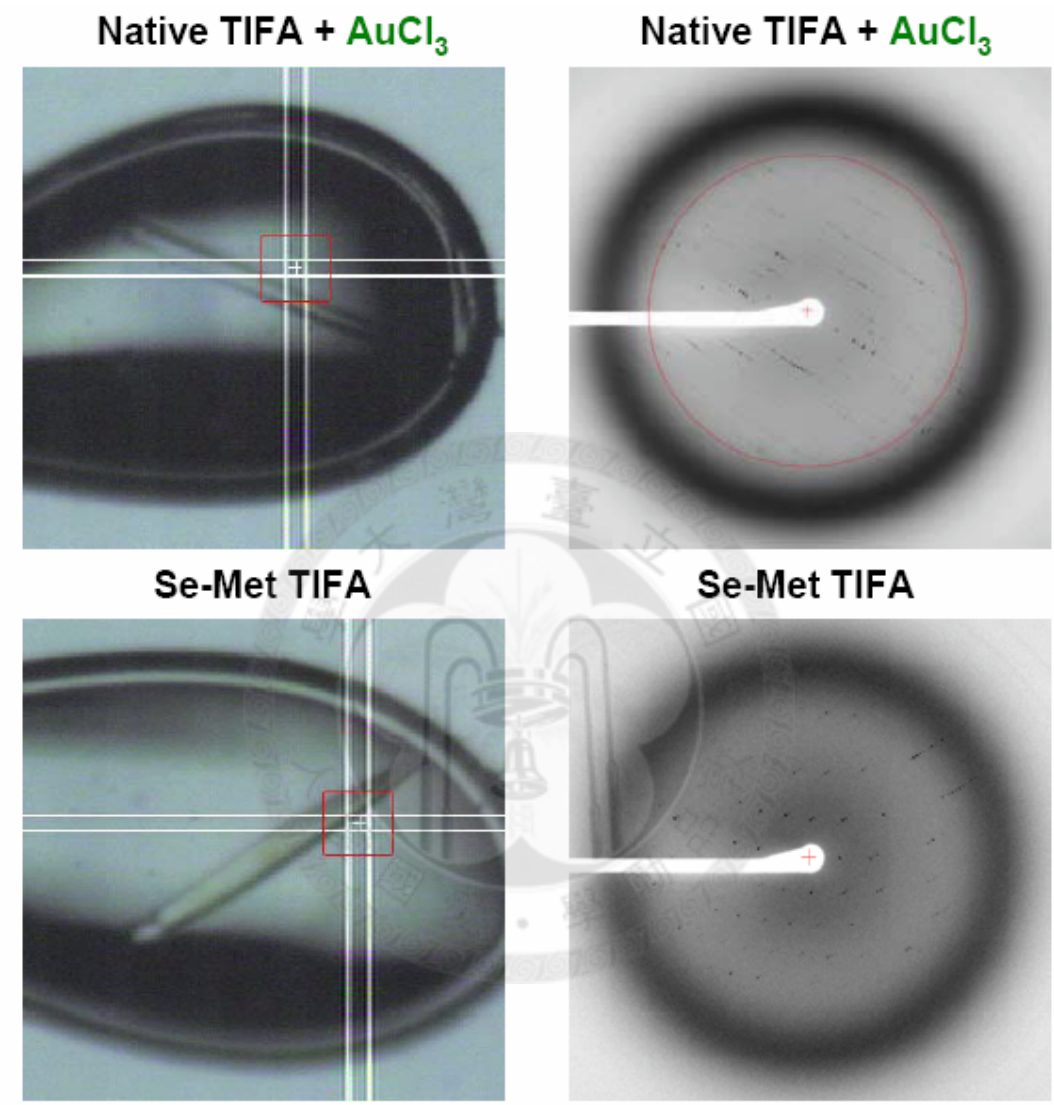

Figure 5. (F) Native TIFA crystals soaked with heavy atom Au or Se-Met labeled TIFA crystals mounted in cryo-loops (left) were subjected to synchrotron radiation. The advance collecting mode allowed the beam to move gradually along the long axis of the targeted crystal during data collection. Red squares indicate the regions exposed to radiation. Diffraction patterns (right) for these crystals.

Figure 6. TIFA pT9-FHA interaction is required for TIFA oligomerization.

Figure 6A. Oligomerization status of TIFA WT and mutants.

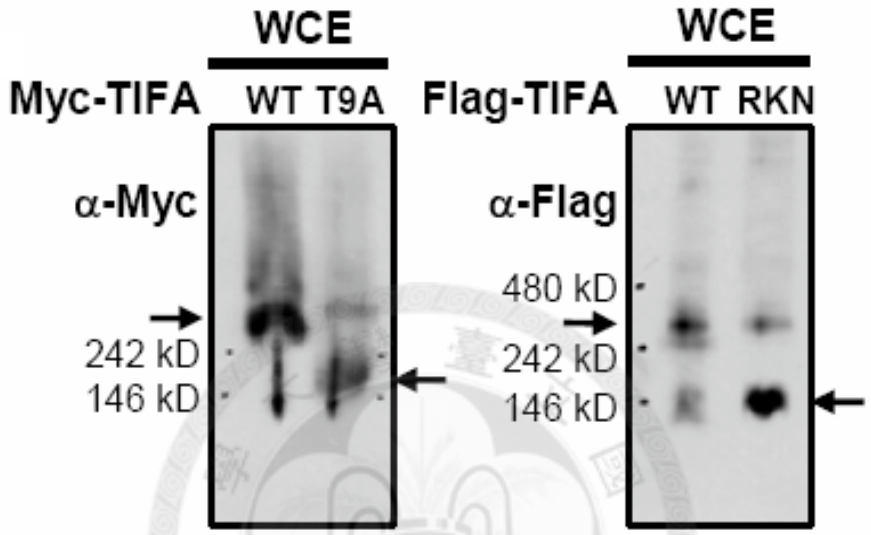

Figure 6. (A) The exogenously expressed Myc-TIFA, Flag-TIFA, and their T9A and RKN mutants were separated by native gel and detected by Western blot. Arrows indicate the major bands.

Figure 6B. *In vitro* kinase assay with native gel.

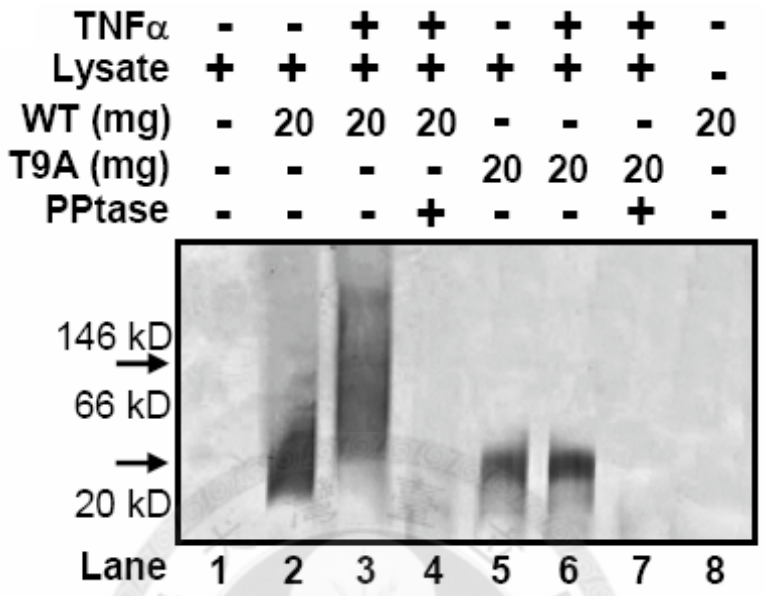

Figure 6. (B) Autoradiography of native gel shows that the phosphorylated His-TIFA WT in TNFα-treated cell lysate was up-shifted to a larger molecular weight (indicated by arrows). No signal was detected when samples were treated with alkaline phosphatase.

Figure 6C. Immunostaining of TIFA WT and mutants.

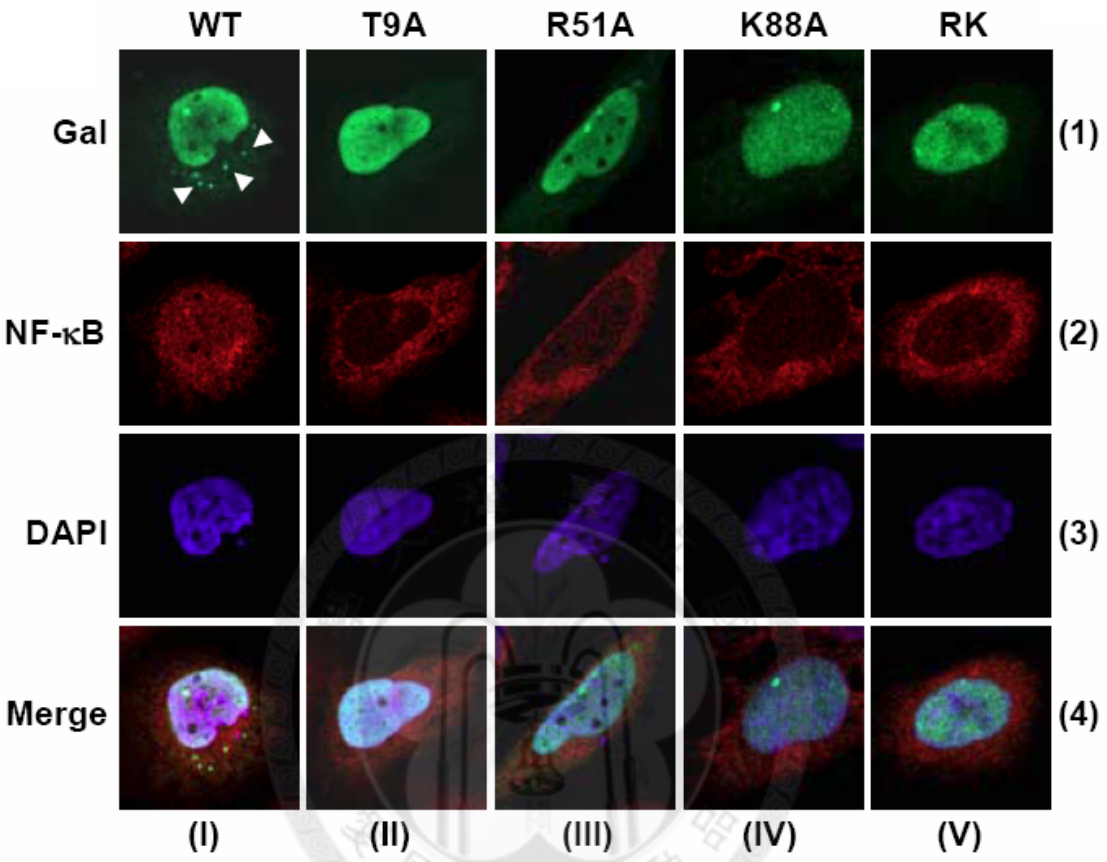

Figure 6. (C) U2OS cells ectopically expressing Gal-tagged TIFA/mutants were fixed and incubated with anti-Gal and anti-NF-κB antibodies followed by FITC-conjugated anti-mouse IgG and rhodamine conjugated anti-rabbit IgG. The nuclei were counterstained with DAPI. The fluorescence images were obtained by a Zeiss LSM 510 confocal microscope. White arrows indicate the aggregations/speckles of Gal-TIFA WT.

Figure 6D. Co-localization of TIFA and TRAF6 *in vivo*.

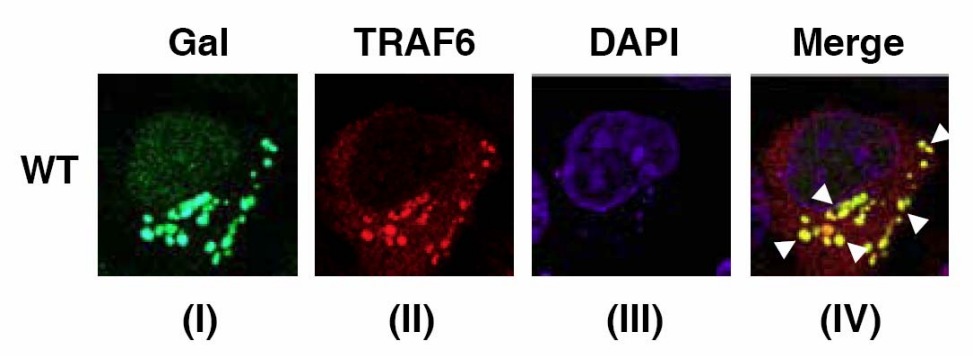

Figure 6. (D) Co-localization of Gal-TIFA WT and Flag-tagged TRAF6 is indicated by white arrows in the superimposed images. The experimental condition was the same as that in (C) except Flag-TRAF6 was recognized by anti-TRAF6 antibody.

Figure 7. The pT9-FHA binding is involved in TNFα-mediated activation of NF-κB.

Figure 7A. NF-κB activation induced by exogenous TIFA/TRAF2.

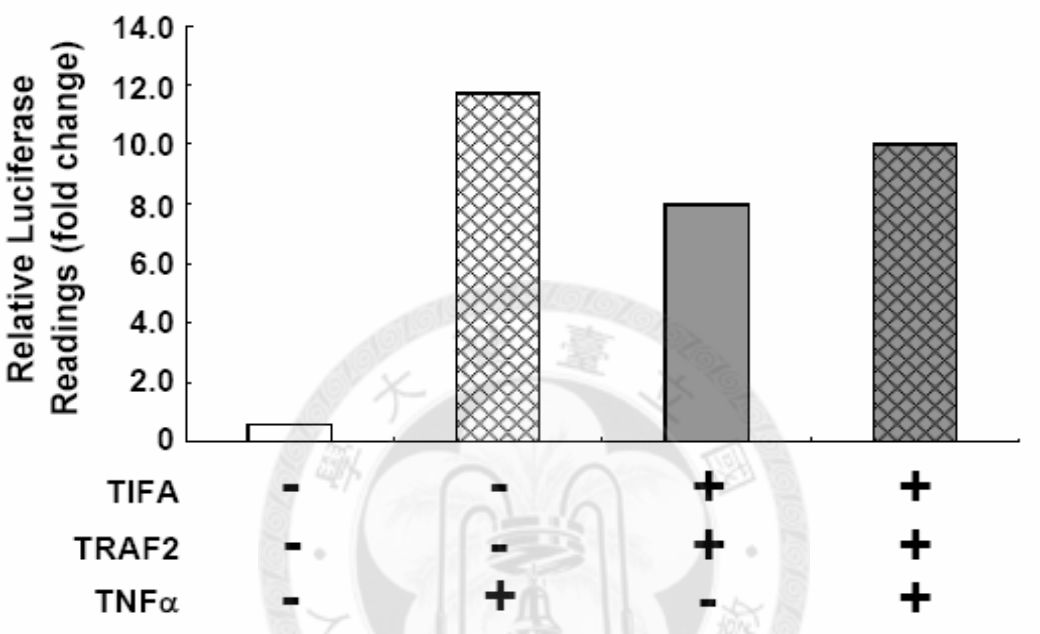

Figure 7. (A) Comparison of activation levels of NF-κB mediated by endogenous TIFA/TRAF2 or over-expressed TIFA/TRAF2 with or without TNFα stimulation.

Figure 7B. NF-κB activation mediated by over-expressed TIFA WT and mutants

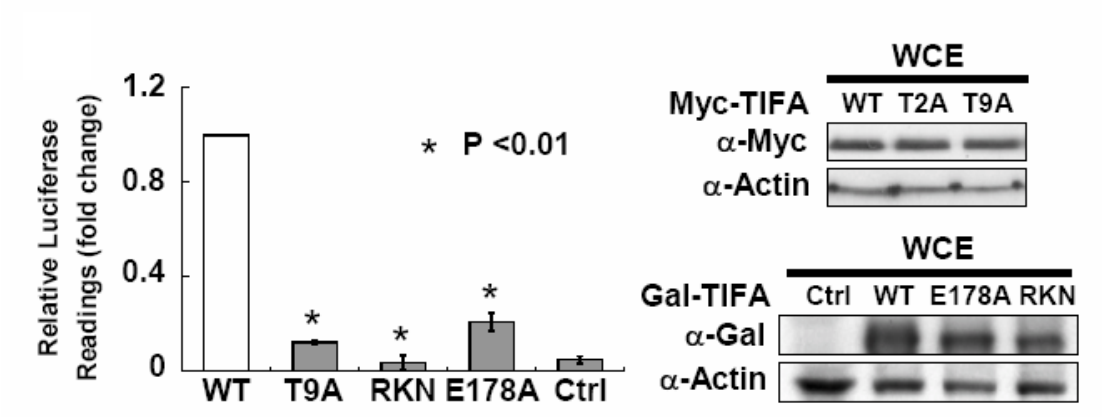

Figure 7. (B) HEK 293T cells were transfected with a NF-κB luciferase reporter together with TIFA WT or its various mutants. NF-κB activation was evaluated by luciferase activity assays. The bar graph represents fold changes of normalized relative luminescence unit (RLU). The results are mean ± SD from at least 3 independent experiments. Western blotting on the right shows the expression profiles of mutants used in the experiments.

Figure 7C. Amount of endogenous TIFA augments upon stimulations

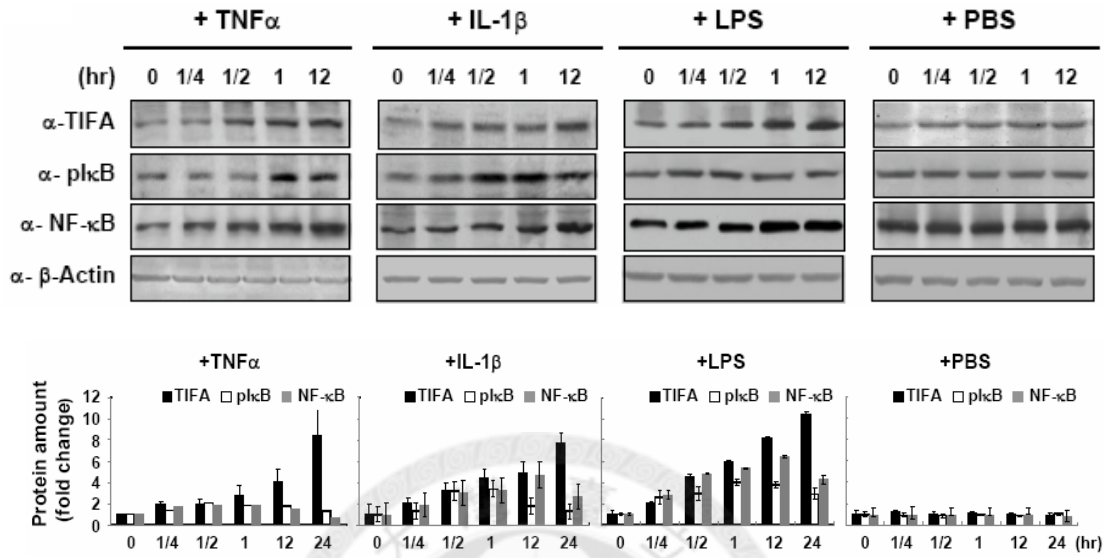

Figure 7. (C) Changes in the level of endogenous TIFA upon TNFα, IL-1β, and LPS stimulations. HEK293T cells were pre-starved at least 8 hours and stimulated. Treated cells were then harvested at different post-incubation time, lysed, and subjected to WB analysis. WB shows the endogenous TIFA protein amount after different inflammatory stimulation in the time course manner. Phospho-IκB (pS32/pS36) and NF-κB (p65) were used as stimulation controls.

Figure 7D. TIFA mRNA level remains the same upon TNFα stimulation.

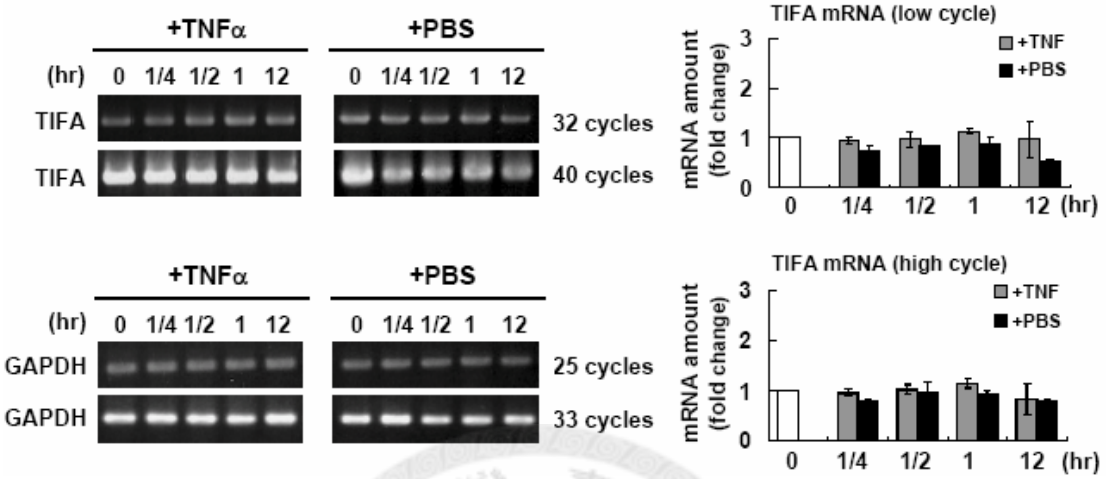

Figure 7. (D) EtBr staining of amplified cDNA by semi-quantitative RT-PCR in two different reaction cycles, representing the relative TIFA mRNA transcription levels of TNFα-stimulated cells. A house keeping gene, GAPDH was used as control. Bar graphs in the lower panel show the quantification of band intensity of the above EtBr staining for *TIFA*. Standard deviations were calculated from at least 3 independent experiments. PBS, non-treatment control.

Figure 7E. Silencing of TIFA with siRNA.

Figure 7. (E) HEK293T cells were transfected with TIFA siRNA or scramble RNA (Ctrl). The efficiency of RNA interference was verified by Western blot from at least 3 independent experiments and plotted as the bar graph shown on the right.

Figure 7F. Attenuation of NF-κB activation in HEK 293T cells with TIFA silenced.

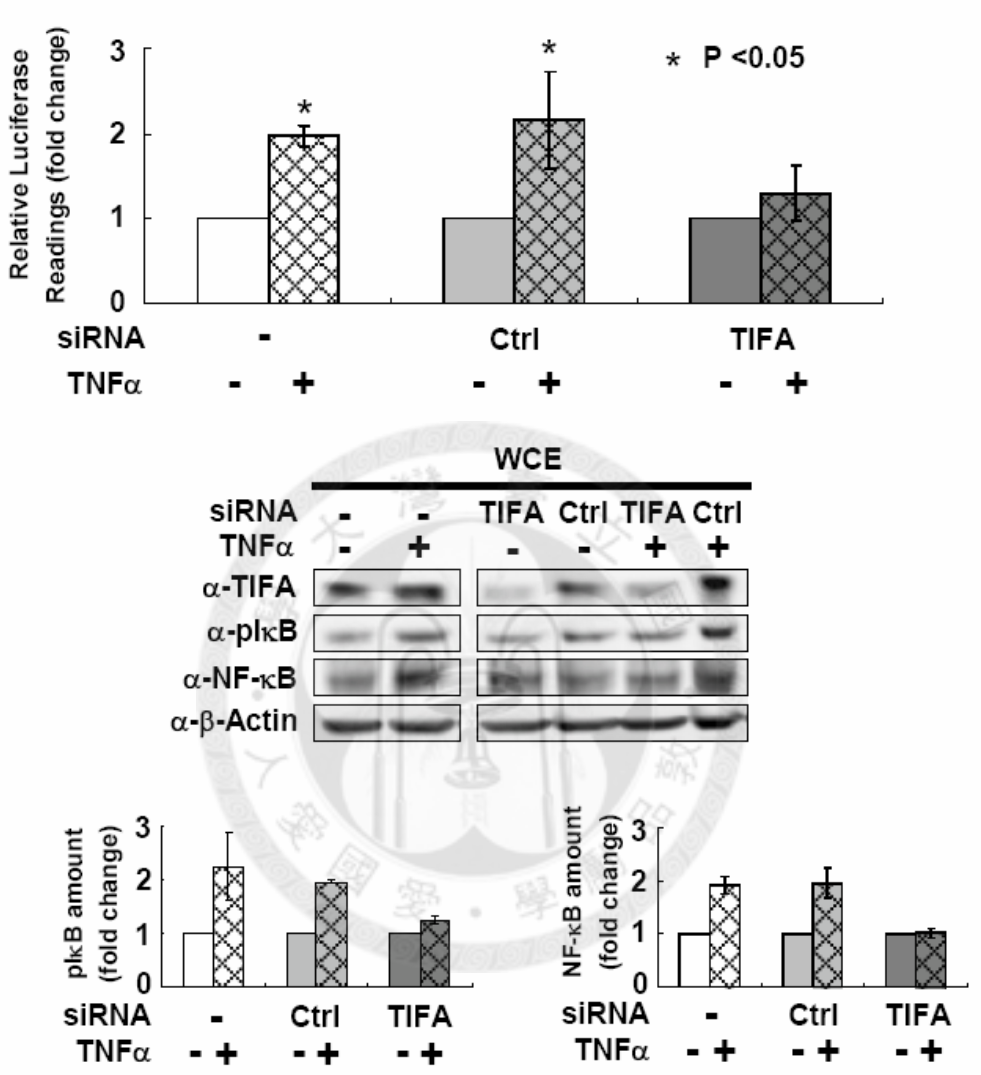

Figure 7. (F) HEK 293T cells receiving TIFA siRNA or scramble RNA (Ctrl) were co-transfected with a NF-κB luciferase reporter and then stimulated with TNFα as indicated. NF-κB activation was evaluated by luciferase activity assays. The untreated groups were set as 1. The cell lysates were also analyzed by Western blot. The bar graphs below represent the fold changes of phosphorylated IκB (pS32/pS36) and total NF-κB (p65) proteins after TNFα treatment.

Figure 7G. Attenuation of NF-κB activation in THP-1 cells with TIFA silenced.

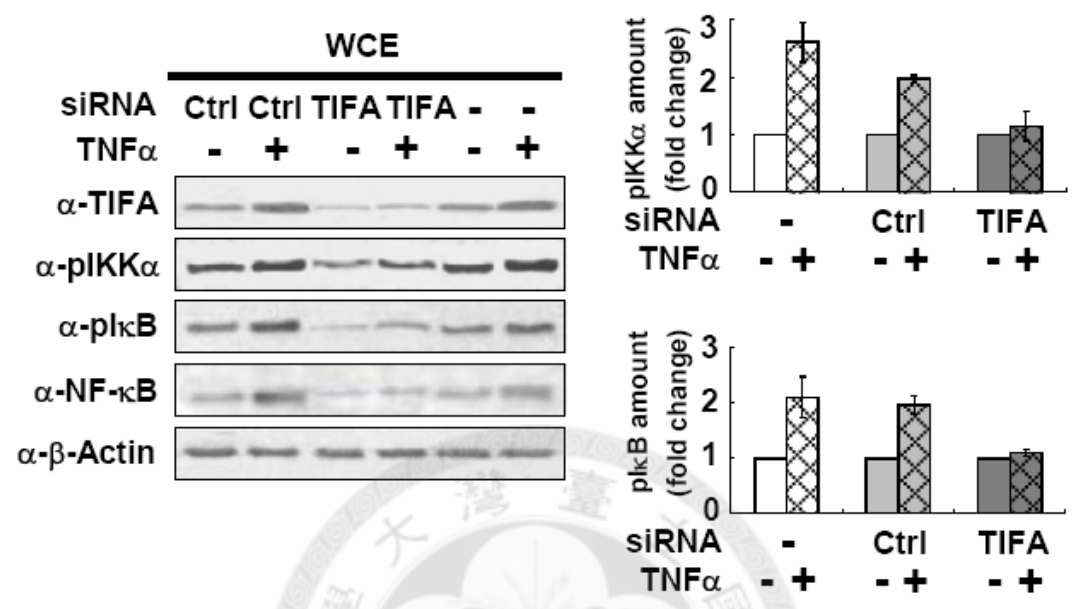

Figure 7. (G) The experimental conditions for siRNA transfection were the same as those described in (E) except the cell line used was THP-1 (human acute monocytic leukemia cell line). The bar graphs represent the fold changes of phosphorylated IKKα (pT23) and phosphorylated IκB (pS32/pS36) after TNFα stimulation.

Figure 8. Interaction of TIFA and TRAF2

Figure 8A. Validation of TIFA-TRAF2 interaction.

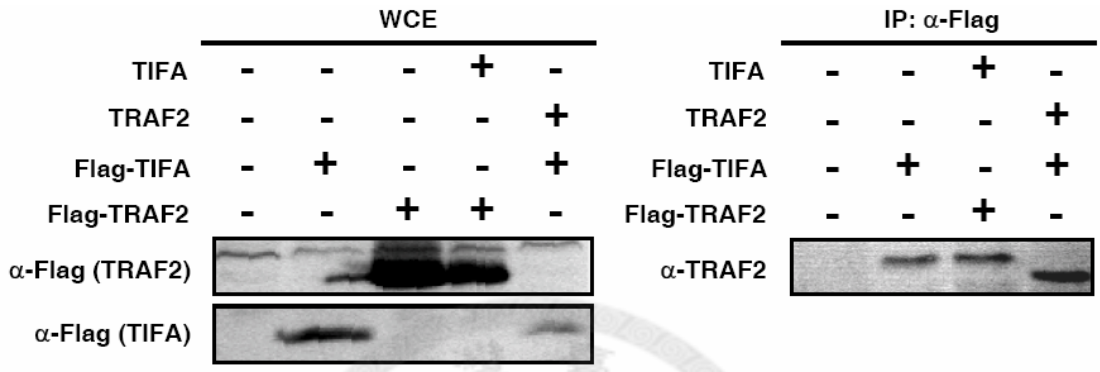

Figure 8. (A) Immunoprecipitation/Co-immunoprecipitation experiment to confirm TIFA-TRAF2 interaction *in vivo*.

Figure 8B. Co-localization of TIFA and TRAF2 *in vivo*.

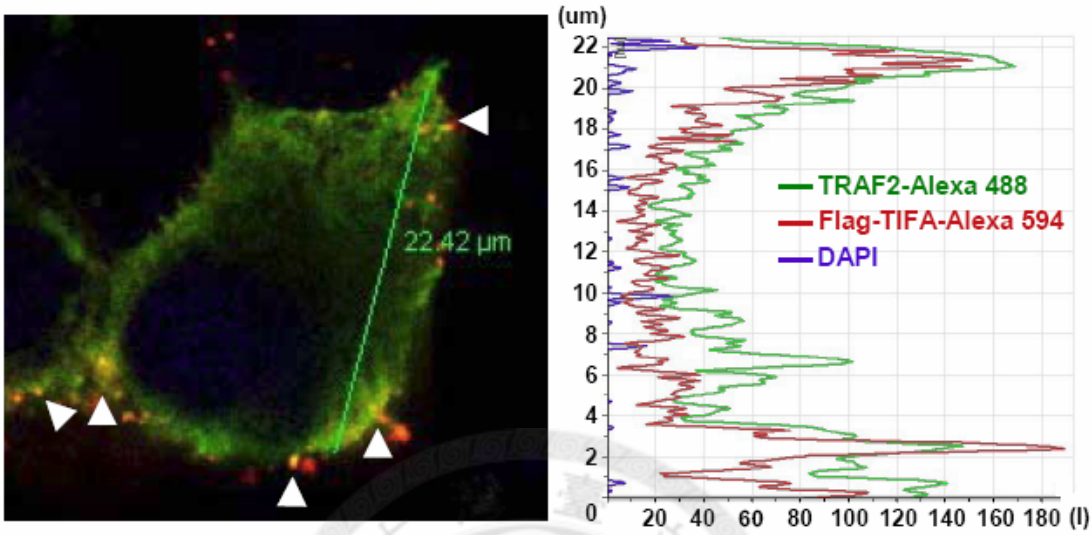

Figure 8. (B) Co-localization of over-expressed Flag-TIFA WT and non-tagged TRAF2 in the cytoplasm of HEK293T cells using confocal microscopy (indicated by white arrows in the superimposed images). The experimental condition was the same as that in Fig. 6(C) and Fig. 6(D) except TRAF2 was recognized by anti-TRAF2 antibody followed by Alexa 488-conjugated anti-mouse IgG and Flag-TIFA was recognized by anti-Flag antibody followed by Alexa 594-conjugated anti-rabbit IgG. The nuclei were counterstained with DAPI.

Figure 8C. TRAF2 domain structure and sequence alignment with hNIFK.

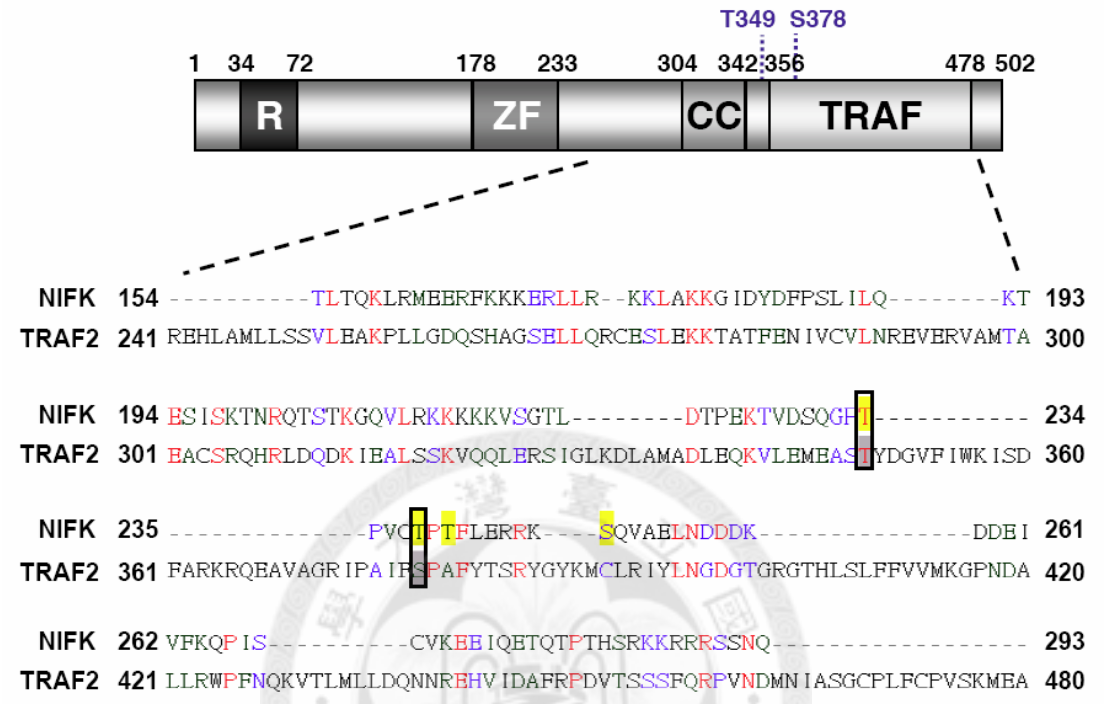

Figure 8. (C) Schematic overview of TRAF2 domain structures (top) and C-terminal sequence alignment of TRAF2 with hNIFK (bottom). Two sites of TRAF2, T349 and S378, that aligned with the two important phosphorylated threonine residues of NIFK (pT234 and pT238) are indicated in black boxes. Two other known phosphorylation sites on hNIFK are highlighted in yellow.

Figure 8D. MTH assay for TIFA WT and TRAF2 mutants.

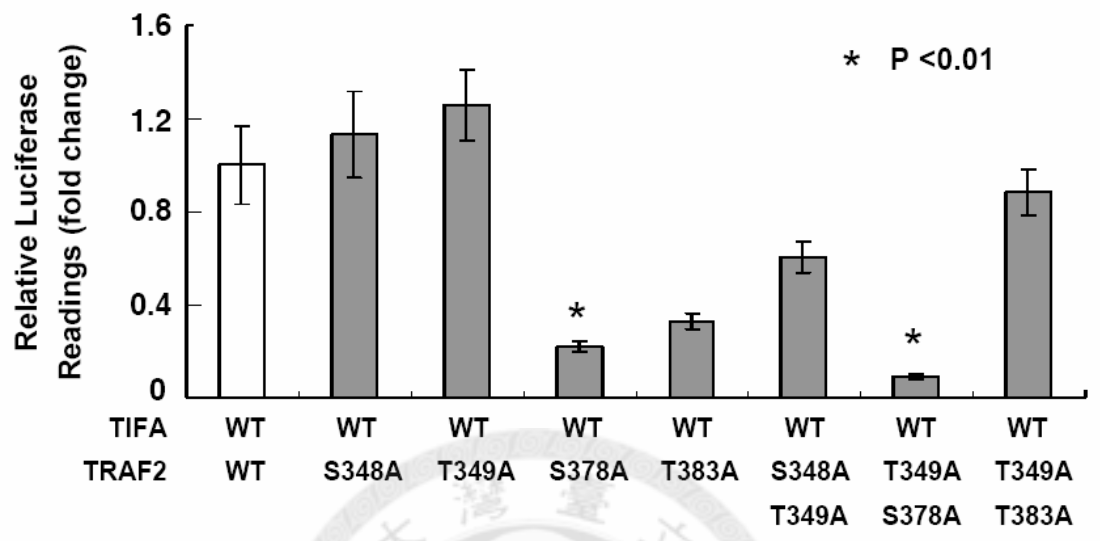

Figure 8. (D) Mammalian Two-Hybrid assay for TRAF2 mutants. T349 and S378 on TRAF2 are two important sites for TIFA-TRAF2 interaction.

Figure 8E. TRAF2 phosphorylation sites identified by MS analysis.

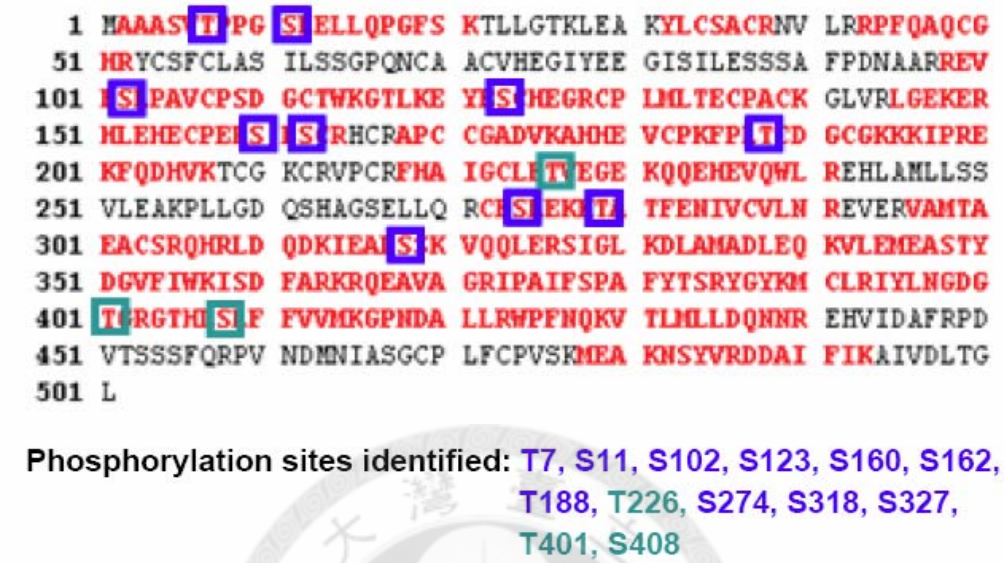

Figure 8. (E) A total of thirteen TRAF2 phosphorylation sites were identified by MS analysis. The matched peptides are highlighted in bold red and the identified sites are boxed in dark and light blue.

Figure 8F. AUC analysis of exogenous full-length TRAF2.

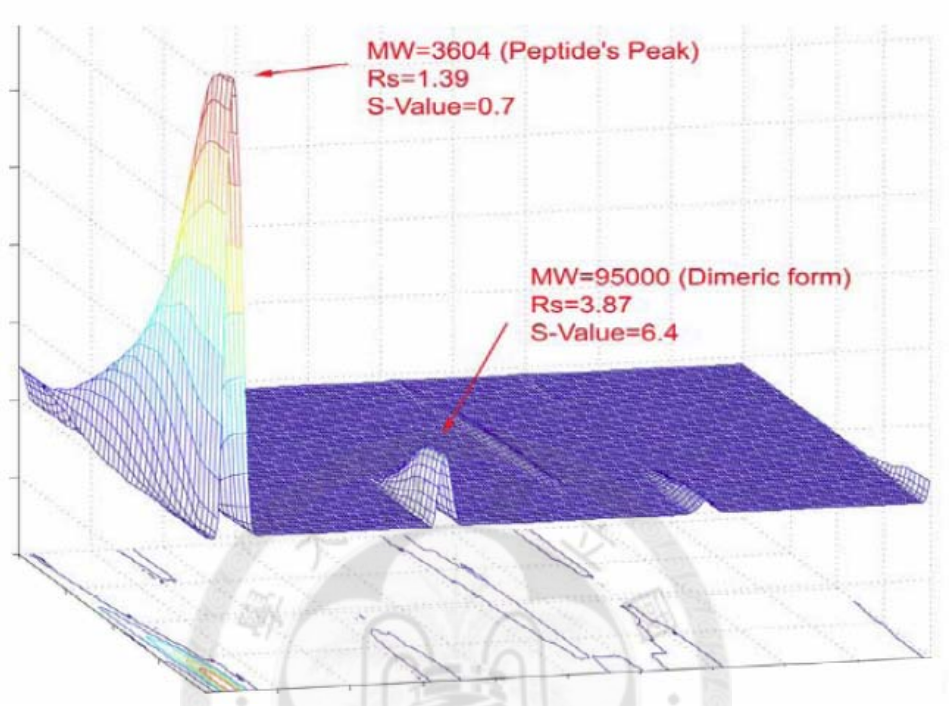

Figure 8. (F) AUC analysis suggests that over-expressed full-length TRAF2 is a dimer in solution.

Figure 8G. Structure of TRAF2 TRAF domain.

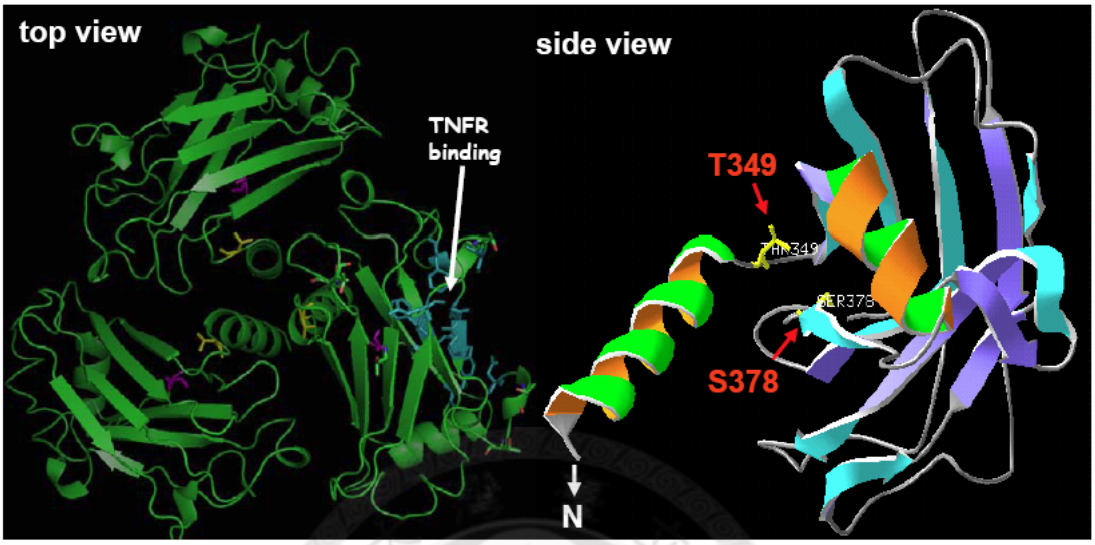

Figure 8. (G) Top and side views of the structures of human TRAF2 TRAF domain solved by Hao Wu's group (**PDB: 1CA4**) using X-ray crystallography. Positions of residues T349 and S378 are indicated as yellow sticks and red labels.

Figure 9. Proposed TIFA oligomerization model.

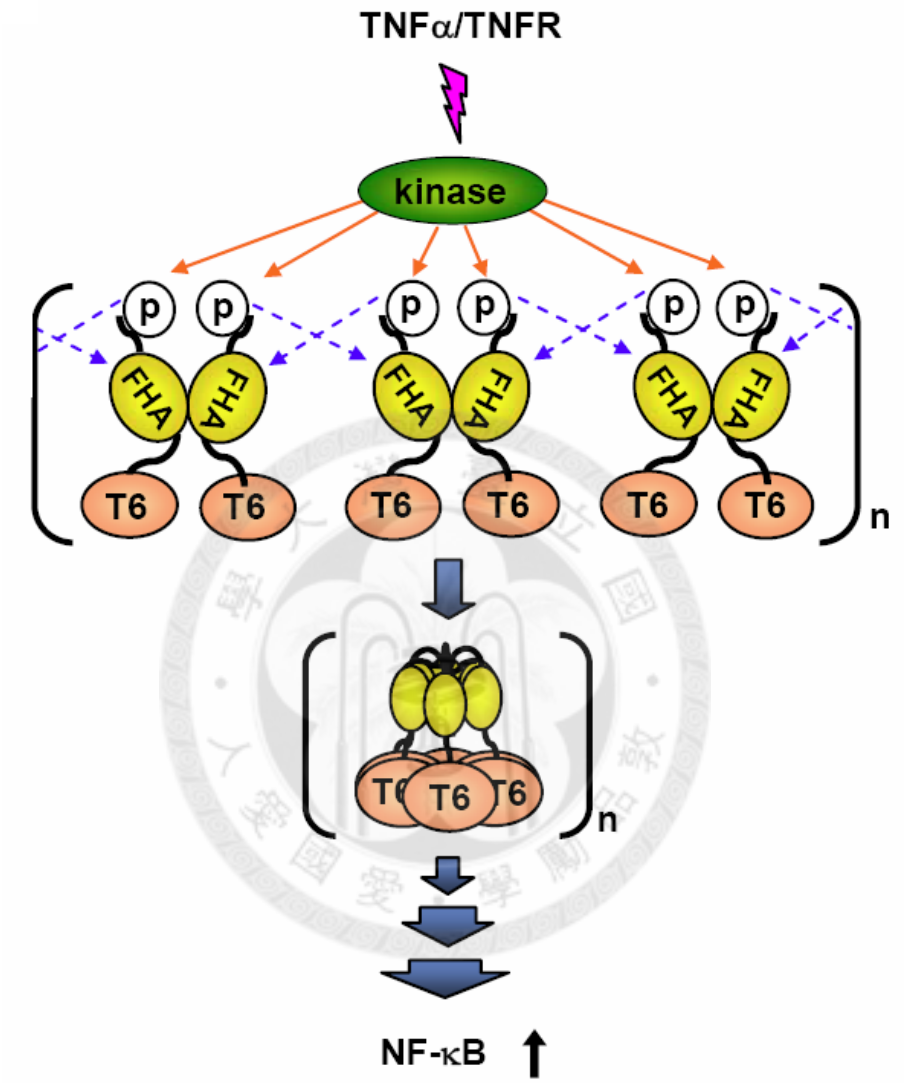

Figure 9. The proposed model for TIFA oligomerization that first takes place via intermolecular FHA-pT9 binding between TIFA dimers upon TNFα stimulation, then leads to TRAF6 (labeled as T6) oligomerization and subsequent NF-κB activation .

Chapter 6. TABLES

Table 1. Expression conditions for recombinant TIFA. The optimal conditions are highlighted in red color.

Expression vectors	pET28a (N and C-terminal His)	pET-Duet (N-terminal His)	pGEX-4T1 (N-terminal GST)	pET43.1 (C-terminus His)
Host cells	BL21 (DE3)	BL21 (Codon Plus)		
Media	LB	Minimal (M9)	Minimal (M9) + N15	Minimal (M9) + Se-Met
IPTG amounts	1mL of 1M IPTG into 1L of cell culture	600μL of 1M IPTG into 1L of cell culture		
Incubation temperatures	37°C	16°C		
Expression lengths	> 14hrs			

Table 2. Purification conditions for recombinant TIFA. The optimal conditions are highlighted in red color.

[Salt]	50mM	100mM	150mM	200mM	250mM	300mM
pH	6.5	7.0	7.5	8.0	8.5	9.0
Temperatures	4°C	25°C				
Buffers	Tris Base	Phosphate				
Reducing agent	β-ME (5mM)					
Glycerol (10%)	+10%					

Table 3. Different truncation constructs for recombinant TIFA. (**E:** expression yield. **S:** solubility and stability. **+:** protein expressed in large quantity or remained stable in solution. **−:** proteins not expressed, expressed in low yield, degraded, or precipitated. **?:** not yet tested. **red highlight:** not yet constructed.)

pET28a	E	S	pGEX-4T (with TEV site)	E	S	pET43.1	E	S
HIS-1~184-HIS	+	-	GST-1~135	?	?	1~184-HIS	+	+
HIS-1~163	+	-	GST-18~135	?	?	1~135-HIS	+	-
HIS-11~163	+	-	GST-1~150	?	?	11~135-HIS	-	-
HIS-11~163-HIS	+	-	GST-18~150	?	?	18~135-HIS	-	-
HIS-1~150	+	-				1~150-HIS	+	-
HIS-11~150	+	-				11~150-HIS	+	-
						18~150-HIS	-	-
						1~163-HIS	?	?
						11~163-HIS	?	?

pET-Duet	E	S	pGEX-4T1	E	S	pYES-2CT	E	S
HIS-1~184 + TRAF2	+	-	GST-1~184	+	-	1~184-HIS	?	?

Table 4. Screenings of crystallization conditions for native TIFA. The optimized conditions that can reproduce proteins crystals are highlighted in red.

Buffers	0.1~0.2M Immidazole malate	0.1~0.2M SPG	0.1~0.2M MES	0.1M Tris-Base
pH	7.5, 8.0, 8.5	7.0, 7.5, 8.0, 8.5, 9.0	5.5, 6.5, 7.5, 8.5	6.5, 7.0, 7.5, 8.0, 8.5, 9.0, 9.5, 10.0
Temperatures	4°C, 20°C	4°C, 20°C	4°C, 20°C	4°C, 8°C, 16°C, 20°C, 25°C
PEG	1~2% PEG 8000	7.5~27.5% PEG 1500	2, 4, 6, 8, 10 ,12% PEG 20000	5, 10, 15% PEG1500 4, 6, 8, 10% PEG8000 3, 4, 5% PEG10000
EtOH	N/A	N/A	N/A	5, 10, 15, 20%
Glycerol	N/A	N/A	N/A	10%
Additives	1.0M lithium sulphate	N/A	N/A	0.1M ATP disodium salt 0.5uL
Concentrations	12mg/mL	14mg/mL	14mg/mL	6, 8, 10, 12, 15, 16, 18mg/mL
Hanging vs. Sitting	Hanging Sitting	Hanging Sitting	Hanging Sitting	Hanging Sitting
Protein: Reservoir (Ratio)	1.0ul : 1.0ul 2.0ul : 1.0ul	1.0ul : 1.0ul 1.5ul : 1.0ul 2.0ul : 1.0ul	0.5ul : 1.0ul 0.8ul : 1.0ul 1.0ul : 1.0ul 1.5ul : 1.0ul 2.0ul : 1.0ul	0.5ul : 1.0ul 0.8ul : 1.0ul 1.0ul : 1.0ul 1.5ul : 1.0ul 2.0ul : 1.0ul 2.0ul : 2.0ul

Table 5. A lot of different cryo-protectants in different percentages were screened for both native and Se-Met labeled TIFA crystals. PEG1500 (ideal percentage highlighted in red color) has provided best cryo-protection for the crystals so far.

Ethylene Glycol	2-Methyl-2,4-pentanediol	Glycerol	PEG1500
20, 30, 100%	10, 15, 25, 100%	10, 15, 20, 25, 30, 100%	15, 22, 26, 27, 28~32, 33~36, 50%

Perfluoropolyether PFO-X125/03	Paraffin Oil	Silicon Oil	AI's Oil
50%	100%	100%	100%

Table 6. Native TIFA crystals were soaked in crystallization buffers containing different heavy atoms. MAD data sets have been collected for those highlighted in red color.

Heavy atom Au (Native TIFA)	Heavy atom Pt (Native TIFA)	Heavy atom Hg (Native TIFA)
Gold (I) Potassium Cyanide	Potassium Tetrachloroplatinate (II)	Ethyl Mercuric Phosphate
Potassium Tetrachloroaurate (III)	Ammonium Tetrachloroplatinate (II)	Ethylmercurithiosalicylic Acid, sodium salt
Sodium Tetrachloroaurate (III)	Potassium Hexachloroplatinate (IV)	Mercury (II) Potassium Iodide
Gold (III) Chloride	Potassium Tetranitroplatinate (II)	Ethylmercury Chloride
Gold Chloride	Potassium Tetracyanoplatinate (II)	Mercury (II) Cyanide
Gold Potassium Bromide	Dichloroethylenediamine Platinum (II)	Methylmercury (II) Bromide
	Potassium Hexabromoplatinate (IV)	
	Platinum Potassium Thiocyanate	

Table 7. Optimized conditions for crystallization of Se-Met labeled TIFA were highlighted in red color.

Methods	Additives (Se-Met TIFA)	Protein: Additive (Ratio)
microseeding	0.1M Praseodymium (III) Acetate	1.0uL : 0.2uL
macroseeding	0.1M Taurine	1.0uL : 0.3uL
microbatch	30% v/v Glycerol	1.0uL : 0.5uL
	3.0M NDSB-195	1.0uL : 0.7uL
	2.0M NDSB-211	1.5uL : 0.5uL
	2.0M NDSB-221	1.5uL : 1.0uL
	40% v/v n-Propanol	

Table 8. Statistics of two best data sets collected from native and Se-Met labeled TIFA protein crystals.

	Native TIFA Crystal			Se-Met TIFA Crystal			
Data collection							
Space group	**P321**			**P321**			
Cell dimensions							
a, *b*, *c* (Å)	**41.21**	**41.21**	**178.91**	**41.21**	**41.21**	**178.91**	
α, β, γ (°)	**90.00**	**90.00**	**120.00**	**90.00**	**90.00**	**120.00**	
Wavelength	**0.9**			**0.979247**		**0.97893**	**0.96400**
Resolution (Å)	**2.3**			**3.0**		**3.0**	**3.0**
Completeness (%)	**99.8**			**99.9**		**99.4**	**99.4**
Redundancy	**8.4**			**7.9**		**7.8**	**7.7**

Table 9. All TIFA mutants in different vectors for different experiments.

pcDNA3.1	pCMV-Tag2a		
G50A	G50A	T12A	R51AS66AR67A
R51A	R51A	T14A	R51AK88AN89A
N52A	N52A	T19A	G50AR51AS66AR67A
S66A	S66A	E178A	Myc + pcDNA3.1
R67A	R67A	T9D	T2A
R51AS66A	K88A	R51AS66A	T9A
G50AR51AS66A	N89A	R51AK88A	T12A
R51AS66AR67A	T2A	R51AN89A	T14A
G50AR51AS66AR67A	T9A	G50AR51AS66A	T19A

pBIND		
G50A	R51AS91A	G50AR51AS66AR67A
R51A	R51AT94A	R51AS66AR67AK88A
N52A	R51AN95A	R51AS66AR67AN89A
S66A	K88AN89A	R51AS66AR67AK88AN89A
R67A	R51AK88A	R51AS66AR67AK93AT94A
K88A	R51AN89A	R51AS66AR67AK93AT94AN95A
N89A	G50AR51AS66A	R51AS66AR67AK92AK93AT94AN95A
E178A	R51AS66AR67A	R51AS66AR67AK88AN89AK92AK93AT94AN95A
R51AS66A	R51AK88AN89A	

pACT	
G50A	R51AS66A
R51A	G50AR51AS66A
N52A	R51AS66AR67A
S66A	G50AR51AS66AR67A
R67A	

pET43.1	
T9A	R51AK88A
R51A	R51AN89A
K88A	R51AK88AN89A
N89A	
G50A	

Table 10. All TRAF2 mutants constructed for mammalian two-hybrid assay.

pcDNA3.1	pCMV-Tag2a	pACT	pBIND
S348A	S348A	S348A	S348A
T349A	T349A	T349A	T349A
S378A	S378A	S378A	S378A
T383A	T383A	T383A	T383A
T349D	T349D	T349D	S348AT349A
S378D	S378D	S378D	T349AS378A
T349E	T349E	T349E	T349AT383A
S378C	S378C	S378C	
S348AT349A	S348AT349A	S348AT349A	
T349AS378A	T349AS378A	T349AS378A	
T349AT383A	T349AT383A	T349AT383A	
T349DS378D	T349DS378D	T349DS378D	
T349ES378C	T349ES378C	T349ES378C	
A420DL421M	A420DL421M	A420DL421M	

Chapter 7. REFERENCES

1. **Adhikari, A., M. Xu, and Z. J. Chen.** 2007. Ubiquitin-mediated activation of TAK1 and IKK. Oncogene **26:**3214-26.
2. **Ahn, J., and C. Prives.** 2002. Checkpoint kinase 2 (Chk2) monomers or dimers phosphorylate Cdc25C after DNA damage regardless of threonine 68 phosphorylation. J Biol Chem **277:**48418-26.
3. **Barthe, P., C. Roumestand, M. J. Canova, L. Kremer, C. Hurard, V. Molle, and M. Cohen-Gonsaud.** 2009. Dynamic and structural characterization of a bacterial FHA protein reveals a new autoinhibition mechanism. Structure **17:**568-78.
4. **Baud, V., Z. G. Liu, B. Bennett, N. Suzuki, Y. Xia, and M. Karin.** 1999. Signaling by proinflammatory cytokines: oligomerization of TRAF2 and TRAF6 is sufficient for JNK and IKK activation and target gene induction via an amino-terminal effector domain. Genes Dev **13:**1297-308.
5. **Blackwell, K., L. Zhang, G. S. Thomas, S. Sun, H. Nakano, and H. Habelhah.** 2009. TRAF2 phosphorylation modulates tumor necrosis factor alpha-induced gene expression and cell resistance to apoptosis. Mol Cell Biol **29:**303-14.
6. **Bonizzi, G., and M. Karin.** 2004. The two NF-kappaB activation pathways and their role in innate and adaptive immunity. Trends Immunol **25:**280-8.
7. **Byeon, I. J., H. Li, H. Song, A. M. Gronenborn, and M. D. Tsai.** 2005. Sequential phosphorylation and multisite interactions characterize specific target recognition by the FHA domain of Ki67. Nat Struct Mol Biol **12:**987-93.
8. **Byeon, I. J., S. Yongkiettrakul, and M. D. Tsai.** 2001. Solution structure of the yeast Rad53 FHA2 complexed with a phosphothreonine peptide pTXXL: comparison with the structures of FHA2-pYXL and FHA1-pTXXD complexes. J Mol Biol **314:**577-88.
9. **Cai, Z., N. H. Chehab, and N. P. Pavletich.** 2009. Structure and activation mechanism of the CHK2 DNA damage checkpoint kinase. Mol Cell **35:**818-29.

10. **Chen, L., W. Dong, T. Zou, L. Ouyang, G. He, Y. Liu, and Y. Qi.** 2008. Protein phosphatase 4 negatively regulates LPS cascade by inhibiting ubiquitination of TRAF6. FEBS Lett **582:**2843-9.

11. **Chung, J. Y., Y. C. Park, H. Ye, and H. Wu.** 2002. All TRAFs are not created equal: common and distinct molecular mechanisms of TRAF-mediated signal transduction. J Cell Sci **115:**679-88.

12. **Clark, K., O. Takeuchi, S. Akira, and P. Cohen.** 2011. The TRAF-associated protein TANK facilitates cross-talk within the IkappaB kinase family during Toll-like receptor signaling. Proc Natl Acad Sci U S A **108:**17093-8.

13. **Dempsey, P. W., S. E. Doyle, J. Q. He, and G. Cheng.** 2003. The signaling adaptors and pathways activated by TNF superfamily. Cytokine Growth Factor Rev **14:**193-209.

14. **Dumitru, C. D., J. D. Ceci, C. Tsatsanis, D. Kontoyiannis, K. Stamatakis, J. H. Lin, C. Patriotis, N. A. Jenkins, N. G. Copeland, G. Kollias, and P. N. Tsichlis.** 2000. TNF-alpha induction by LPS is regulated posttranscriptionally via a Tpl2/ERK-dependent pathway. Cell **103:**1071-83.

15. **Durocher, D., and S. P. Jackson.** 2002. The FHA domain. FEBS Lett **513:**58-66.

16. **Durocher, D., I. A. Taylor, D. Sarbassova, L. F. Haire, S. L. Westcott, S. P. Jackson, S. J. Smerdon, and M. B. Yaffe.** 2000. The molecular basis of FHA domain:phosphopeptide binding specificity and implications for phospho-dependent signaling mechanisms. Mol Cell **6:**1169-82.

17. **Ea, C. K., L. Sun, J. Inoue, and Z. J. Chen.** 2004. TIFA activates IkappaB kinase (IKK) by promoting oligomerization and ubiquitination of TRAF6. Proc Natl Acad Sci U S A **101:**15318-23.

18. **Fan, A. C., D. Deb-Basu, M. W. Orban, J. R. Gotlib, Y. Natkunam, R. O'Neill, R. A. Padua, L. Xu, D. Taketa, A. E. Shirer, S. Beer, A. X. Yee, D. W. Voehringer, and D. W. Felsher.** 2009. Nanofluidic proteomic assay for serial analysis of oncoprotein activation in clinical specimens. Nat Med **15:**566-71.

19. **Fang, C. Y., H. Y. Chen, M. Wang, P. L. Chen, C. F. Chang, L. S. Chen, C. H. Shen, W. C. Ou, M. D. Tsai, P. H. Hsu, and D. Chang.** 2010. Global analysis of modifications of the human BK virus structural proteins by LC-MS/MS. Virology **402:**164-76.

20. **Force, W. R., A. A. Glass, C. A. Benedict, T. C. Cheung, J. Lama, and C. F. Ware.** 2000. Discrete signaling regions in the lymphotoxin-beta receptor for tumor necrosis factor receptor-associated factor binding, subcellular localization, and activation of cell death and NF-kappaB pathways. J Biol Chem **275:**11121-9.

21. **Habelhah, H., S. Takahashi, S. G. Cho, T. Kadoya, T. Watanabe, and Z. Ronai.** 2004. Ubiquitination and translocation of TRAF2 is required for activation of JNK but not of p38 or NF-kappaB. EMBO J **23:**322-32.

22. **Hauer, J., S. Puschner, P. Ramakrishnan, U. Simon, M. Bongers, C. Federle, and H. Engelmann.** 2005. TNF receptor (TNFR)-associated factor (TRAF) 3 serves as an inhibitor of TRAF2/5-mediated activation of the noncanonical NF-kappaB pathway by TRAF-binding TNFRs. Proc Natl Acad Sci U S A **102:**2874-9.

23. **Hayden, M. S., and S. Ghosh.** 2004. Signaling to NF-kappaB. Genes Dev **18:**2195-224.

24. **Hofmann, K., and P. Bucher.** 1995. The FHA domain: a putative nuclear signalling domain found in protein kinases and transcription factors. Trends Biochem Sci **20:**347-9.

25. **Huang, Q., J. Yang, Y. Lin, C. Walker, J. Cheng, Z. G. Liu, and B. Su.** 2004. Differential regulation of interleukin 1 receptor and Toll-like receptor signaling by MEKK3. Nat Immunol **5:**98-103.

26. **Ishida, T., S. Mizushima, S. Azuma, N. Kobayashi, T. Tojo, K. Suzuki, S. Aizawa, T. Watanabe, G. Mosialos, E. Kieff, T. Yamamoto, and J. Inoue.** 1996. Identification of TRAF6, a novel tumor necrosis factor receptor-associated factor

protein that mediates signaling from an amino-terminal domain of the CD40 cytoplasmic region. J Biol Chem **271:**28745-8.

27. **Jungmichel, S., J. A. Clapperton, J. Lloyd, F. J. Hari, C. Spycher, L. Pavic, J. Li, L. F. Haire, M. Bonalli, D. H. Larsen, C. Lukas, J. Lukas, D. Macmillan, M. L. Nielsen, M. Stucki, and S. J. Smerdon.** 2012. The molecular basis of ATM-dependent dimerization of the Mdc1 DNA damage checkpoint mediator. Nucleic Acids Res.

28. **Kanamori, M., H. Suzuki, R. Saito, M. Muramatsu, and Y. Hayashizaki.** 2002. T2BP, a novel TRAF2 binding protein, can activate NF-kappaB and AP-1 without TNF stimulation. Biochem Biophys Res Commun **290:**1108-13.

29. **Lee, H., C. Yuan, A. Hammet, A. Mahajan, E. S. Chen, M. R. Wu, M. I. Su, J. Heierhorst, and M. D. Tsai.** 2008. Diphosphothreonine-specific interaction between an SQ/TQ cluster and an FHA domain in the Rad53-Dun1 kinase cascade. Mol Cell **30:**767-78.

30. **Li, H., and X. Lin.** 2008. Positive and negative signaling components involved in TNFalpha-induced NF-kappaB activation. Cytokine **41:**1-8.

31. **Li, J., I. A. Taylor, J. Lloyd, J. A. Clapperton, S. Howell, D. MacMillan, and S. J. Smerdon.** 2008. Chk2 oligomerization studied by phosphopeptide ligation: implications for regulation and phosphodependent interactions. J Biol Chem **283:**36019-30.

32. **Li, J., B. L. Williams, L. F. Haire, M. Goldberg, E. Wilker, D. Durocher, M. B. Yaffe, S. P. Jackson, and S. J. Smerdon.** 2002. Structural and functional versatility of the FHA domain in DNA-damage signaling by the tumor suppressor kinase Chk2. Mol Cell **9:**1045-54.

33. **Li, S., L. Wang, M. A. Berman, Y. Zhang, and M. E. Dorf.** 2006. RNAi screen in mouse astrocytes identifies phosphatases that regulate NF-kappaB signaling. Mol Cell **24:**497-509.

34. **Li, S., L. Wang, and M. E. Dorf.** 2009. PKC phosphorylation of TRAF2 mediates IKKalpha/beta recruitment and K63-linked polyubiquitination. Mol Cell **33:**30-42.

35. **Liang, X., and S. R. Van Doren.** 2008. Mechanistic insights into phosphoprotein-binding FHA domains. Acc Chem Res **41:**991-9.

36. **Liao, H., C. Yuan, M. I. Su, S. Yongkiettrakul, D. Qin, H. Li, I. J. Byeon, D. Pei, and M. D. Tsai.** 2000. Structure of the FHA1 domain of yeast Rad53 and identification of binding sites for both FHA1 and its target protein Rad9. J Mol Biol **304:**941-51.

37. **Liu, J., S. Luo, H. Zhao, J. Liao, J. Li, C. Yang, B. Xu, D. F. Stern, X. Xu, and K. Ye.** 2012. Structural mechanism of the phosphorylation-dependent dimerization of the MDC1 forkhead-associated domain. Nucleic Acids Res.

38. **Lloyd, J., J. R. Chapman, J. A. Clapperton, L. F. Haire, E. Hartsuiker, J. Li, A. M. Carr, S. P. Jackson, and S. J. Smerdon.** 2009. A supramodular FHA/BRCT-repeat architecture mediates Nbs1 adaptor function in response to DNA damage. Cell **139:**100-11.

39. **Lomaga, M. A., W. C. Yeh, I. Sarosi, G. S. Duncan, C. Furlonger, A. Ho, S. Morony, C. Capparelli, G. Van, S. Kaufman, A. van der Heiden, A. Itie, A. Wakeham, W. Khoo, T. Sasaki, Z. Cao, J. M. Penninger, C. J. Paige, D. L. Lacey, C. R. Dunstan, W. J. Boyle, D. V. Goeddel, and T. W. Mak.** 1999. TRAF6 deficiency results in osteopetrosis and defective interleukin-1, CD40, and LPS signaling. Genes Dev **13:**1015-24.

40. **Luo, K., J. Yuan, and Z. Lou.** 2011. Oligomerization of MDC1 is important for proper DNA damage response. J Biol Chem.

41. **Mahajan, A., C. Yuan, H. Lee, E. S. Chen, P. Y. Wu, and M. D. Tsai.** 2008. Structure and function of the phosphothreonine-specific FHA domain. Sci Signal **1:**re12.

42. **Mahajan, A., C. Yuan, B. L. Pike, J. Heierhorst, C. F. Chang, and M. D. Tsai.** 2005. FHA domain-ligand interactions: importance of integrating chemical and biological approaches. J Am Chem Soc **127:**14572-3.

43. **Malinin, N. L., M. P. Boldin, A. V. Kovalenko, and D. Wallach.** 1997. MAP3K-related kinase involved in NF-kappaB induction by TNF, CD95 and IL-1. Nature **385:**540-4.

44. **Matsumura, T., J. Kawamura-Tsuzuku, T. Yamamoto, K. Semba, and J. Inoue.** 2009. TRAF-interacting protein with a forkhead-associated domain B (TIFAB) is a negative regulator of the TRAF6-induced cellular functions. J Biochem **146:**375-81.

45. **Matsumura, T., K. Semba, S. Azuma, S. Ikawa, J. Gohda, T. Akiyama, and J. Inoue.** 2004. TIFAB inhibits TIFA, TRAF-interacting protein with a forkhead-associated domain. Biochem Biophys Res Commun **317:**230-4.

46. **Minoda, Y., K. Saeki, D. Aki, H. Takaki, T. Sanada, K. Koga, T. Kobayashi, G. Takaesu, and A. Yoshimura.** 2006. A novel Zinc finger protein, ZCCHC11, interacts with TIFA and modulates TLR signaling. Biochem Biophys Res Commun **344:**1023-30.

47. **Muzio, M., and A. Mantovani.** 2001. Toll-like receptors (TLRs) signalling and expression pattern. J Endotoxin Res **7:**297-300.

48. **Naito, A., S. Azuma, S. Tanaka, T. Miyazaki, S. Takaki, K. Takatsu, K. Nakao, K. Nakamura, M. Katsuki, T. Yamamoto, and J. Inoue.** 1999. Severe osteopetrosis, defective interleukin-1 signalling and lymph node organogenesis in TRAF6-deficient mice. Genes Cells **4:**353-62.

49. **Nott, T. J., G. Kelly, L. Stach, J. Li, S. Westcott, D. Patel, D. M. Hunt, S. Howell, R. S. Buxton, H. M. O'Hare, and S. J. Smerdon.** 2009. An intramolecular switch regulates phosphoindependent FHA domain interactions in Mycobacterium tuberculosis. Sci Signal **2:**ra12.

50. **O'Neill, R. A., A. Bhamidipati, X. Bi, D. Deb-Basu, L. Cahill, J. Ferrante, E. Gentalen, M. Glazer, J. Gossett, K. Hacker, C. Kirby, J. Knittle, R. Loder, C. Mastroieni, M. Maclaren, T. Mills, U. Nguyen, N. Parker, A. Rice, D. Roach, D. Suich, D. Voehringer, K. Voss, J. Yang, T. Yang, and P. B. Vander Horn.** 2006. Isoelectric focusing technology quantifies protein signaling in 25 cells. Proc Natl Acad Sci U S A **103:**16153-8.

51. **Park, Y. C., V. Burkitt, A. R. Villa, L. Tong, and H. Wu.** 1999. Structural basis for self-association and receptor recognition of human TRAF2. Nature **398:**533-8.

52. **Pennell, S., S. Westcott, M. Ortiz-Lombardia, D. Patel, J. Li, T. J. Nott, D. Mohammed, R. S. Buxton, M. B. Yaffe, C. Verma, and S. J. Smerdon.** 2010. Structural and functional analysis of phosphothreonine-dependent FHA domain interactions. Structure **18:**1587-95.

53. **Pomerantz, J. L., and D. Baltimore.** 2002. Two pathways to NF-kappaB. Mol Cell **10:**693-5.

54. **Pullen, S. S., H. G. Miller, D. S. Everdeen, T. T. Dang, J. J. Crute, and M. R. Kehry.** 1998. CD40-tumor necrosis factor receptor-associated factor (TRAF) interactions: regulation of CD40 signaling through multiple TRAF binding sites and TRAF hetero-oligomerization. Biochemistry **37:**11836-45.

55. **Rothe, M., S. C. Wong, W. J. Henzel, and D. V. Goeddel.** 1994. A novel family of putative signal transducers associated with the cytoplasmic domain of the 75 kDa tumor necrosis factor receptor. Cell **78:**681-92.

56. **Sanz, L., M. T. Diaz-Meco, H. Nakano, and J. Moscat.** 2000. The atypical PKC-interacting protein p62 channels NF-kappaB activation by the IL-1-TRAF6 pathway. EMBO J **19:**1576-86.

57. **Seibenhener, M. L., J. R. Babu, T. Geetha, H. C. Wong, N. R. Krishna, and M. W. Wooten.** 2004. Sequestosome 1/p62 is a polyubiquitin chain binding protein involved in ubiquitin proteasome degradation. Mol Cell Biol **24:**8055-68.

58. **Shi, C. S., and J. H. Kehrl.** 2003. Tumor necrosis factor (TNF)-induced germinal center kinase-related (GCKR) and stress-activated protein kinase (SAPK) activation depends upon the E2/E3 complex Ubc13-Uev1A/TNF receptor-associated factor 2 (TRAF2). J Biol Chem **278:**15429-34.

59. **Sun, Z., J. Hsiao, D. S. Fay, and D. F. Stern.** 1998. Rad53 FHA domain associated with phosphorylated Rad9 in the DNA damage checkpoint. Science **281:**272-4.

60. **Tada, K., T. Okazaki, S. Sakon, T. Kobarai, K. Kurosawa, S. Yamaoka, H. Hashimoto, T. W. Mak, H. Yagita, K. Okumura, W. C. Yeh, and H. Nakano.** 2001. Critical roles of TRAF2 and TRAF5 in tumor necrosis factor-induced NF-kappa B activation and protection from cell death. J Biol Chem **276:**36530-4.

61. **Takatsuna, H., H. Kato, J. Gohda, T. Akiyama, A. Moriya, Y. Okamoto, Y. Yamagata, M. Otsuka, K. Umezawa, K. Semba, and J. Inoue.** 2003. Identification of TIFA as an adapter protein that links tumor necrosis factor receptor-associated factor 6 (TRAF6) to interleukin-1 (IL-1) receptor-associated kinase-1 (IRAK-1) in IL-1 receptor signaling. J Biol Chem **278:**12144-50.

62. **Takeuchi, M., M. Rothe, and D. V. Goeddel.** 1996. Anatomy of TRAF2. Distinct domains for nuclear factor-kappaB activation and association with tumor necrosis factor signaling proteins. J Biol Chem **271:**19935-42.

63. **Thomas, G. S., L. Zhang, K. Blackwell, and H. Habelhah.** 2009. Phosphorylation of TRAF2 within its RING domain inhibits stress-induced cell death by promoting IKK and suppressing JNK activation. Cancer Res **69:**3665-72.

64. **Trauzold, A., C. Roder, B. Sipos, K. Karsten, A. Arlt, P. Jiang, J. I. Martin-Subero, D. Siegmund, S. Muerkoster, L. Pagerols-Raluy, R. Siebert, H. Wajant, and H. Kalthoff.** 2005. CD95 and TRAF2 promote invasiveness of pancreatic cancer cells. FASEB J **19:**620-2.

65. **Wang, C., L. Deng, M. Hong, G. R. Akkaraju, J. Inoue, and Z. J. Chen.** 2001. TAK1 is a ubiquitin-dependent kinase of MKK and IKK. Nature **412:**346-51.

66. **Wang, K. Z., D. L. Galson, and P. E. Auron.** 2010. TRAF6 is autoinhibited by an intramolecular interaction which is counteracted by trans-ubiquitination. J Cell Biochem **110:**763-71.

67. **Wang, K. Z., N. Wara-Aswapati, J. A. Boch, Y. Yoshida, C. D. Hu, D. L. Galson, and P. E. Auron.** 2006. TRAF6 activation of PI 3-kinase-dependent cytoskeletal changes is cooperative with Ras and is mediated by an interaction with cytoplasmic Src. J Cell Sci **119:**1579-91.

68. **Weston, V. J., B. Austen, W. Wei, E. Marston, A. Alvi, S. Lawson, P. J. Darbyshire, M. Griffiths, F. Hill, J. R. Mann, P. A. Moss, A. M. Taylor, and T. Stankovic.** 2004. Apoptotic resistance to ionizing radiation in pediatric B-precursor acute lymphoblastic leukemia frequently involves increased NF-kappaB survival pathway signaling. Blood **104:**1465-73.

69. **Wu, C. J., D. B. Conze, X. Li, S. X. Ying, J. A. Hanover, and J. D. Ashwell.** 2005. TNF-alpha induced c-IAP1/TRAF2 complex translocation to a Ubc6-containing compartment and TRAF2 ubiquitination. EMBO J **24:**1886-98.

70. **Wu, H. H., P. Y. Wu, K. F. Huang, Y. Y. Kao, and M. D. Tsai.** 2012. Structural delineation of MDC1-FHA domain binding with CHK2-pThr68. Biochemistry **51:**575-7.

71. **Xu, L. G., L. Y. Li, and H. B. Shu.** 2004. TRAF7 potentiates MEKK3-induced AP1 and CHOP activation and induces apoptosis. J Biol Chem **279:**17278-82.

72. **Xu, X., L. M. Tsvetkov, and D. F. Stern.** 2002. Chk2 activation and phosphorylation-dependent oligomerization. Mol Cell Biol **22:**4419-32.

73. **Yang, J., Y. Lin, Z. Guo, J. Cheng, J. Huang, L. Deng, W. Liao, Z. Chen, Z. Liu, and B. Su.** 2001. The essential role of MEKK3 in TNF-induced NF-kappaB activation. Nat Immunol **2:**620-4.

74. **Ye, H., J. R. Arron, B. Lamothe, M. Cirilli, T. Kobayashi, N. K. Shevde, D. Segal, O. K. Dzivenu, M. Vologodskaia, M. Yim, K. Du, S. Singh, J. W. Pike, B.**

G. Darnay, Y. Choi, and H. Wu. 2002. Distinct molecular mechanism for initiating TRAF6 signalling. Nature **418:**443-7.

75. **Yin, Q., S. C. Lin, B. Lamothe, M. Lu, Y. C. Lo, G. Hura, L. Zheng, R. L. Rich, A. D. Campos, D. G. Myszka, M. J. Lenardo, B. G. Darnay, and H. Wu.** 2009. E2 interaction and dimerization in the crystal structure of TRAF6. Nat Struct Mol Biol **16:**658-66.

76. **Zapata, J. M., K. Pawlowski, E. Haas, C. F. Ware, A. Godzik, and J. C. Reed.** 2001. A diverse family of proteins containing tumor necrosis factor receptor-associated factor domains. J Biol Chem **276:**24242-52.

77. **Zhang, L., K. Blackwell, A. Altaeva, Z. Shi, and H. Habelhah.** 2011. TRAF2 phosphorylation promotes NF-kappaB-dependent gene expression and inhibits oxidative stress-induced cell death. Mol Biol Cell **22:**128-40.

78. **Zhang, L., K. Blackwell, Z. Shi, and H. Habelhah.** 2010. The RING domain of TRAF2 plays an essential role in the inhibition of TNFalpha-induced cell death but not in the activation of NF-kappaB. J Mol Biol **396:**528-39.

79. **Zhang, L., K. Blackwell, G. S. Thomas, S. Sun, W. C. Yeh, and H. Habelhah.** 2009. TRAF2 suppresses basal IKK activity in resting cells and TNFalpha can activate IKK in TRAF2 and TRAF5 double knockout cells. J Mol Biol **389:**495-510.

80. **Zhao, Q., and F. S. Lee.** 1999. Mitogen-activated protein kinase/ERK kinase kinases 2 and 3 activate nuclear factor-kappaB through IkappaB kinase-alpha and IkappaB kinase-beta. J Biol Chem **274:**8355-8.

81. **Zheng, C., V. Kabaleeswaran, Y. Wang, G. Cheng, and H. Wu.** 2010. Crystal structures of the TRAF2: cIAP2 and the TRAF1: TRAF2: cIAP2 complexes: affinity, specificity, and regulation. Mol Cell **38:**101-13.

Appendix

List of Supplementary Figures

List of Abbreviations

1. **1-D:** one dimension
2. **Ala or A:** alanine
3. **AP-1:** activator protein 1
4. **Arg or R:** arginine
5. **Asn or D:** aspartic acid
6. **ATP:** adenosine-5'-triphosphate
7. **AUC:** analytical ultra centrifugation
8. **BSA:** bovine serum albumin
9. **CC:** coiled coil
10. **CD:** circular dichroism
11. **CHAPS:** {3-[(3-cholamidopropyl)-dimethylammonio]-1-propanesulfonate}
12. **CHK2:** checkpoint kinase 2
13. **CO_2:** carbon dioxide
14. **Cys or C:** cysteine
15. **Da:** Dalton
16. **DAPI:** 4',6'-diamidino-2-phenylindole
17. **DDM:** n-dodecyl β-D-maltoside
18. **DMEM:** Dulbecco's modified Eagle medium
19. **DMSO:** dimethyl sulfoxide
20. **DTT:** dithiothreitol
21. **ERK:** extracellular-signal-regulated kinases
22. **EtOH:** ethanol
23. **FBS:** fetal bovine serum
24. **FHA:** forkhead-associated
25. **FITC:** fluorescein isothiocyanaate
26. **FPLC:** fast protein liquid chromatography
27. **Glu or E:** glutamic acid

28. **GST:** glutathione S-transferase
29. **HEK 293T:** human embryonic kidney 293 cell line with large T-antigen from SV40 virus transformed
30. **His:** histidine
31. **HRP:** Horseradish peroxidase
32. **HSQC:** Heteronuclear Single Quantum Correlation
33. **IBC:** Institute of Biological Chemistry, Academia Sinica
34. **IEF:** isoelectric focusing
35. **IFA:** Immunofluorescence assay
36. **IgG:** Immunoglobulin G
37. **IKK:** IκB kinase
38. **IL-1R:** interleukin-1 receptor
39. **IL-1β:** interleukin-1β
40. **IP:** immunoprecipitation
41. **IRAK:** interleukin-1 receptor-associated kinase
42. **ITC:** isothermal titration calorimetry
43. **IκB:** inhibitor of kappa B
44. **JNK:** c-Jun amino-terminal kinase
45. **KAPP:** kinase-associated protein phosphatase
46. **LC-MS/MS:** liquid chromatography-tandem MS
47. **LPS:** lipopolysaccharide
48. **LTQ-FT:** linear quadrupole ion trap-Fourier transform
49. **Lys or K:** lysine
50. **mAb:** monoclonal antibody
51. **MAD:** multi-wavelength anomalous dispersion
52. **MAP3K:** mitogen-activated protein kinase kinase kinase
53. **MATH:** meprin and TRAF homology domain
54. **MDC1:** mediator of DNA damage checkpoint protein 1

55. **MEKK:** MAPK/ERK kinase kinase
56. **MR:** molecular replacement
57. **MS:** Mass
58. **MTH:** mammalian-two-hybrid
59. **MyD88:** myeloid differentiation 88
60. **Nbs:** Nijmegen breakage syndrome
61. **NEMO:** NF-κB essential modulator
62. **NF-κB:** nuclear factor kappa-light-chain-enhancer of activated B cells
63. **Ni:** nickel
64. **NIFK:** nucleolar protein interacting with the FHA domain of pKI-67
65. **NIK:** NF-κB-inducing kinase
66. **NMR:** nuclear magnetic resonance
67. **NSRRC:** National Synchrotron Radiation Research Center, a 1.5 GeV third-generation synchrotron located in the Hsin-Chu Science Park, Taiwan
68. **O.D.:** optical density
69. **OdhI:** oxoglutarate dehydrogenase inhibitor
70. **PBS:** phosphate buffered saline
71. **PI3K:** phosphoinositide 3-kinase
72. **PKC:** protein kinase C
73. **PMSF:** phenylmethylsulfonyl fluoride
74. **PP4:** protein phosphatase 4
75. **PPase:** alkaline phosphatase
76. **pT:** phosphothreonine
77. **PVDF:** polyvinylidene difluoride
78. **RAcP:** receptor accessory protein
79. **RING:** really interesting new gene
80. **RIPL:** arginine, isoleucine, proline, leucine
81. **RLU:** relative luciferase units

82. **RNAi:** RNA interference
83. **RPMI-1640:** Roswell Park Memorial Institute medium
84. **RT-PCR:** reverse transcription polymerase chain reaction
85. **SA:** streptavidin
86. **Se-Met:** selenomethionine
87. **Ser or S:** serine
88. **siRNA:** small interfering RNA
89. **Spring-8:** Super Photon Ring – 8 GeV, a synchrotron radiation facility located in Hyōgo Prefecture, Japan
90. **T2BP:** TRAF2 binding protein
91. **TAB2:** TAK1-binding protein 2
92. **TAK:** transforming growth factor β-activated kinase
93. **TBST:** Tris-buffered saline-Tween 20
94. **Thr:** threonine
95. **TIFA:** TRAF-interacting protein with a FHA domain
96. **TIR:** toll/interleukin-1 receptor
97. **TLR:** toll-like receptor
98. **TNFR:** tumor necrosis factor receptor
99. **TNFα:** tumor necrosis factor alpha
100. **Tpl2:** tumor progression locus 2
101. **TRAF:** TNF receptor associated factor
102. **TROSY:** Transverse relaxation optimized spectroscopy
103. **Ub:** ubiquitin
104. **Ubc13:** ubiquitin-conjugating enzyme E2 13
105. **Uev1A:** ubiquitin-conjugating enzyme E2 variant 1A
106. **WT:** wild-type
107. **ZF:** zinc finger
108. **β-ME:** beta-mercaptoethanol

Molecular and Cellular Biology

Intermolecular Binding between TIFA-FHA and TIFA-pT Mediates Tumor Necrosis Factor Alpha Stimulation and NF-κB Activation

Chia-Chi Flora Huang, Jui-Hung Weng, Tong-You Wade Wei, Pei-Yu Gabriel Wu, Pang-Hung Hsu, Yu-Hou Chen, Shun-Chang Wang, Dongyan Qin, Chin-Chun Hung, Shui-Tsung Chen, Andrew H.-J. Wang, John Y.-J. Shyy and Ming-Daw Tsai

Mol. Cell. Biol. **2012, 32(14):2664. DOI: 10.1128/MCB.00438-12.**
Published Ahead of Print 7 May 2012.

MCB
Journals.ASM.org

Intermolecular Binding between TIFA-FHA and TIFA-pT Mediates Tumor Necrosis Factor Alpha Stimulation and NF-κB Activation

Chia-Chi Flora Huang,[a,b,c,d] Jui-Hung Weng,[a,b,c,e] Tong-You Wade Wei,[a,d] Pei-Yu Gabriel Wu,[a,b] Pang-Hung Hsu,[a,b] Yu-Hou Chen,[a,b] Shun-Chang Wang,[a] Dongyan Qin,[b] Chin-Chun Hung,[a] Shui-Tsung Chen,[a] Andrew H.-J. Wang,[a] John Y.-J. Shyy,[f] and Ming-Daw Tsai[a,b,c,d]

Institute of Biological Chemistry, Academia Sinica, Taipei, Taiwan[a]; Genomics Research Center, Academia Sinica, Taipei, Taiwan[b]; Taiwan International Graduate Program, Academia Sinica, Taipei, Taiwan[c]; Institute of Biochemical Sciences, National Taiwan University, Taipei, Taiwan[d]; Department of Chemistry, National Tsing Hua University, Hsinchu, Taiwan[e]; and Division of Biomedical Sciences, University of California, Riverside, California, USA[f]

The forkhead-associated (FHA) domain recognizes phosphothreonine (pT) with high specificity and functional diversity. TIFA (TRAF-interacting protein with an FHA domain) is the smallest FHA-containing human protein. Its overexpression was previously suggested to provoke NF-κB activation, yet its exact roles in this signaling pathway and the underlying molecular mechanism remain unclear. Here we identify a novel threonine phosphorylation site on TIFA and show that this phosphorylated threonine (pT) binds with the FHA domain of TIFA, leading to TIFA oligomerization and TIFA-mediated NF-κB activation. Detailed analysis indicated that unphosphorylated TIFA exists as an intrinsic dimer and that the FHA-pT9 binding occurs between different dimers of TIFA. In addition, silencing of endogenous TIFA resulted in attenuation of tumor necrosis factor alpha (TNF-α)-mediated downstream signaling. We therefore propose that the TIFA FHA-pT9 binding provides a previously unidentified link between TNF-α stimulation and NF-κB activation. The intermolecular FHA-pT9 binding between dimers also represents a new mechanism for the FHA domain.

The forkhead-associated (FHA) domain, discovered in 1995 (10) and first suggested to bind phosphoproteins in 1998 (24), is known to specifically recognize phosphothreonine (pT) to exert its function (5, 20). Although the sequence homology among different FHA-containing proteins is relatively low, the structural architecture of FHA domains is highly conserved. It contains a six-stranded β-sheet and another five-stranded β-sheet, forming a β-sandwich. The FHA-pT binding has been shown to regulate diverse biological functions, ranging from DNA damage repair to cell cycle checkpoints to signal transduction (18). Furthermore, the mechanism of FHA-phosphoprotein binding varies greatly among different FHA-containing proteins. The structure, specificity, mechanism, and biological functions of FHA domains have been summarized in recent reviews (16, 18).

TRAF-interacting protein with an FHA domain (TIFA) was first identified as a tumor necrosis factor (TNF) receptor-associated factor 2 (TRAF2) binding protein. Consisting of 184 amino acids, TIFA is the smallest FHA domain-containing protein in humans (Fig. 1A). In the absence of TNF-α stimulation, TIFA overexpression in HEK 293T cells can activate NF-κB and AP-1 (14), suggesting a direct involvement of TIFA in TNF-mediated immune responses. This involvement of TIFA was further attributed to the binding of TRAF2, which requires the TRAF domain of TRAF2 and almost the entire TIFA protein (residues 1 to 162) (14). TIFA was also reported to bind to TNF-associated factor 6 (TRAF6) (25). The consensus binding site of TIFA for TRAF6 was mapped to be glutamic acid 178 (E178) (11, 25), indicating different binding mechanisms in TIFA-TRAF2 and TIFA-TARF6 interactions. In addition, TIFA overexpression, even in the absence of interleukin-1 (IL-1), was shown to activate NF-κB and c-Jun amino-terminal kinase (JNK), possibly through its enhancement of TRAF6 binding to IL-1 receptor-associated kinase 1 (IRAK-1). On the other hand, mutation of E178 abolished the binding of TIFA to TRAF6 and the ensuing activation of NF-κB (25). In a follow-up report, TIFA was shown to promote oligomerization and ubiquitination of TRAF6, leading to activation of IκB kinase (IKK), based on *in vitro* studies (6).

Although the studies of Takatsuna et al. (25) and Ea et al. (6) have previously established the key function of TIFA in its interaction with TRAF6, several issues still remain inconclusive. For example, TIFA has been suggested to be phosphorylated, and the integrity of the FHA domain of TIFA is essential for its function (6, 25), but little information has been unveiled about the molecular basis of TIFA phosphorylation and its functional consequences.

In this work, we report that threonine 9 (T9) is a newly identified phosphorylation site of TIFA and that the phosphorylation level of T9 increases upon TNF-α treatment. Based on data collected here, we concluded that TIFA-FHA binds to this pT9 site. Such a TIFA-FHA/pT9 binding directs TIFA self-association and promotes NF-κB activation through the oligomerization process. We also observed *in vivo* speckle formation of oligomerized TIFA which colocalizes with TRAF6. Further biophysical analyses indicate that TIFA-FHA/pT9 binding occurs between dimers of TIFA, leading to oligomerization. Moreover, our studies suggest that the TNF-α-mediated signaling is attenuated when endogenous TIFA is knocked down. Thus, we propose that FHA/pT9 binding of TIFA is a critical link between TNF-α stimulation and NF-κB activation. Our findings provide not only a new molecular insight

Received 2 April 2012 Returned for modification 24 April 2012
Accepted 30 April 2012
Published ahead of print 7 May 2012
Address correspondence to Ming-Daw Tsai, mdtsai@gate.sinica.edu.tw.

doi:10.1128/MCB.00438-12

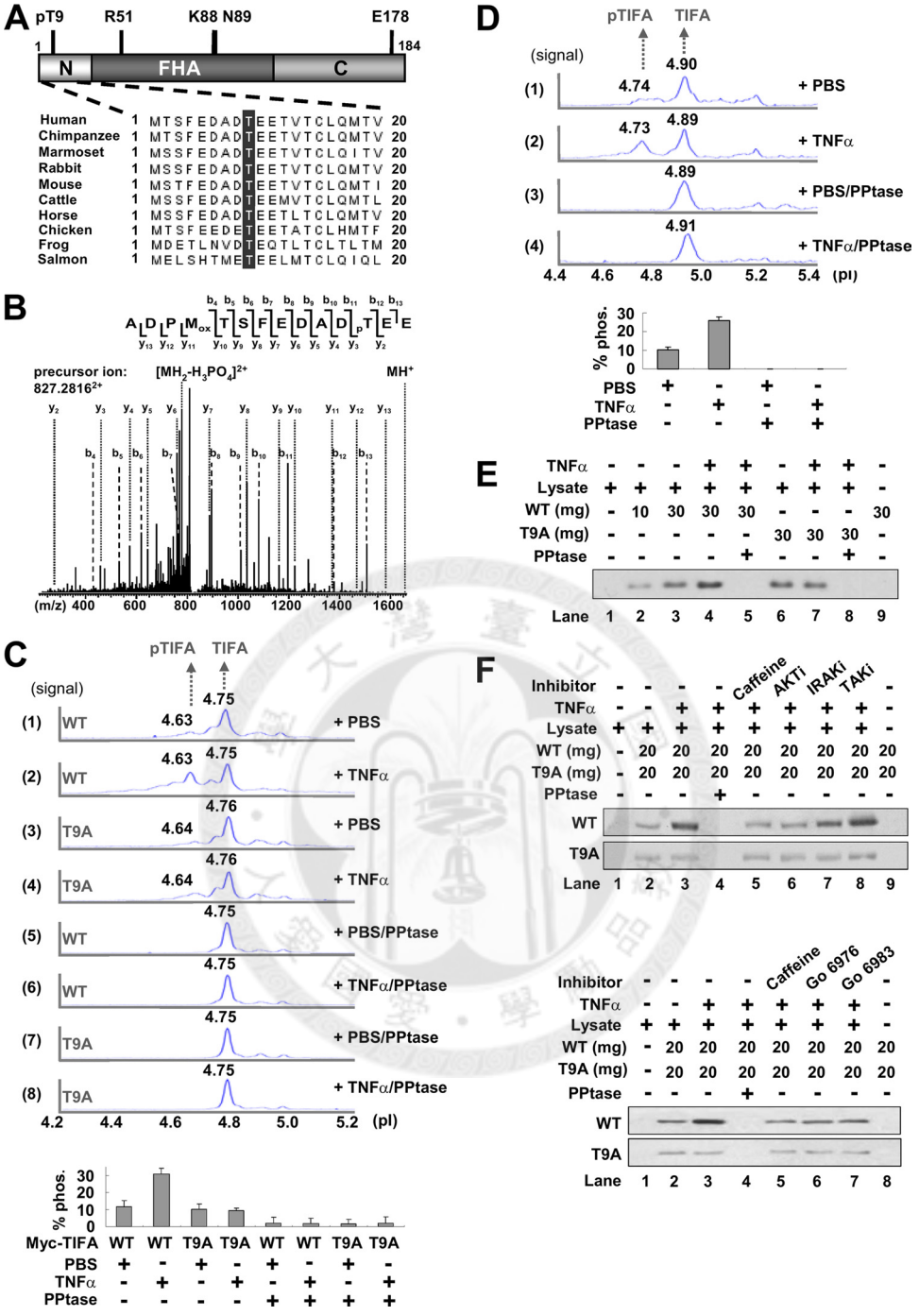

FIG 1 Enhancement of TIFA phosphorylation by TNF-α stimulation. (A) Schematic overview of TIFA domain structure (top) and N-terminal sequences of TIFA orthologues from different species (bottom). T9 is highlighted in dark gray. (B) MS/MS spectrum of the peptide containing pT9 in TIFA. The precursor ion 827.2816^{2+} is from ADPMTSFEDAD(pT)EE. (C) NanoPro immunoassay demonstrates the phosphorylation status of overexpressed Myc-tagged WT and T9A mutant TIFA with or without TNF-α and phosphatase treatment. The peaks at pI 4.75 and pI 4.63 are assigned to unphosphorylated TIFA and singly phosphorylated TIFA, respectively. The bar graph in the lower panel represents the ratios of peak areas of singly phosphorylated TIFA to total TIFA. The results represent means ± standard deviations (SD) from at least 3 independent experiments. (D) NanoPro immunoassay of endogenous TIFA. The conditions were the same as those for panel C. The pI values differ from the peaks in panel C due to lack of the Myc tag. (E) Recombinant TIFA or the T9A mutant was incubated with [γ-^{32}P]ATP and lysates from cells treated with or without TNF-α for 30 min. During incubation, alkaline phosphatase (PPtase) was added as indicated. The reaction mixtures were separated by SDS-PAGE, and the bands were revealed by autoradiography. (F) The experimental conditions were the same as those for panel E except for the inclusion of caffeine or inhibitor cocktails for AKT, IRAK, TAK, or PKC (Go 6976 and Go 6983).

into the TNF-α-mediated signaling pathway but also a new functional mechanism of FHA-containing proteins.

MATERIALS AND METHODS

Cell culture. The human embryonic kidney (HEK) 293T cell line and human osteosarcoma cell line U2OS were cultured in Dulbecco's modified Eagle medium (DMEM) (Gibco). The human acute monocytic leukemia cell line THP-1 was cultured in Roswell Park Memorial Institute medium (RPMI 1640) (Gibco). All media were supplemented with 10% heat-inactivated fetal bovine serum (FBS) (Gibco), 200 mM L-glutamine (Gibco), 100 U/ml penicillin (Gibco), 100 μg/ml streptomycin (Gibco), and 1% sodium pyruvate (Gibco). Cells were kept in a 37°C incubator with 5% CO_2. Cells were starved by replacing the complete medium with serum-free DMEM 8 to 10 h prior to the addition of 50 ng/ml of TNF-α at the indicated time points.

TIFA plasmids and recombinant protein. The His-tagged human TIFA wild-type (WT) protein and various mutants were expressed in *Escherichia coli* BL21 Codon Plus and affinity purified with nickel resin (Millipore). Approximately 30 mg of purified recombinant His-TIFA was applied to a HiLoad 16/60 Superdex 75-pg column or a Superdex 75 10/300 GL column (GE Healthcare). The separated fractions were analyzed by 15% SDS-PAGE, and proteins were visualized by Coomassie blue staining. Other plasmids involved in this study, including Flag-tagged pCMV-Tag2a (Stratagene), pcDNA3.1-Myc (EQKLISEEDL) (Invitrogen), pNF-κB-Luc (Clontech), His-tagged pET43.1a (Novagen), and Gal-tagged pBIND (Promega), were obtained from commercial sources.

RNA interference. Two hundred picomoles of double-stranded small interfering RNA (siRNA) oligomers (Invitrogen) corresponding to the sequence of TIFA (UCAGGACAAACAGGUUUCCCGAGUU) or scramble control oligomers (Invitrogen) was transfected into HEK 293T or THP-1 cells. Cells were collected after 72 h of incubation.

Antibodies. The anti-TIFA monoclonal antibody (MAb) was produced by the core facility at IBC, Academia Sinica. Other MAbs used in the current study are anti-Flag (Sigma), anti-Myc (Millipore), anti-Gal (Abcam), anti-β-actin (GeneTex), anti-His (Signal Chem), anti-pIKKα (pT23) (Abcam), anti-pIκB (pS32/pS36) (Santa Cruz), and anti-NF-κB p65 (Millipore). The polyclonal antibodies used in this work are anti-NF-κB p65 (Santa Cruz), horseradish peroxidase (HRP)-conjugated anti-mouse IgG (Millipore), fluorescein isothiocyanate (FITC)-conjugated anti-mouse IgG (Millipore), and rhodamine-conjugated anti-rabbit IgG (Millipore).

NanoPro immunoassay. The NanoPro immunoassay method involves separation of cell lysates in the capillary isoelectric focusing (IEF) step, followed by analysis of specific protein isoforms (i.e., different phosphorylation forms of TIFA) using conventional immune detection (19). Cells were collected and centrifuged at 1.0 krpm for 5 min. The cell pellet was then resuspended in 250 μl Bicine-CHAPS {3-[(3-cholamidopropyl)-dimethylammonio]-1-propanesulfonate} lysis buffer plus 1× dimethyl sulfoxide (DMSO) inhibitor mix and 1× aqueous inhibitor mix. The cell lysates were cleared by centrifugation at 13.2 krpm for 1 h at 4°C. When indicated, 5 mg total cell lysate was incubated with alkaline phosphatase (Fermentas) together with 10× reaction buffer at 37°C for 1 h. Final supernatants were transferred to a fresh tube and snap-frozen with liquid nitrogen. The nanofluidic proteomic immunoassay was performed with the NanoPro-1000 system. Cell lysate was diluted to 2× the final protein concentration in Bicine-CHAPS buffer in the presence of DMSO inhibitor mix and 20 mM dithiothreitol (DTT). Diluted cell lysate was combined with an equal volume of IEF buffer solution (50% [vol/vol] pH 3 to 10 premix solution, 50% [vol/vol] Servalyte, pH 3 to 6), 1 μM pI standard 4.4, and 1 μM pI standard 5.5. The charge-based separation was performed in a capillary at 45,000 μW for 40 min, and immobilization was by 80 s of irradiation with UV light. After separation and immobilization, the sample was incubated with primary antibody for 120 min. Each overexpressed sample was then incubated with HRP-conjugated goat anti-mouse IgG for 1 h. Endogenous sample was detected by biotin-labeled goat anti-rabbit IgG for 1 h followed by 10 min of incubation with streptavidin (SA)-HRP-conjugated antibody. Chemiluminescence signals for the target proteins were detected by adding luminol and peroxide XDR detection reagents and analyzed with the Compass software.

***In vitro* kinase assay.** After washing with phosphate-buffered saline (PBS), TNF-α-stimulated or nonstimulated 293T cells were lysed with CHAPS lysis buffer. The cell lysates were precleaned with sheep anti-mouse IgG M-280 Dynabeads (Invitrogen) at 25°C for 30 min and then incubated with the recombinant His-tagged wild-type or T9 mutant TIFA in a buffer containing 40 mM HEPES (pH 7.5), 20 mM $MgCl_2$, 100 μM ATP, and 1 mCi/ml [γ-^{32}P]ATP (Perkin-Elmer) at 37°C for 30 min. His-TIFA was pulled down with M-280 Dynabeads coated with anti-His MAb. The reaction was terminated by addition of SDS sample buffer and heating at 95°C for 10 min prior to SDS-PAGE.

Coimmunoprecipitation analysis. The protein-coding sequences of TIFA cDNA were subcloned into the expression vector pCMV-Flag or pcDNA3.1-Myc. HEK 293T cells (~2×10^7) were cotransfected with 3 μg of the expression vectors containing Flag-TIFA and Myc-TIFA using Jet-PEI (Polyplus transfection). After 36 h, cells were lysed with TNE buffer, containing 10 mM Tris-HCl (pH 7.8), 1% NP-40, 0.15 M NaCl, 1 mM EDTA, 1 mM phenylmethylsulfonyl fluoride (PMSF), and 1× protease inhibitor cocktail. An amount of 6.5 μg of anti-Flag MAb was precoated with M-280 Dynabeads overnight at 4°C. The cell lysates were incubated with anti-Flag–Dynabeads at 4°C overnight. The protein-bead complex was then washed with TNE buffer and 1× Tris-buffered saline–Tween 20 (TBST) buffer. The immunoprecipitates were then eluted using 50 μg of the 3× Flag peptide (Sigma) and subjected to Western blot analysis.

Western blotting. For Western blotting, cell lysates were separated by 15% SDS-PAGE and transferred onto a polyvinylidene difluoride (PVDF) membrane (Perkin-Elmer). The membranes were then blotted with primary antibody at 4°C overnight followed by HRP-conjugated anti-mouse IgG. The blotted protein bands were revealed by the ECL system (Millipore).

Native PAGE experiment. For the native PAGE experiment, cells were lysed using the NativePAGE (Invitrogen) sample buffer in the presence of 10% *n*-dodecyl β-D-maltoside (DDM) and 5% digitonin. After centrifugation at 4°C for 1 h, the whole-cell lysates were separated by gradient PAGE (4 to 16%). A buffer containing 0.5 M Tris base (pH 9.2) and 0.5 M glycine was used for protein transfer. After transfer, the PVDF membrane was incubated in 20 ml of 7.5% acetic acid for 15 min at room temperature to fix the proteins. The membrane was subsequently rinsed with methanol and deionized water to remove the residual Coomassie blue G-250 dye. Finally, TIFA proteins were detected by Western blot analysis using mouse anti-Flag antibody or mouse anti-Myc antibody.

NF-κB activation assay. 293T cells in 6-well plates were transiently transfected with 1.5 μg of the TIFA WT or mutant expression plasmids together with 1.5 μg of the pNF-κB-Luc reporter. After 36 h, cells were lysed with 1× passive lysis buffer (Promega) and 20 μl of cell lysates was dispensed into a 96-well plate, followed by addition of 100 μl of lyophilized luciferase assay substrate (LARII) (Promega) and 100 μl of Stop & Glo reagent (Promega). The luciferase activity was measured as relative luminescence units (RLU). When indicated, Western blot analysis for the total cell lysate was carried out in parallel in order to confirm the expression levels of each sample. The firefly luciferase readings were then normalized to the internal *Renilla* luciferase readings as well as the corresponding band intensities of the samples.

Immunostaining. An amount of 7×10^5 U2OS cells seeded on coverslips was transfected with 3 μg of TIFA or mutant vectors. At 36 h posttransfection, cells were washed with cold PBS and fixed with 4% paraformaldehyde (Electron Microscopy Sciences) for 30 min. Cells were permeabilized with 0.2% Triton X-100, blocked with PBS containing 10% bovine serum albumin (BSA), and then incubated with primary antibodies, fluorescence-labeled secondary antibodies, and DAPI (4′,6′-diamidino-2-phenylindole) sequentially. Fluorescence image sections were taken by Zeiss LSM 510 confocal microscopy.

Mass spectrometry (MS) analysis. The phosphorylation sites were analyzed using high-resolution and high-mass-accuracy nanoflow liquid chromatography-tandem MS (LC-MS/MS) on a linear quadrupole ion trap-Fourier transform (LTQ-FT) ion cyclotron resonance mass spectrometer (Thermo Fisher Scientific) with procedures described previously (8).

ITC analysis. Isothermal titration calorimetry (ITC) experiments were performed using a MicroCal iTC200 instrument (Northampton, MA). Two TIFA N-terminal peptides, i.e., MTSFEDADTEETVT and MTSFEDAD(pT)EETVT (2 mM), were used to titrate TIFA protein (100 μM) at 25°C in the calorimeter cell (0.2044 ml) with automatic injections of 1.6 μl each time. With the use of software provided by the manufacturer, each peak corresponding to the injection was integrated and corrected with baseline. The titration heat had been calculated to eliminate the effect of heat generated from diluting the ligand into buffer. Thermal data were fitted to a two-independent-site binding model to yield the value of the equilibrium dissociation constant (K_d).

Analytical ultracentrifugation (AUC) analysis. Sample and buffer were loaded into a 12-mm standard double-sector Epon charcoal-filled centerpiece and mounted in an An-60 or An-50 Ti rotor of a Beckman Coulter XL-I analytical ultracentrifuge (Fullerton, CA). The rotor speed was 40,000 rpm at 20°C. The signal was monitored at 280 nm. The partial specific volume of TIFA protein is 0.724. The raw experimental data were analyzed by Sedfit (http://www.analyticalultracentrifugation.com/default.htm), and the plots of *c*(*s*, *fr*) and molecular mass versus the *s* value were generated by MATLAB (MathWork, Inc.).

RESULTS

TIFA phosphorylation at Thr9. Given the presence of an FHA domain in the middle of TIFA and five Thr residues at its N terminus (T2, T9, T12, T14, and T19) (Fig. 1A), we investigated whether one of these Thr residues could be phosphorylated and thereby recognized by the FHA domain. The exogenously expressed Flag-TIFA was immunoprecipitated from HEK 293T cells and then subjected to mass spectrometry (MS) analysis. With 80% sequence coverage, the MS data revealed that Flag-TIFA was phosphorylated at T9 (Fig. 1B).

Because both TNF-α stimulation and TIFA overexpression can activate NF-κB (14, 25), it is likely that T9 phosphorylation is correlated with TNF-α-elicited signaling. We thus used the recently developed NanoPro immunoassay (7, 19) to examine the effect of TNF-α treatment on T9 phosphorylation. The method involves separation of cell lysates in the capillary isoelectric focusing step, followed by analysis of specific protein isoforms (i.e., different phosphorylation forms of TIFA) using conventional immune detection (19). As shown in Fig. 1C, trace 1, the exogenously expressed Myc-TIFA, revealed by the anti-Myc antibody, exhibited a major peak at pI 4.75. This was close to the theoretical pI value of 4.92 deduced by the Scansite database (http://scansite.mit.edu/calc_mw_pi.html). Among the several smaller peaks detected, the one with pI 4.63 was consistent with singularly phosphorylated TIFA, since addition of one phosphate group is expected to decrease the pI by 0.12. Treatment with TNF-α also led to an increase of the peak with pI 4.63 (traces 2), suggesting phosphorylation at one single amino acid residue. However, TNF-α did not have such an effect on the T9A mutant (traces 3 and 4). When traces 1 to 4 were repeated in the presence of alkaline phosphatase (traces 5 to 8, respectively), only one single peak at pI 4.75 was observed. These results support that the exogenously expressed TIFA was phosphorylated (at T9 based on the MS result) and that the phosphorylation increased upon TNF-α treatment. To examine whether TNF-α induces T9 phosphorylation of the endogenous TIFA, we raised a monoclonal antibody (MAb) against bacterially expressed full-length TIFA. The endogenous TIFA from 293T cells detected by NanoPro immunoassay showed the same results as seen in Fig. 1C (comparing traces 1 to 4 in Fig. 1D with traces 1, 2, 5, and 6 in Fig. 1C). Of note, since the endogenous TIFA was not tagged, the pI values differed slightly from those in Fig. 1C.

An *in vitro* kinase assay was then used to further confirm that TIFA T9 phosphorylation is TNF-α dependent. We incubated recombinant TIFA with TNF-α-stimulated cell extracts in the presence of [γ-^{32}P]ATP. Revealed by autoradiography, the band intensity of ^{32}P-labeled His-TIFA increased when TNF-α-stimulated cell extract was used, relative to that from control cells (Fig. 1E, lanes 3 and 4). On the other hand, there was no TNF-α-dependent increase in the band intensity for the T9A mutant (Fig. 1E, lanes 6 and 7), indicating that TNF-α-increased TIFA phosphorylation most likely occurs at T9. In the control lanes 1, 5, 8, and 9, no ^{32}P-labeled TIFA band was observed when the sample was treated with phosphatase or when TIFA protein or cell lysate was omitted.

To explore the kinase that mediates the TNF-α-dependent T9 phosphorylation, cells were treated with caffeine, a general inhibitor of the phosphatidylinositol 3-kinase (PI3K) pathway, or with kinase inhibitor cocktails for AKT, IRAK, TAK, and protein kinase C (PKC) before TNF-α treatment. Autoradiography (Fig. 1F) showed that caffeine and AKT and PKC inhibitors, but not IRAK or TAK inhibitors, decreased the level of TNF-α-induced phosphorylation of wild-type (WT) His-TIFA, while none of these inhibitors affected the basal phosphorylation level of T9A. These results suggest the involvement of Ser/Thr kinases in the PI3K-AKT signaling pathway in T9 phosphorylation.

pT9 and FHA domain are important for TIFA self-association. Because TIFA molecules can associate with each other to form homo-oligomers (25), we examined whether the phosphorylated T9 binding to TIFA-FHA is the basis of TIFA-TIFA self-association. Flag-tagged WT TIFA and Myc-tagged TIFA (WT or mutants) were overexpressed in HEK 293T cells. The Myc-tagged WT TIFA was detected in the anti-Flag pulldown (Fig. 2A, lane 1). Incubation of anti-Flag pulled-down samples with phosphatase reduced the interaction between Myc- and Flag-tagged WT TIFA (lane 2), while this reduction was rescued by the inclusion of EDTA to block the phosphatase activity (lane 3). In contrast, the T9A mutant was marginally detected under the same conditions, with or without phosphatase (lanes 4 to 6), supporting that T9 phosphorylation is critical for the TIFA self-association.

We next tested whether FHA mutants impair the TIFA-TIFA association. On the basis of sequence alignment of different FHA domains shown in Fig. 2B, we replaced two of the highly conserved residues, Arg51 and Asn89, and a nonconserved but potentially important (due to its charge neighboring to the conserved Asn89) residue, Lys88, with Ala. As shown in Fig. 2C, Gal-tagged mutant TIFA could no longer be detected in the anti-Flag immunoprecipitates, indicating that each of the three residues is essential for the TIFA-TIFA interaction. A similar result was observed in previous study using a G50E S66A double mutant (25), although the role of pT9 was not then known.

By using isothermal titration calorimetry (ITC), we evaluated further the binding between the FHA domain and pT9 residue of TIFA. The expressed His-tagged WT TIFA and two FHA mutants were purified using a nickel column and then analyzed for associ-

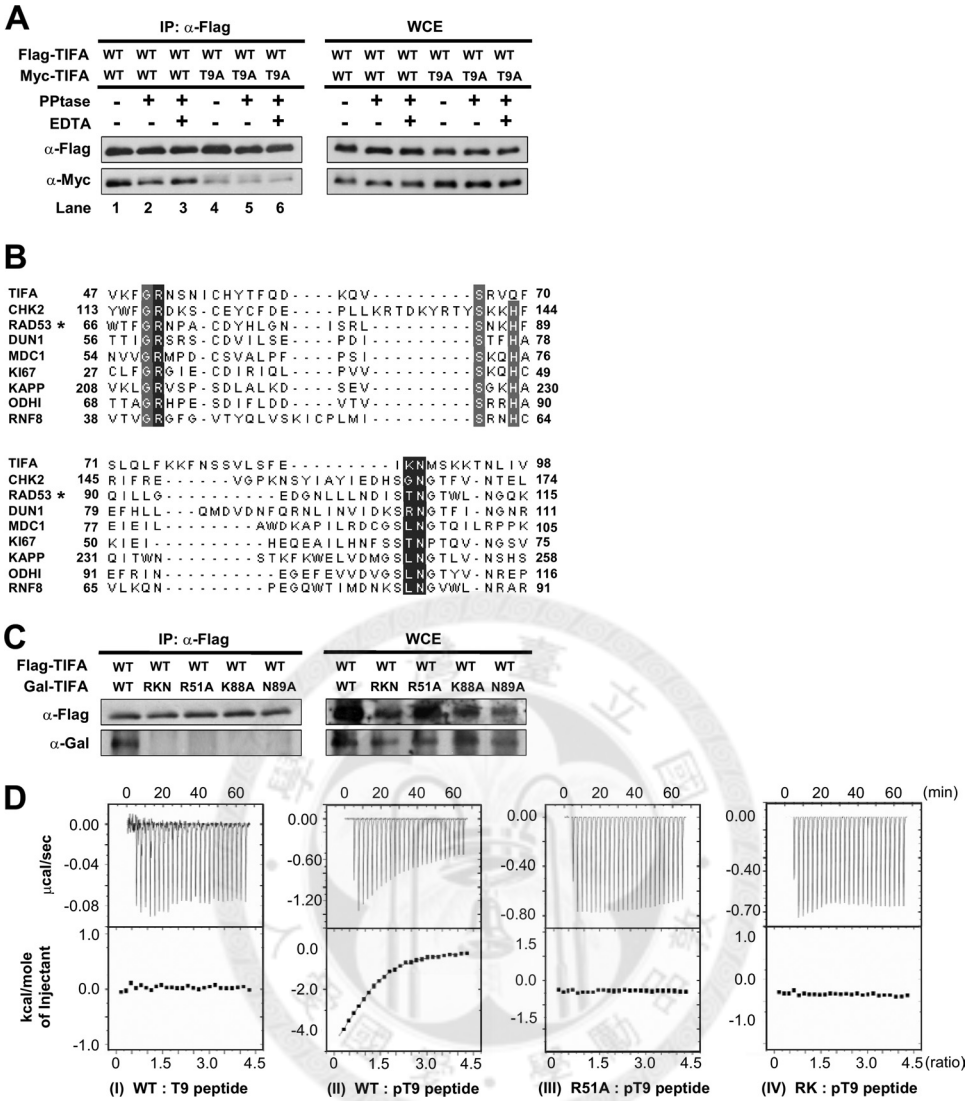

FIG 2 pT9 and the FHA domain are required for TIFA self-association. (A) Flag-tagged WT and Myc-tagged WT and T9A TIFA were coexpressed in HEK 293T cells. Anti-Flag-coated Dynabeads was used in immunoprecipitation (IP). The coprecipitated proteins were detected by anti-Myc antibody in immunoblotting. The whole-cell extracts (WCE) used as IP inputs are shown in the right panel. PPtase or EDTA was included as indicated. (B) Sequence alignment of the conserved pT-contacting residues within the FHA domains of different FHA domain-containing proteins. Conserved residues among homologues are in light gray. The residues chosen for mutation in this work are in dark gray. RAD53*, RAD53 FHA1. (C) Effect of FHA domain mutations on the self-association of TIFA. The experiments were performed as described for panel A except that the coprecipitated TIFA and its mutants were detected by anti-Gal antibody. RKN, R51A K88A N89A mutant. (D) ITC analysis of the *in vitro* binding of WT TIFA and its R51A and R51A K88A (RK) mutants with the T9-containing peptide ([1]MTSFEDADTEETVT[14]) or pT9-containing peptide [[1]MTSFEDAD(pT)EETVT[14]]. Binding was observed only when the WT TIFA was incubated with the pT9-containing peptide.

ation with a synthetic pT9-containing peptide spanning residues 1 to 14 of TIFA. As shown in Fig. 2D (panel II), ITC showed that the pT9-containing peptide binds to the unphosphorylated recombinant wild-type TIFA with a K_d of 50 ± 1.3 μM (stoichiometry, N = 1.04). In contrast, ITC could not detect binding for the corresponding unphosphorylated peptide with wild-type TIFA (panel I) or for the pT9-containing peptide with mutants R51A and R51A K88A (RK) (panels III to IV). These results reinforce the notion that the TIFA self-association is mediated through binding of pT9 to the FHA domain of TIFA.

The TIFA intrinsic dimer is the basic unit for self-association and oligomerization. As a hallmark of the TRAF family, oligomer formation appears to be critical for TNF-α signaling (2, 12, 21). Since TIFA is able to promote oligomerization of TRAF6 (6), the self-associated TIFA may serve as building blocks for oligomerization. This in turn raises the question of whether the quaternary state of TIFA may exist in high-order protein architecture. The recombinant TIFA has been reported to exist in trimers (25), even though the vast majority of FHA domains are known to exist as monomers (18). Unexpectedly, the results from our experiments using fast protein liquid chromatography (FPLC) (Fig. 3A) or AUC (Fig. 3B) indicated that unphosphorylated WT TIFA existed as a 46-kDa intrinsic dimer which was stable between pH 7.5 and 8.5 in a range of protein concentrations (Fig. 3C). This finding suggests that the TIFA self-association observed in Fig. 2 represents oligomer formation (dimer associates with dimer) through

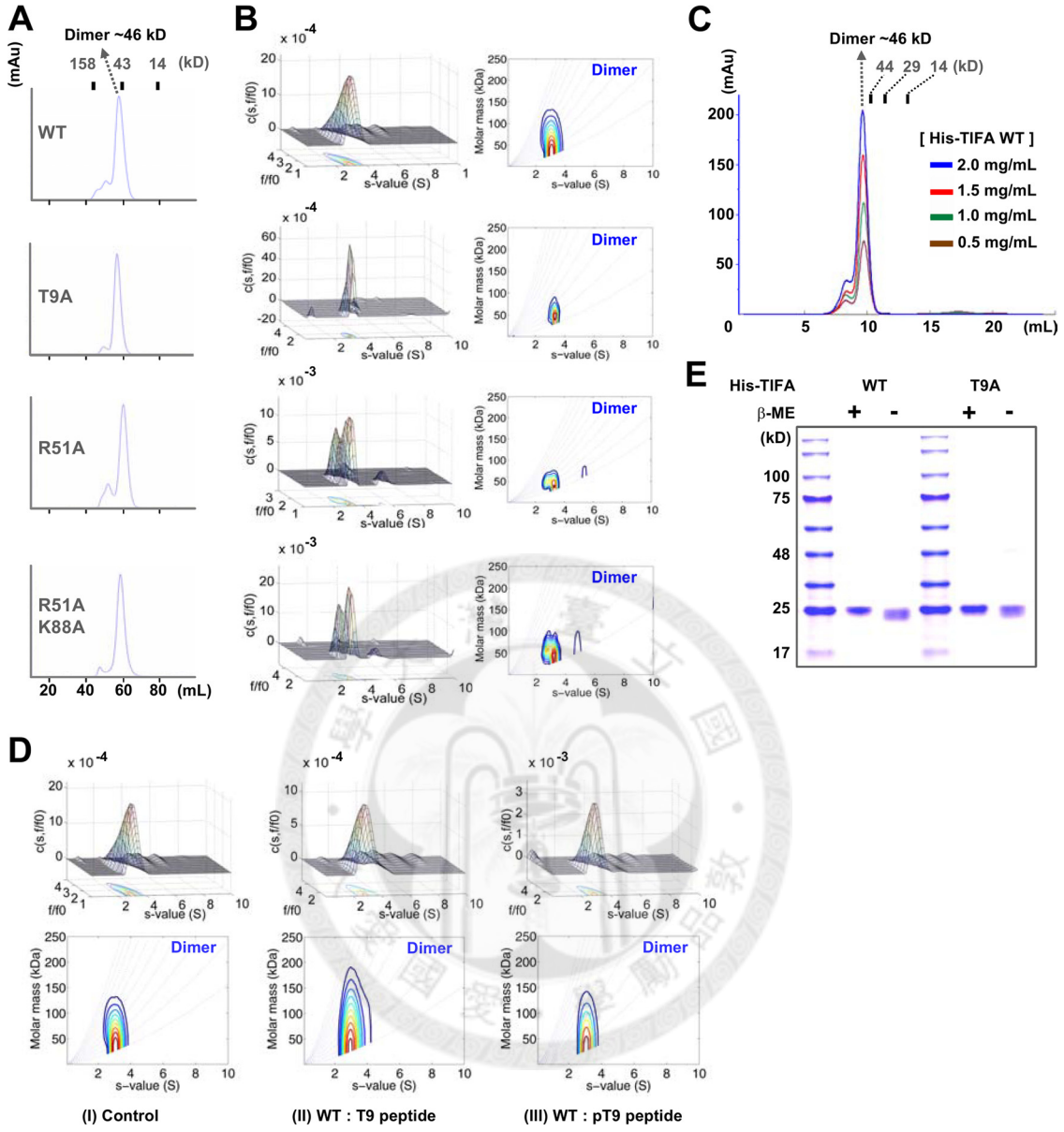

FIG 3 TIFA exists as an intrinsic dimer in solution. (A and B) Size exclusion chromatography (HiLoad 16/60 Superdex 75 pg column) (A) and AUC analysis (B) show that recombinant TIFA and mutants exist as dimers in solution. (C) Recombinant WT TIFA appeared as a dimer from low (0.5 mg/ml) to high (2 mg/ml) protein concentrations in size exclusion chromatography (Superdex 75 10/300 GL column). (D) AUC analysis of WT recombinant TIFA alone (I) or with the T9-containing peptide (II) or the pT9-containing peptide (III). The concentration of WT TIFA used was 10 mM, and the peptides were presented at a molar ratio of 1:10 (protein/peptide). (E) TIFA remained in the monomeric form on SDS-PAGE under a nonreduced condition, demonstrating that TIFA did not dimerize through disulfide bonds.

FHA-pT9 interaction rather than dimer formation (monomer associates with monomer). To further investigate the dimerization mechanism of TIFA, we performed FPLC and AUC again to analyze three mutants, the T9A, R51A, and RK mutants. Since these mutants showed reduced self-association (Fig. 2A and C), they should not exist in stable dimers if the self-association reflects the formation of dimers. As the mutants still exist as dimers as shown in Fig. 3A and B, the results provide further support that TIFA exists as intrinsic dimers. In addition, the fact that the peptide-protein complex in Fig. 3D (panel III) remained as a dimer suggests that the dimeric interface does not involve the pT-FHA binding sites so that the dimer is not disrupted by the pT9-containing peptide. Finally, we found that WT TIFA did not dissociate into monomers under nonreduced conditions (Fig. 3E), excluding involvement of disulfide bonds in the intrinsic dimer.

FHA-pT9 binding promotes TIFA oligomerization that colocalizes with TRAF6. To provide further support that pT9-FHA binding does promote TIFA oligomerization, we evaluated the molecular weights of native TIFA proteins using nondenaturing gels. We examined overexpressed Myc-tagged or Flag-tagged TIFA and mutants from mammalian HEK 293T cells and found that native T9A and R51A K88A N89A (RKN) mutants of TIFA

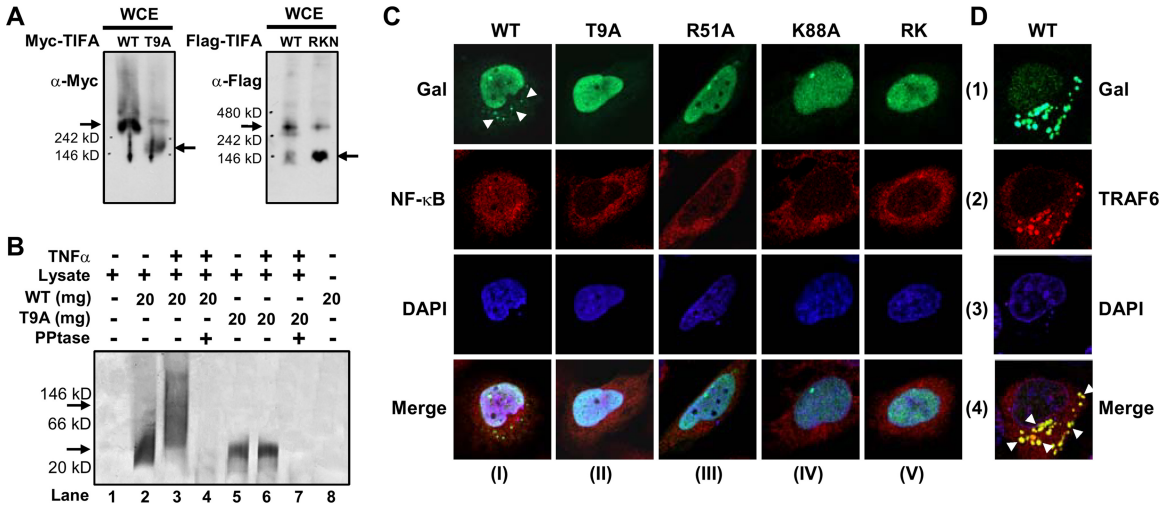

FIG 4 TIFA pT9-FHA interaction is required for TIFA oligomerization. (A) The exogenously expressed Myc-TIFA, Flag-TIFA, and their T9A and RKN mutants were separated by native gel and detected by Western blotting. Arrows indicate the major bands. (B) Autoradiography of the native gel shows that the phosphorylated WT His-TIFA in TNF-α-treated cell lysate was upshifted to a higher molecular mass (indicated by arrows). No signal was detected when samples were treated with alkaline phosphatase. (C) U2OS cells ectopically expressing Gal-tagged TIFA mutants were fixed and incubated with anti-Gal and anti-NF-κB antibodies followed by FITC-conjugated anti-mouse IgG and rhodamine-conjugated anti-rabbit IgG. The nuclei were counterstained with DAPI. The fluorescence images were obtained with a Zeiss LSM 510 confocal microscope. Arrowheads indicate the aggregations/speckles of WT Gal-TIFA. (D) Colocalization of WT Gal-TIFA and Flag-tagged TRAF6 is indicated by arrowheads in the superimposed images. The experimental conditions were the same as for panel C except that Flag-TRAF6 was recognized by anti-TRAF6 antibody.

protein migrated faster than the WT protein during electrophoresis, suggesting that the mutations repressed the formation of oligomeric TIFA (Fig. 4A). We also performed an *in vitro* kinase assay and analyzed the native samples. As a result, the recombinant His-TIFA WT protein that had been phosphorylated by TNF-α-treated cell lysates upshifted to a higher molecular weight, whereas the PBS-treated control WT and both T9A samples remained at a lower molecular weight (Fig. 4B). Taken together, our results suggest that unphosphorylated TIFA forms intrinsic dimers in solution and that the binding between FHA and pT9 of TIFA in cells likely occurs through intermolecular interaction between dimers, presumably leading to oligomerization. This represents a new mechanism for the FHA domain function.

Next, we employed immunostaining to study the role of FHA-pT9 binding in TIFA oligomerization in cells. U2OS cells were transfected with Gal-tagged WT TIFA or its various mutants. As shown in the first panel of Fig. 4C (column I, row 1), a number of discrete punctate spots recognized by anti-Gal (indicated by arrowheads) were found in the perinuclear region of the cytoplasm of U2OS cells (representing possible protein aggregates or oligomers) transfected with WT Gal-TIFA. In parallel experiments in which cells were transfected with T9A or FHA domain mutants (columns II to V, row 1), no aggregates of Gal-TIFA were observed.

Moreover, since this newly found aggregation/oligomerization of exogenously expressed TIFA behaved similarly to what has been observed for members involved in the same inflammatory signaling pathway, including TRAF6, IRAK, P62, sequestosome, etc. (9, 22, 23, 26, 27, 30), we extrapolated that the speckles observed in cells exogenously expressing TIFA could be part of this huge signalosome protein complex. Indeed, the confocal section (Fig. 4D) shows that when WT and Flag-tagged TRAF6 were coexpressed, most of the punctuate spots of TIFA (row 1) colocalized with that of TRAF6 (row 2) in the cytoplasm of the cells (indicated by arrowheads) (row 4). These results suggest that the pT9-FHA binding is crucial for TIFA/TRAF6 oligomerization.

FHA-pT9 binding is required for TNF-α-mediated activation of NF-κB. Previous reports showed that oligomeric forms of TIFA can activate IKK (6) and that interaction of TIFA with TRAF6 is indispensable for NF-κB activation (25). Given that TIFA-TIFA interaction occurs via pT9-FHA binding between TIFA dimers leading to oligomerization, we tested whether the pT9-FHA interaction is necessary for NF-κB activation. HEK 293T cells were transfected with a NF-κB luciferase reporter together with expressing plasmids encoding WT TIFA or its various mutants. As shown in Fig. 5A, the NF-κB-driven luciferase activity was much lower in cells cotransfected with the unphosphorylatable T9A or RKN FHA domain mutant than in those cotransfected with WT TIFA. In line with previous observations (25), the NF-κB activity mediated by E178A mutant was also drastically decreased, which supports that TRAF6 binds to TIFA via E178. We next monitored the subcellular localization of endogenous NF-κB affected by exogenously expressed TIFA. In agreement with the reporter assay, Gal-tagged wild-type TIFA in U2OS cells did promote the nuclear translocation of NF-κB (Fig. 4C, column I, row 2). Such a nuclear translocation of NF-κB was not observed when the T9A, R51A, K88A, or RK mutant was transfected (Fig. 4C, columns II to V, row 2).

In a complementary experiment, small interfering RNA (siRNA) was used to silence the endogenous TIFA in HEK 293T cells, which was down to approximately 20% of the original level (Fig. 5B). Reporter assay and Western blot analysis were performed again to examine NF-κB activation while endogenous TIFA was silenced in HEK 293T cells. Compared with those in positive controls using nontransfected cells or cells transfected with scramble RNA, the TNF-α-induced activation of NF-κB (Fig. 5C, upper bar graph) and elevation level of phosphorylated IκB and total NF-κB proteins (Fig. 5C, lower bar graphs) were

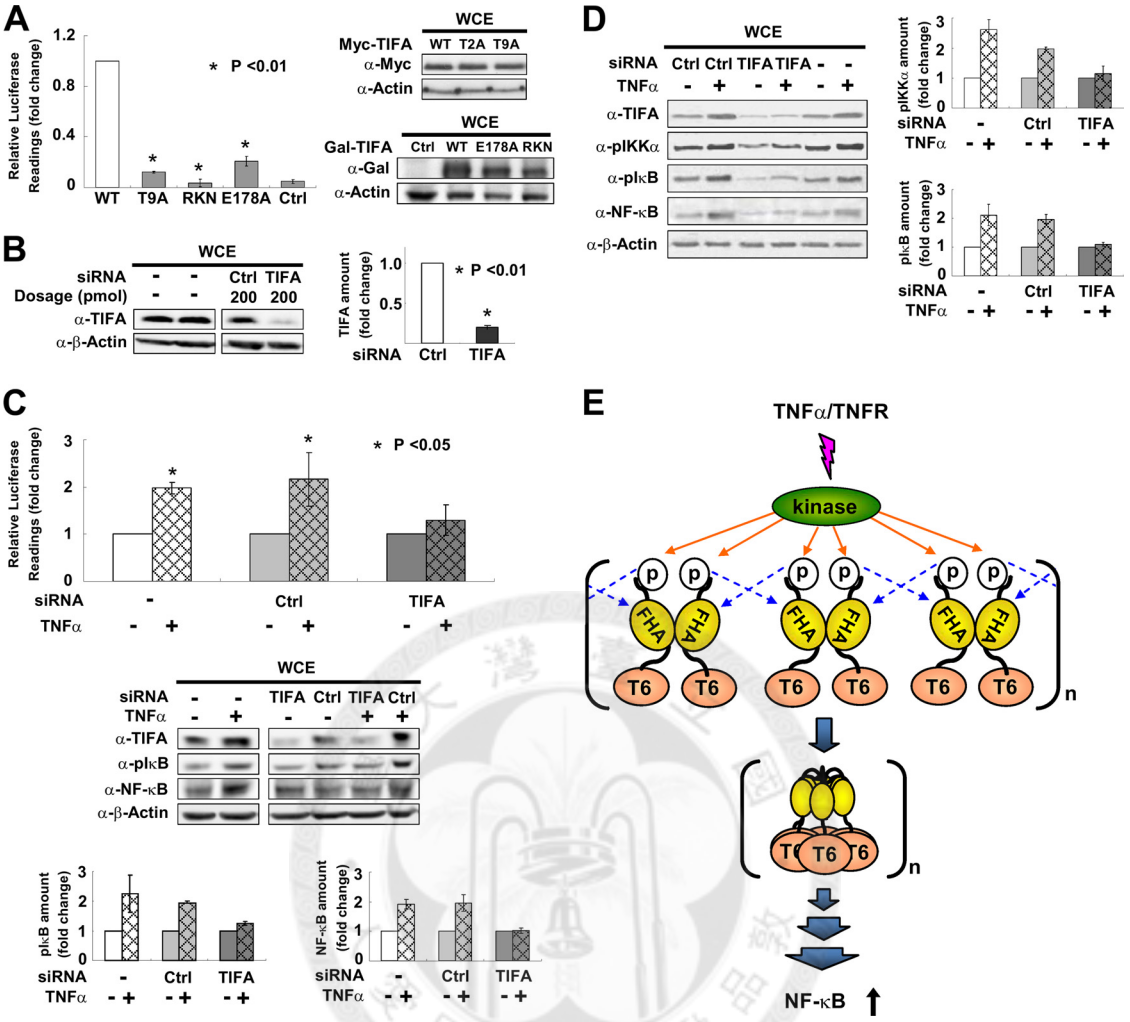

FIG 5 pT9-FHA binding is involved in TNF-α-mediated activation of NF-κB. (A) HEK 293T cells were transfected with an NF-κB luciferase reporter together with WT TIFA or its various mutants. NF-κB activation was evaluated by luciferase activity assays. The bar graph represents fold changes of normalized relative luminescence units (RLU). The results are mean ± SD from at least 3 independent experiments. Western blotting on the right shows the expression profiles of mutants used in the experiments. (B) HEK 293T cells were transfected with TIFA siRNA or scramble RNA (Ctrl). The efficiency of RNA interference was verified by Western blotting in at least 3 independent experiments and plotted in the bar graph shown on the right. (C) HEK 293T cells receiving TIFA siRNA or scramble RNA (Ctrl) were cotransfected with an NF-κB luciferase reporter and then stimulated with TNF-α as indicated. NF-κB activation was evaluated by luciferase activity assays. The values for the untreated groups were set as 1. The cell lysates were also analyzed by Western blotting. The bar graphs at the bottom represent the fold changes of phosphorylated IκB (pS32/pS36) and total NF-κB (p65) proteins after TNF-α treatment. (D) The experimental conditions for siRNA transfection were the same as those described for panel C except that the cell line used was THP-1 (a human acute monocytic leukemia cell line). The bar graphs represent the fold changes of phosphorylated IKKα (pT23) and phosphorylated IκB (pS32/pS36) after TNF-α stimulation. (E) Proposed model for TIFA oligomerization, which first takes place via intermolecular FHA-pT9 binding between TIFA dimers upon TNF-α stimulation and then leads to TRAF6 (labeled T6) oligomerization and subsequent NF-κB activation.

reduced to levels similar to those for the PBS control for the TIFA-silenced group. Similar attenuation of TNF-α-mediated signaling was also observed when endogenous TIFA was silenced in the human acute monocytic leukemia cell line, THP-1 (Fig. 5D). These findings together demonstrate that TIFA is necessary, and the FHA-pT9-induced TIFA oligomerization is important, for TNF-α-mediated NF-κB activation.

DISCUSSION

The principal finding of the current study is that TIFA oligomerizes through intermolecular FHA-pT9 binding between TIFA dimers upon TNF-α stimulation, which leads to TRAF6 oligomerization and subsequent NF-κB activation. Such a mechanism indicates that TIFA is an imperative molecule linking inflammatory cytokines, such as TNF-α, to the NF-κB-driven gene expression. Based on the deduced mechanism, a model is proposed for the function of TIFA, as shown in Fig. 5E. Upon TNF-α stimulation, an activated serine/threonine kinase involved in the PI3K-AKT pathway phosphorylates Thr9 of TIFA. This phosphorylation event then triggers the pT9-FHA interaction between different dimers of TIFA, leading to their oligomerization. Since TRAF6 constitutively binds to TIFA E178 located at the C terminus of TIFA, the oligomerization of TIFA then induces TRAF6 oligomerization, which in turn enhances the E3 ligase activity of the RING ("really interesting new gene") domain of TRAF6 and activates the downstream signaling (6). Thus, this newly defined mechanism

has important translational implications, particularly for inflammatory responses in mammalian cells.

Using MS, NanoPro immunoassay, and *in vitro* kinase assay, we confirmed the T9 phosphorylation and semiquantified its changes responding to TNF-α stimulation. These assays also showed that in addition to T9, there are other basal phosphorylations for both exogenous and endogenous TIFA (Fig. 1C and D, traces 1). However, it is not clear whether these basal phosphorylations are specific. The exact kinases responsible for the TNF-α-induced phosphorylation of T9 and the basal phosphorylation of TIFA remain to be established. Furthermore, because the pT9-FHA binding plays a pivotal role not only in mediating TIFA self-association/oligomerization but also in provoking TRAF6 oligomerization/NF-κB activation, antagonizing such a putative kinase may interfere with the TNF-α-related inflammation.

Based on recent reports, the mechanism of FHA domain function appears to be highly diversified (18). The "mechanism" here is defined as how, at the protein level, the FHA domain binds to its biological ligand and confers its biological function. To date, three mechanisms have been characterized: (i) a monomer of the FHA domain binds the pT residue(s) of a different monomer of its biological ligand intermolecularly (3), (ii) a monomer of the FHA domain binds with the pT residue of another monomer of the same FHA protein intermolecularly to enhance homodimerization (4, 15, 29), and (iii) intramolecular binding occurs between an FHA domain and a pT site within the same protein molecule (1). The model for the aggregation of TIFA therefore uncovers a new mechanism for FHA domain functions: the unphosphorylated FHA domain-containing protein exists as an intrinsic dimer that oligomerizes via the intermolecular FHA-pT bindings between dimers. Interestingly, the FHA domains of both human and mouse MDC1 (mediator of DNA damage checkpoint 1) proteins were recently shown to exist as intrinsic dimers in solution and in crystals (13, 17, 28).

Finally, the detailed atomic structure of full-length TIFA dimer complexed with a pT9-containing peptide, when available, will be very valuable for interpretation of molecular mechanisms of the signaling pathway. Most importantly, it will provide us chances to design regulatory compounds against NF-κB activation and properly manage inflammatory responses, autoimmune diseases, viral infection, and cancer development.

Overall, our work here, along with previous reports, has provided a mechanistic insight into TIFA oligomerization and the critical role of TIFA in NF-κB activation. The TIFA pT9-directed oligomerization of molecules involved in TNF-α-mediated inflammatory responses may have a broad impact on understanding of mammalian immunity. Our results have provided a basis for future studies into these significant issues.

ACKNOWLEDGMENTS

We thank Y.-M. Chou and P. K. Tai of Cold Spring Harbor Inc. (Taipei, Taiwan) and members of Cell Biosciences Inc. for their contributions to the NanoPro immunoassay, Y.-Y. Kao for preliminary ITC analysis, Y.-L. Huang for peptide synthesis, L.-P. Ting (National Yang-Ming University) for the pNF-κB-Luc plasmid, and E. S.-W. Chen, M.-I. Su, and R. H. Chen for useful discussions.

This work was supported by National Health Research Institute grant NHRI-EX100-10002NI and the Academia Sinica Investigator Award to M.-D.T.

C.-C.F.H., P.-Y.G.W., J.-H.W.,T.-Y.W.W., D.Q., and M.-D.T. designed the research; C.-C.F.H., J.-H.W., T.-Y.W.W., P.-H.H., Y.-H.C., S.-C.W., C.-C.H., and S.-T.C. performed the research; C.-C.F.H., P.-Y.G.W., J.-H.W., T.-Y.W.W., A.H.-J.W., J.Y.-J.S., and M.-D.T. interpreted the data; and C.-C.F.H., P.-Y.G.W., J.-H.W., J.Y.-J.S., and M.-D.T. wrote the paper.

We declare that we have no competing interests.

REFERENCES

1. **Barthe P, et al.** 2009. Dynamic and structural characterization of a bacterial FHA protein reveals a new autoinhibition mechanism. Structure **17**:568–578.
2. **Baud V, et al.** 1999. Signaling by proinflammatory cytokines: oligomerization of TRAF2 and TRAF6 is sufficient for JNK and IKK activation and target gene induction via an amino-terminal effector domain. Genes Dev. **13**:1297–1308.
3. **Byeon IJ, Li H, Song H, Gronenborn AM, Tsai MD.** 2005. Sequential phosphorylation and multisite interactions characterize specific target recognition by the FHA domain of Ki67. Nat. Struct. Mol. Biol. **12**:987–993.
4. **Cai Z, Chehab NH, Pavletich NP.** 2009. Structure and activation mechanism of the CHK2 DNA damage checkpoint kinase. Mol. Cell **35**:818–829.
5. **Durocher D, Jackson SP.** 2002. The FHA domain. FEBS Lett. **513**:58–66.
6. **Ea CK, Sun L, Inoue J, Chen ZJ.** 2004. TIFA activates IkappaB kinase (IKK) by promoting oligomerization and ubiquitination of TRAF6. Proc. Natl. Acad. Sci. U. S. A. **101**:15318–15323.
7. **Fan AC, et al.** 2009. Nanofluidic proteomic assay for serial analysis of oncoprotein activation in clinical specimens. Nat. Med. **15**:566–571.
8. **Fang CY, et al.** 2010. Global analysis of modifications of the human BK virus structural proteins by LC-MS/MS. Virology **402**:164–176.
9. **Force WR, et al.** 2000. Discrete signaling regions in the lymphotoxin-beta receptor for tumor necrosis factor receptor-associated factor binding, subcellular localization, and activation of cell death and NF-kappaB pathways. J. Biol. Chem. **275**:11121–11129.
10. **Hofmann K, Bucher P.** 1995. The FHA domain: a putative nuclear signalling domain found in protein kinases and transcription factors. Trends Biochem. Sci. **20**:347–349.
11. **Inoue J, et al.** 2005. Identification and characterization of Xenopus laevis homologs of mammalian TRAF6 and its binding protein TIFA. Gene **358**:53–59.
12. **Ishida T, et al.** 1996. Identification of TRAF6, a novel tumor necrosis factor receptor-associated factor protein that mediates signaling from an amino-terminal domain of the CD40 cytoplasmic region. J. Biol. Chem. **271**:28745–28748.
13. **Jungmichel S, et al.** 2012. The molecular basis of ATM-dependent dimerization of the Mdc1 DNA damage checkpoint mediator. Nucleic Acids Res. **40**:3913–3928.
14. **Kanamori M, Suzuki H, Saito R, Muramatsu M, Hayashizaki Y.** 2002. T2BP, a novel TRAF2 binding protein, can activate NF-kappaB and AP-1 without TNF stimulation. Biochem. Biophys. Res. Commun. **290**:1108–1113.
15. **Li J, et al.** 2008. Chk2 oligomerization studied by phosphopeptide ligation: implications for regulation and phosphodependent interactions. J. Biol. Chem. **283**:36019–36030.
16. **Liang X, Van Doren SR.** 2008. Mechanistic insights into phosphoprotein-binding FHA domains. Acc. Chem. Res. **41**:991–999.
17. **Liu J, et al.** 2012. Structural mechanism of the phosphorylation-dependent dimerization of the MDC1 forkhead-associated domain. Nucleic Acids Res. **40**:3898–3912.
18. **Mahajan A, et al.** 2008. Structure and function of the phosphothreonine-specific FHA domain. Sci. Signal. **1**:re12. doi:10.1126/scisignal.151re12.
19. **O'Neill RA, et al.** 2006. Isoelectric focusing technology quantifies protein signaling in 25 cells. Proc. Natl. Acad. Sci. U. S. A. **103**:16153–16158.
20. **Pennell S, et al.** 2010. Structural and functional analysis of phosphothreonine-dependent FHA domain interactions. Structure **18**:1587–1595.
21. **Pullen SS, et al.** 1998. CD40-tumor necrosis factor receptor-associated factor (TRAF) interactions: regulation of CD40 signaling through multiple TRAF binding sites and TRAF hetero-oligomerization. Biochemistry **37**:11836–11845.
22. **Sanz L, Diaz-Meco MT, Nakano H, Moscat J.** 2000. The atypical PKC-

interacting protein p62 channels NF-kappaB activation by the IL-1-TRAF6 pathway. EMBO J. **19**:1576–1586.
23. **Seibenhener ML, et al.** 2004. Sequestosome 1/p62 is a polyubiquitin chain binding protein involved in ubiquitin proteasome degradation. Mol. Cell. Biol. **24**:8055–8068.
24. **Sun Z, Hsiao J, Fay DS, Stern DF.** 1998. Rad53 FHA domain associated with phosphorylated Rad9 in the DNA damage checkpoint. Science **281**: 272–274.
25. **Takatsuna H, et al.** 2003. Identification of TIFA as an adapter protein that links tumor necrosis factor receptor-associated factor 6 (TRAF6) to interleukin-1 (IL-1) receptor-associated kinase-1 (IRAK-1) in IL-1 receptor signaling. J. Biol. Chem. **278**:12144–12150.
26. **Wang KZ, Galson DL, Auron PE.** 2010. TRAF6 is autoinhibited by an intramolecular interaction which is counteracted by trans-ubiquitination. J. Cell Biochem. **110**:763–771.
27. **Wang KZ, et al.** 2006. TRAF6 activation of PI 3-kinase-dependent cytoskeletal changes is cooperative with Ras and is mediated by an interaction with cytoplasmic Src. J. Cell Sci. **119**:1579–1591.
28. **Wu HH, Wu PY, Huang KF, Kao YY, Tsai MD.** 2012. Structural delineation of MDC1-FHA domain binding with CHK2-pThr68. Biochemistry **51**:575–577.
29. **Xu X, Tsvetkov LM, Stern DF.** 2002. Chk2 activation and phosphorylation-dependent oligomerization. Mol. Cell. Biol. **22**:4419–4432.
30. **Zapata JM, et al.** 2001. A diverse family of proteins containing tumor necrosis factor receptor-associated factor domains. J. Biol. Chem. **276**: 24242–24252.